INVESTIGATION OF WORMHOLE PENETRATION IN CARBONATE ROCKS UNDER HIGH PRESSURE

BY

Sarmad Zafar Khan

A Thesis Presented to the
DEANSHIP OF GRADUATE STUDIES

KING FAHD UNIVERSITY OF PETROLEUM & MINERALS
DHAHRAN, SAUDI ARABIA

In Partial Fulfillment of the
Requirements for the Degree of

MASTER OF SCIENCE
In

PETROLEUM ENGINEERING

MAY, 2013

KING FAHD UNIVERSITY OF PETROLEUM & MINERALS

DHAHRAN 31261, SAUDI ARABIA

DEANSHIP OF GRADUATE STUDIES

This thesis, written by SARMAD ZAFAR KHAN under the direction of his thesis adviser and approved by his thesis committee, has been presented to and accepted by the Dean of Graduate Studies, in partial fulfillment of the requirements for the degree of MASTER OF SCIENCE IN PETROLEUM ENGINEERING.

Thesis Committee

Dr. Abdullah S. Sultan
(Advisor)

Dr. Mahmoud Doklah
(Member)

Darren Malekzadeh
Dr. Darren Malekzadeh
(Member)

M. A. Mahmoud
Dr. Mohamed Mahmoud
(Member)

Frank Chang
Dr. Frank Chang
(Member)

25 JUN 2013
for
Dr. Abdullah Sultan
(Department Chairman)

Dr. Salam A. Zummo
(Dean of Graduate Studies)

30/6/13
Date

INVESTIGATION OF WORMHOLE PENETRATION IN CARBONATE ROCKS UNDER HIGH PRESSURE

by

SARMAD ZAFAR KHAN

A Thesis Presented to the

DEANSHIP OF GRADUATE STUDIES

in Partial Fulfillment of the Requirements for the degree
MASTERS OF SCIENCE

IN

PETROLEUM ENGINEERING

KING FAHD UNIVERSITY OF PETROLEUM & MINERALS

Dhahran, Saudi Arabia

MAY, 2013

KING FAHD UNIVERSITY OF PETROLEUM & MINERALS

DHAHRAN 31261 , SAUDI ARABIA

DEANSHIP OF GRADUATE STUDIES

This thesis, written by SARMAD ZAFAR KHAN under the direction of his thesis adviser and approved by his thesis committee, has been presented to and accepted by the Dean of Graduate Studies, in partial fulfillment of the requirements for the degree of MASTER OF SCIENCE IN PETROLEUM ENGINEERING.

Thesis Committee

____
Dr. Abdullah S. Sultan
(Advisor)

____
Dr. Mahmoud Doklah
(Member)

____
Dr. Darren Malekzadeh
(Member)

____
Dr. Mohamed Mahmoud
(Member)

____
Dr. Frank Chang
(Member)

____
Dr. Abdullah Sultan
(Department Chairman)

____
Dr. Salam A. Zummo
(Dean of Graduate Studies)

____
Date

Dedication

This effort is dedicated to my parents

ACKNOWLEDGEMENT

I am grateful to Almighty Allah for blessing me with courage and determination for fulfillment of this dream. I cannot express my thanks to him in words.

I truly acknowledge my advisor, Dr. Sultan, for providing me with the opportunity to work on an area of my interest. His guidance, support and encouragement were extremely helpful.

I would also like to express my gratitude towards King Fahd University of Petroleum and Minerals for the award of scholarship to me throughout the course of my study in the Masters Program. My stay here is one of the most memorable period of my life.

I thank my thesis committee members Dr. Doklah, Dr. Darren, Dr. Mahmoud, and Dr. Chang for their valuable input in the data analysis of my experiments.

I also thank Schlumberger Dhahran Carbonate Research Center (SDCR) for funding this project (CPM-2298) and I really appreciate the support of Steve Dyer, Abdul Muqtadir and Xiadong from SDCR for providing me all the help during the coreflood experiments.

I thank my parents, family and friends for their continuous support.

TABLE OF CONTENTS

LIST OF FIGURES

LIST OF TABLES

ABSTRACT

Full Name : Sarmad Zafar Khan

Thesis Title : Investigation of Wormhole Penetration in Carbonate Rocks Under High Pressure

Major Field : Petroleum Engineering

Date of Degree : May, 2013

Matrix acidizing is a classic stimulation technique through which the permeability of a formation is altered by injecting an acid which result in dissolution of rock. In carbonate reservoirs, this process actually creates flow channels for the hydrocarbons in the near wellbore area known as “wormholes”. The objective of this project was to study the phenomenon of “wormholing” in deep carbonate formations at high pressure.

The primary focus was to establish good understanding of the rock dissolution under high pressure and moderate temperature conditions for tight reservoirs. There are various parameters involved in such studies which include but not limited to the flow rate of acid, the concentration of the acid, rock type, rock properties, temperature and pressure. There have been vast studies reported in the literature; however, experiments with such high pressures have not been conducted before.

In this project, we studied the propagation of wormhole by conducting experiments using new coreflooding system capable of handling high pressure and longer cores. These experiments provided new insights regarding the phase of CO_2 on the process of wormholing at different pressures. On contrary to the assumptions in the modeling, CO_2 was found to be at gaseous state moderate pressures, hampering the process of wormholing. With abundant data from coreflood experiments, the effect of pressure and flow rate studied. The long cores used in the experiments along with the special setup on the coreflood system helped us to establish relation between the length of the core and the dissolution. It was found that length plays an important role when the pressures are moderate. Description of wormhole speed and wormhole diameter profile at different conditions has been covered in detail. CT scans, thin section and SEM were used to understand the shape and propagation of the wormhole morphology.

ABSTRACT (ARABIC)

الاسم: سرمد ظفر خان

عنوان الرسالة: دراسة تفاعل حمض الكلوريك فى الصخور الكربونية وتشكيل الحفر الدودية تحت تاثير الضغط العالى

الدرجة العلمية: ماجستير العلوم الهندسية

التخصص: هندسة البترول

تاريخ التخرج: مايو، 2013 م

الملخص

ذوبان الصخر بالأحامض هو طريقة محاكاة تقليدية قديمة حيث يتم فيها تغيير نفاذية الطبقة القريبة من منبع البئر النفطية عن طريق حقن حامض حيث يتفاعل مع الصخر ويُحسن النفاذية. فى مكامن الصخور الكربونية، هذه العملية فعليا تُودي الى تكوين قنوات لسريات الهايدروكربونات بالقرب من منطقة البئر وهذه القنوات تعرف ب"القنوات الدودية". الهدف من هذا المشروع هو دراسة مصطلح "القناة الدودية" فى اعماق الطبقات الكربونية.

وكان التركيز الأساسى هو انشاء فهم جيد لتفاعل الصخور الكربونية تحت ظروف ضغط عالى ودرجة حرارة متوسطة للمكامن ذات النفاذية المنخفضة. هناك متغيرات عدة تكون ينبغي دراستها والتى تشمل و التي تشتمل على معدل تدفق الحمض، تركيز الحمض، نوع الصخر، خواص الصخور، درجة الحرارة والضغط. كما ذكر سابقا، نُفذّت هذه الدراسة تحت ضغط عالى باستخدام صخور الكربونية ذات نفاذية منخفضة. وبالنظر في الدراسات السابقة يلاحظ أنه لم تتم تجارب تحت ضغط عالى قد أُنجزت من قبل.

فى هذا المشروع، درسنا انتشار القناة الدودية عن طريق اجراء تجارب باستخدام جهازالتدفق فى العينات الصخرية قادر على محاكاة تمثيل سريان الموائع في المكامن. حيث قدمت هذه التجارب رؤى جديدة فيما يتعلق بطبيعة ثانى اكسيد الكربون فى عملية تشكل القنوات الدودية تحت ضغوط مختلفة. وقد توفرت بيانات كثيرة من تجارب غمر العينة، و تأثير الضغط، و معدل التدفق و طول العينة وتأثيرها على سرعة وقطر الثقب الدودي فى الظروف المختلفة

كما تم استخدام المسح الالكتروني المقطعى، و عمل مقاطع دقيقة فى العينة و تصويرها تحت المجهر الالكترونى لدراسة طريقة تشكّل الثقب الدودى في الظروف المختلفة.

CHAPTER 1

INTRODUCTION

Advancement in the research towards better description of in-situ processes is a very important step in the way ahead for the hydrocarbon industry in order to meet the ever increasing demands of the hydrocarbon thirsty world. This study deals with analysis of the matrix acidizing in carbonates under high temperature and high pressure with its implications on low permeability reservoirs.

The basic idea of matrix acidizing is to increase the permeability of the formation in the vicinity of the borehole by the dissolution of carbonated from injected acid.

$$2HCl + CaCO_3 \longrightarrow CaCl_2 + H_2O + CO_2$$

Most experimental studies conducted for understanding the wormholing phenomenon made an incorrect assumption that 1,000 psi is sufficient to keep CO_2 in the solution. Hence extracting data from experiments conducted at 1,000 psi to model acid penetration in typical oil and gas reservoir can cause significant error.

The second drawback in modeling wormholing phenomena is the lack of kinetics data of spent acids. As wormholes penetrate into the reservoir, the acid concentration at the fine tips could be significantly lower than that of the fresh acid, especially in low permeability rocks. Current models use the same kinetics parameters of fresh acid throughout the length of the wormhole, leading to overestimate in wormhole penetration. Moreover, there is very limited data available that studies the core length effects on the wormholing process and this shortcoming must be addressed.

To overcome the above stated drawbacks, coreflood experiments were conducted at increasing system pore pressure (up to 5,000 psi) and realistic reservoir temperatures (up to 150^{o}F) to study the effect of CO_2 phase on wormholing velocity. Carbonate cores were CT scanned before and after acidizing to observe the wormhole morphology against porosity distribution. These steps allowed us to accurately understand wormholing process and hence to quantitatively model the wormhole penetration dynamics through a comprehensive interpretation of the wormhole formation as it propagates along the length of the core.

1.1 Statement of Problem

Current understanding of wormholing process during carbonate matrix acidizing is based on acidizing experiments conducted in short cores under 1,000 psi system pressure. It has been assumed that 1,000 psi is sufficient to keep evolved CO_2 in solution. Thermodynamic study has shown that CO_2 solubility is a strong function of pressure and temperature. Under most reservoir temperature, 1,000 psi is not sufficient to keep CO_2 dissolved in the aqueous phase. Using experimental studies at 1,000 psi could cause significant misconception about acid and carbonate reaction in real reservoirs.

As mentioned earlier, most models do not take into consideration the variation in the concentration of the acid along the length of the wormhole. The tip of the wormhole could be saturated with reaction products (calcium and magnesium ions), which hinder further reaction by limiting mass transfer of hydrogen ions to the rock surface. The capacity of acid to extend wormhole is therefore significantly reduced. The dissolution kinetics at the tip of the wormhole is dictated by the reaction kinetics parameters of spent acid. Current practices lead to overestimation in wormhole penetration.

The effect of core length on the breakthrough volume for acidizing has been discussed very rarely in the literature. It is believed that an extensive experimental data relating the length of core with optimum flow rate and the breakthrough volume will help improve the wormholing model significantly.

1.2 Thesis Objectives

There are two primary objectives of this work:

1. To conduct core acidizing experiments at pressures up to 5,000 psi and 150°F to study pressure effects on the phenomenon of wormholing. It is expected that as the pressure builds up, the solubility of CO_2 in the solution will increase and its effects will be studied.

2. The effect of core length (up to 24 inches) with varying pressure conditions will also be studied. The advanced equipment will render more detailed experimental data than available in the literature.

Most coreflood acidizing experiments in the past have been conducted at about a maximum of 2,000 psi and such extensive experiments at high pressures are being conducted for the first time and will be a valuable addition to the literature. Moreover, this work is a part of a greater project which will integrate the data from these experiments with other Rotating Disk experiments for fresh and spent acids to finally develop a better wormhole model.

CHAPTER 2

LITERATURE REVIEW

2.1 Matrix Acidizing of Carbonates

Stimulation techniques include matrix acidizing, propped hydraulic fracturing, and acid fracturing. The selection of the stimulation technique depends upon the rock type of reservoir, the production objectives and economics. Matrix acidizing is a common well stimulation technique in which acid is injected into the producing reservoir. The main purpose of the process is to remove wellbore formation damage and/or dissolve a portion of the rock and hence, enhance the permeability in the near well-bore region. Matrix acidizing is normally less expensive than other techniques.

2.1.1 Description of wormhole growth

Wormholes are basically flow channels produced in the rock formation when the rock is acidized below the fracturing pressure of the formation. Hung and Hill [1] presented a mathematical model that describes the growth and competition of wormholes during acidizing treatment in a carbonate formation. The model is initialized with the distribution of the largest pores. Wormhole characteristics (size, length and distribution) were found to be controlled by acid injection, diffusion and fluid loss rates. It was concluded that wormholes are formed from the largest pores or surface defects on the rock surface.

2.1.2 Existence of Damkohler Number

Hoefner & Fogler [2] carried out coreflood experiments to study the fluid velocity and reaction rate effects during carbonate acidizing. A network model developed to study flow and matrix dissolution in carbonates. They found out that wormholing in carbonates is controlled by the relative rates of flow and dissolution which are characterized by Damkohler number, N_{DA}, for the process. Acid penetrates as a function of wormholing and well defined channels will not form if N_{DA} is either very high or low. The experiments they carried out were done upon water/plaster systems. Aqueous solution of HCl was injected at a pressure of 1,000 psi and room temperature. Molten Wood's alloy was injected into the core after the formation of the wormholes and then the metal was allowed to solidify and then the whole core was dissolved to obtain the actual structures of the wormholes (Fig. 1).

It was found out that if the flow rate is increased for limestone, less volume is required for breakthrough. Similarly, if the reaction rate is lowered by decreasing the diffusion rate, similar effects are observed. The effect of both the situations is that acid and wormhole go farther in the formation easily. However, for dolomite the effect is quite opposite as the increase in injection rate and decrease in reaction rate require more volume of acid to achieve breakthrough.

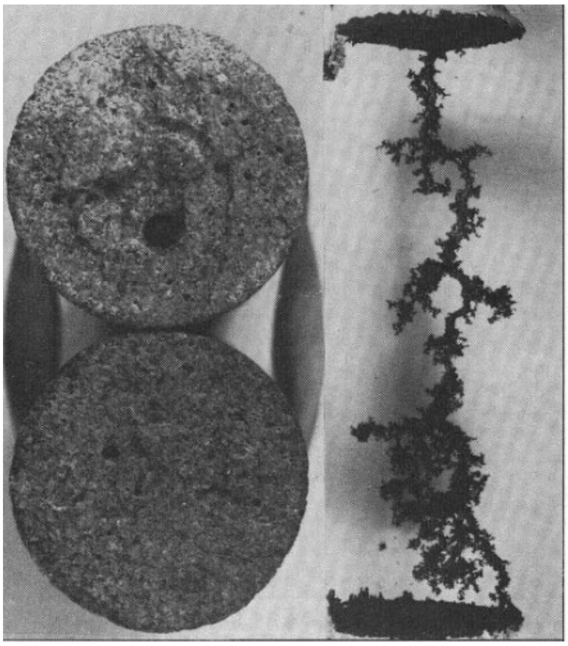

Figure 1 Wood's alloy procedure for Hoefner's experiment

Fredd and Fogler [3] performed acidizing experiments on a wide range of fluid systems including strong acids, weak acids, and chelating agents. These fluid systems are influenced by a variety of transport and reaction processes such as the transport of reactants to the surface, the reversible surface reactions, and the transport of products away from the surface**.** When these transport and reaction processes were taken into account, a common dependence of the dissolution phenomenon on the Damkohler number was observed. There exists an optimum Damkohler number at which a minimum number of pore volumes are required for channel breakthrough. In addition, an optimum kinetic parameter exists at which wormhole formation is most efficient. Together, the Damkohler number and the kinetic parameter provide a complete description of the dissolution phenomenon.

All the experiments carried out by Fredd & Fogler [3] were conducted at pressure ranges of 1,000–2,000 psi and temperatures of about 50°C and 70°C. The degree of transport/reaction limitations was quantified by a kinetic parameter, Γ. The dimensionless kinetic parameter is defined as the ratio of the surface reaction rate constant to the overall dissolution rate constant.

The number of pore volumes to breakthrough and the wormhole structures were found to be influenced by the degree of transport/reaction limitations. These limitations were quantified by the dimensionless kinetic parameter. For a particular value of the Damkohler number and the kinetic parameter, both the number of pore volumes to breakthrough and the wormhole structures are similar.

2.1.3 Optimum Injection Rate Theory

Wang and Hill [4] presented an optimum acid injection rate theory for the acidizing processes of carbonates. The main result of that work was the discovery of an optimum acid injection rate to obtain acid breakthrough in linear corefloods of carbonates using a minimum total acid volume. Low rates result in acid spending at the core surface while high rates result in the formation of multiple, highly ramified wormholes. At the optimum intermediate rate, a single, small wormhole penetrates the core. The optimum acid rate is found to be a function of the rock composition and reaction temperature as well as the pore size distribution of the virgin formation rock. All of these factors are included in the work done by Wang & Hill which provides a quantitative prediction of the optimum rate. Lab experiments were conducted with dolomite and two types of limestone, Indiana and Glen Rose. For various set of experiments, temperatures of 50°C, 75°C and room temperature were maintained whereas the applied pressure was about 1,000 psi.

From the curves for pore volumes to breakthrough (PV_{BT}) against injection rate, it was observed that as the injection rate increased, the volume required to breakthrough decreased, reached a minimum and then increased slowly. For both cores the curve was steep on the left side of the optimum injection rate and relatively flat for rates greater than the optimum, indicating that the effect of injection rate is more pronounced for rates below the optimum rate.

Huang and Hill [5] later postulated that there are three wormhole patterns that are formed as a result of acid injection. Firstly, compact dissolution in which most of the acid is spent near the rock surface (for low acid flux). Secondly, the regular wormhole pattern (for optimum flux) and lastly uniform dissolution in which many pores are enlarged.

It was found that fluid losses limit the distances of wormhole propagation. It was also found out that transition from one pattern to other depends upon the Damkohler number which is the key factor at large pores on the tip of the wormhole for predicting the optimal rate of injection.

According to Wang [4], the effects of temperature and concentration theory were more or less the same on the reaction as described in the rest of literature whereas mineralogy plays an important role in the formation of wormholes. The optimum injection rate, q_T is dependent upon the acid flux at the tip of the wormhole, u_e, radius of the wormhole, r_{wh}, flow rate at the tip of the wormhole, q_e, and the cylindrical length of the wormhole L_e. The acid flux at the tip of the wormhole is determined from

$$u_e = \frac{E_f C_o^{m-1}}{\mathrm{N_{DA}}} \tag{2.1}$$

Where E_f is the rate of reaction, C_o is the initial acid concentration, m is the order of reaction and N_{DA} is the Damkohler number. r_{wh} is found by the following approximation

$$r_{wh} = \left[\frac{DL}{2u_e}\right]^{1/2} \tag{2.2}$$

Where D is the diffusion coefficient and L is the length of the wormhole.

The flow rate at the tip of the wormhole is obtained by

$$q_e = \pi r_{wh}^2 u_e \tag{2.3}$$

The optimum flow rate, q_T is obtained from Fig. 2, using the parameters determined above.

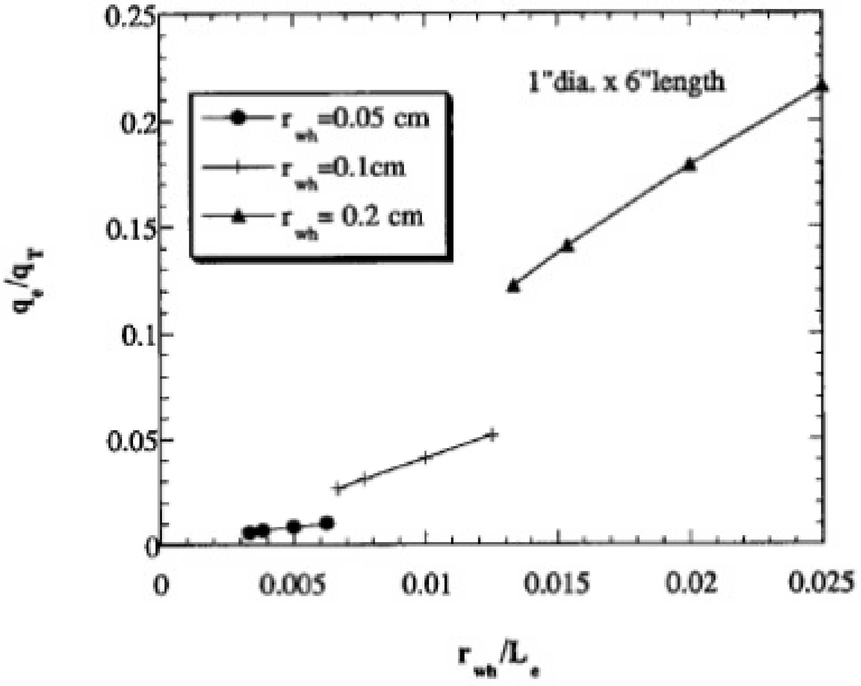

Figure 2 Graph for calculation of qT [4]

Glasbergen et al. [6], however recently concluded from his work that application of optimum coreflood test to a field is virtually impossible because of heterogeneities in the permeability. From many field cases, they also found out that at times the calculated optimum flow rate exceeds the maximum allowed flow rate.

Shedid [7] came up with his study of effects of various varying parameters on the acidizing of permeability damaged carbonate formation. The previously-reviewed experimental studies created an ambiguous design of matrix acidizing since they developed the required optimum volume and rate of acid for matrix acidizing for virgin formations, which do not actually simulate the damaged reservoir rock due to mud invasion or other sources of damage. The purpose of Shedid's work was to solve this issue by investigating the effects of acid injection rate, acid concentration, and acid volume for acidizing the carbonate rocks under different conditions of temperatures and for actually permeability-damaged carbonate reservoir rocks.

Temperatures were kept in the range of 50°C to 70°C and the pressure about 500 psig. It was found that the design of matrix acidizing has to consider the damage condition of carbonate rocks since the Bentonite water-base mud damage causes permeability reduction in the range of 79 % to 97 % of initial rock permeability. According to his interpretation, the increase of acid injection rate and/or acid concentration increases the recovered permeability by matrix acidizing. An oil reservoir of higher temperature requires more acid volume to be injected than that one of lower temperature for the same applied injection rate and acid concentration.

A Global Model for Carbonate Acidizing Behavior – Beyond Damkohler Number

Most of the research work pertaining to acidizing is focused to find an optimum injection rate. The goal is to find a surface injection rate that creates a network of highly conductive wormholes with the least possible amount of acid used. Several authors have observed that the core length, diameter, or aspect ratio can have an impact on the optimum injection rate. Some authors have performed experimental series at different temperatures and acid concentrations. Further, many different types of rocks with different permeability and porosity have been used. Almost all calculations rely upon the Damkohler number to determine the optimum injection rate. Damkohler number is in turn dependent upon wormhole radius and surface reaction both of which are mostly unknown in many cases.

Talbot and Gdanski [8] proposed a global model of the wormholing behavior of HCl and calcium carbonate ($CaCO_3$) by combining all the data from the previous research work using which the optimum injection rate can be found. They have utilized porosity, permeability, aspect ratio, concentration of acid and temperature as the variables which determines the optimum injection rate using properties like morphology factor, wormhole efficiency factor and a wormhole factor which are dependent on the above mentioned varying parameters. In this way reliance on the Damkohler number has been eliminated and easier and reliable solutions have been achieved.

2.1.5 Effect of various factors on the phenomenon of Wormholing

There are various aspects of wormholing upon which different varying parameters affect in differing manners. The rate of reaction which is the primary factor involved increases with increase in temperature, concentration of acid and surface area and decreases with increase in pressure.

Hayatdavoudi et al. [9] studied the effects of pressure on the quantity of unspent acid. They postulated that in the deeper wells with the increase of pressure, the quantity of acid which is left unspent also increases and these statements were validated from the experiments they carried out. In all the prior work the calculation were made considering the reaction to be a homogeneous one as it was believed that CO_2 gets dissolved in the aqueous solution but it is not the case all the time.

The phase of CO_2, in this study, is a matter of prime importance. It was believed that at 1,000 psi very little CO_2 gets dissolved in the solution of HCl whereas as the pressure increases the solubility of CO_2 increases. To quantify the solubility of CO_2, a thermodynamic software OLI was used to simulate the solubility at different pressures. The basis of this simulation is the experimental data available in the literature. Fig. 3 shows that post 1,000 psi, the solubility increases gradually but at around 2,800 psi, a sharp increase can be noted and at around 4,100 psi, all the CO_2 goes into the solution. Although, these number might not be accurate as they are based on limited experimental data available but they form very strong reference point and our findings later will show at great degree of agreement with this model.

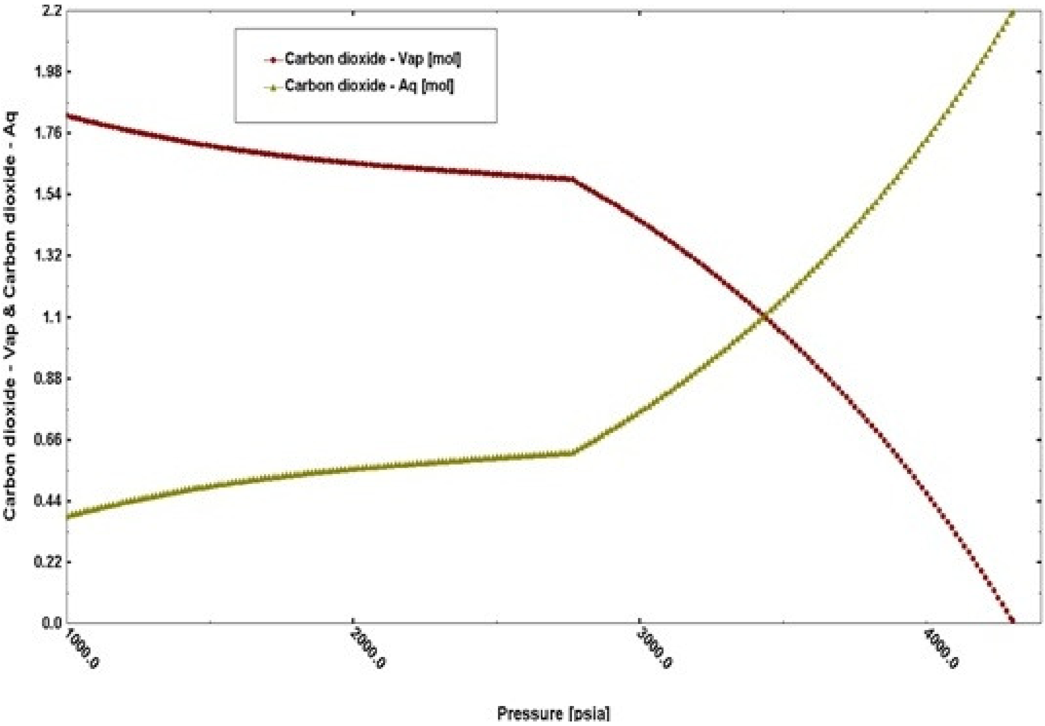

Figure 3 Solubility of CO_2 in a solution of 15% HCl generated by the thermodynamic software OLI

Hill and Hung [1] in their description of wormhole growth had suggested that wormhole lengths increase with injection rate, decrease with increase in fluid losses and with increased diffusion rates. It was also found out that a dominant wormhole is more likely with high diffusion rate or a low fluid loss rate.

Wang and Hill [4] from their work on fluid losses concluded that the effect of concentration is opposite in theory and experiments. According to the theory, increase in concentration should decrease the reaction rate but the experiments show opposite behavior. This phenomenon actually opens some room for further research in the area. This work concludes that since fluid losses are greater in field, so propagation is less. Charts of optimal flux against inverse of temperature were generated for guidelines in selection and formulation of injection fluid.

Shukla, Zhu and Hill [10] explained that the loss of acid across the walls of wormholes decrease the extent to which a wormhole can propagate. If the fluid loss can be controlled, then more of the acid can reach the wormhole tip, and therefore the penetration of wormholes can be increased. They investigated the effect of having immiscible phase saturation in the carbonate rock before the injection of acid. The presence of an immiscible phase can reduces the relative permeability to the acid and the fluid loss from the main wormhole is reduced, thus allowing for deeper penetration of wormholes with a given acid volume. It was found that gas injection prior to acid injection does significantly reduce the volume of acid required to propagate wormholes through cores by a factor of 3. Less branching was observed when an immiscible phase was introduced in the core prior to acid injection.

2.1.6 Wormhole Population Density Model

Huang, Zhu and Hill [11] investigated the wormhole population density, which means how many wormholes per area of rock surface or per wellbore length will be created. The study is based on the following strategy. For a given rock/acid system, the optimal acid injection flux at which dominant wormholes are initiated is obtained from the wormhole propagation theory. For a given formation, a corresponding pressure gradient at the optimal acid flux is calculated. This pressure gradient is also called the wormhole initiation pressure gradient. When a wormhole is initiated at an arbitrary point along the wellbore, the local pressure distribution is disturbed, resulting in lower pressure gradients into the formation in the region surrounding the wormholes. In this region of reduced pressure gradient and hence, reduced flux, initiation of other wormholes is suppressed. At a sufficient distance from the initial wormhole, the pressure field is undisturbed and other wormholes will develop. Fluid loss through the walls of the wormholes and wellbore, optimal acid injection flux, and wormhole propagation rate are also taken into account.

It was concluded that the wormhole population is predicted by modeling the pressure field around a wormhole. Combining the wormhole population density model with a wormhole propagation model, the acid volume needed to propagate wormholes by a given distance can be determined. It was found out that for a typical carbonate reservoir being acidized with 15% HCl, the population density model predicts about 12 wormholes/ft will be created from an open hole.

2.1.7 Use of alternative fluids for matrix acidizing

Various research articles have been published in the recent years about the experimental studies on the use of alternative fluids in place of hydrochloric acid to stimulate carbonate formations. Some of the eminent work is being presented here.

Acetic acid

Huang and Hill [12] in their work claimed that at high reservoir temperature, the optimal rate of hydrochloric acid is usually too high, and it sometimes is beyond the maximum injection allowed (the rate to avoid fracturing formation). In this case, weak acids, such as acetic acid, are alternative fluids to stimulate the wells because the optimal injection rate for weak acids is relatively lower than the one for strong acids. If hydrochloric acid is used below its optimal rate, it causes face dissolution and requires more volume to breakthrough. Although optimal volume of acetic acid required is more than the optimal HCl, but the optimal rate is significantly low and acetic acid also produces wormholes of greater radius. At elevated temperatures, the rate of reaction of acetic acid is expected to increase which will reduce the volume of acid required making it the preferable fluid to be used for stimulation.

Mixture of Organic Acids/HCl

Chang et al. [13] addressed two major drawbacks associated with using concentrated HCl solutions in deep wells. The first is its high reaction rate with carbonate rocks, which limits acid penetration in the formation. The second is its corrosivity to well tubulars. Hence organic acids become viable material for matrix acidizing to alleviate these two problems. Though organic acids provide the benefit of retardation and low corrosivity, their low dissolving capacity may still limit the wormhole penetration leading to insufficient stimulation of the formation. Therefore, opportunity exists to mix HCl with an organic acid to achieve productivity enhancement by optimizing the wormhole penetration and profile.

Chang et al. [13] discussed the required information to properly design an organic acid or HCl plus organic acid treatment. In addition to reaction kinetics, data such as carbonate dissolving capacity at reservoir temperature and pressure, solubility of reaction products, and the effect of HCl to organic acid ratio are needed to better design field treatments.

From the extensive study done, it was concluded that 1,000 psi system pressure is sufficient for testing acid dissolving capacity, but a much higher pressure is required for kinetics studies. The interaction between Ca^{2+} and organic anions is a direct function of organic acid dissociation. Moreover mixing HCl with acetic or formic acid also provides benefits in acid penetration depth due to delayed dissociation of organic acid in the presence of live HCl.

Chelating Agents

Different shortcomings of the use of simple hydrochloric acid have been addressed by various researchers. Mahmoud, Mohamed and Nasr-El-Din [14] believed that hydrochloric acid must not be used in well where the completion has Cr- based alloy because it causes corrosion problem. They also believed that use of HCl in formations where the fracture pressure is low must be avoided as the process is rendered inefficient because of face dissolution.

They investigated two chelating agents; hydroxyethylenediaminetriaceticacid (HEDTA), and L-glutamic acid –N, N-diacetic acid (GLDA) to solve the aforementioned issues.

Experiments proved that at same conditions the injection rate required for GLDA and HEDTA were pretty lower than that for HCl. At same conditions it was also found out that the chelating agents did not caused face dissolutions. Moreover, optimal injection rate was also found to be a function of core length for HCl whereas it is not a function of core length for the case of chelating agents which keeps the optimal rate to a low for chelating agents no matter what the core length is.

The chelating agents were also tested at high temperature where the reaction rates become higher but no dissolution was reported at optimal injection rates but GLDA performed better at low injection rates too. They also found out that GLDA was thermally stable up to 300°F and reacts faster on calcite than dolomite.

2.2 Wormholes and CT Images

The combination of matrix acidizing experiments with visualization techniques is commonly used to elucidate the details of wormhole networks formed during matrix acidizing of carbonate reservoir rock. At a given temperature, the ability of a particular acid to generate wormholes is largely dependent on the acid injection rate or “acid flux”, as illustrated in Fig. 4. Shown is an example of a “wormhole efficiency curve” developed for core plugs of quarried dolomite rock. There is a certain optimal acid flux for which wormholes will most efficiently propagate along the main axis of the core plug. Below the optimal flux, dissolution is mostly confined to the rock face nearest to the acid injection point; above the optimal flux, dissolution occurs more uniformly throughout the entire core plug rather than forming dominant individual wormhole channels.

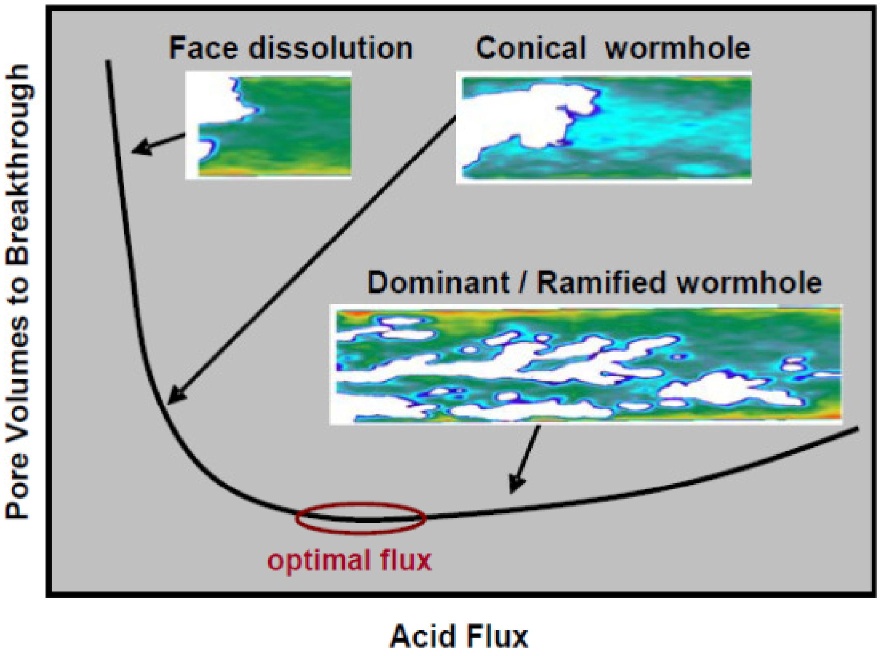

Figure 4 Wormhole Efficiency Curve

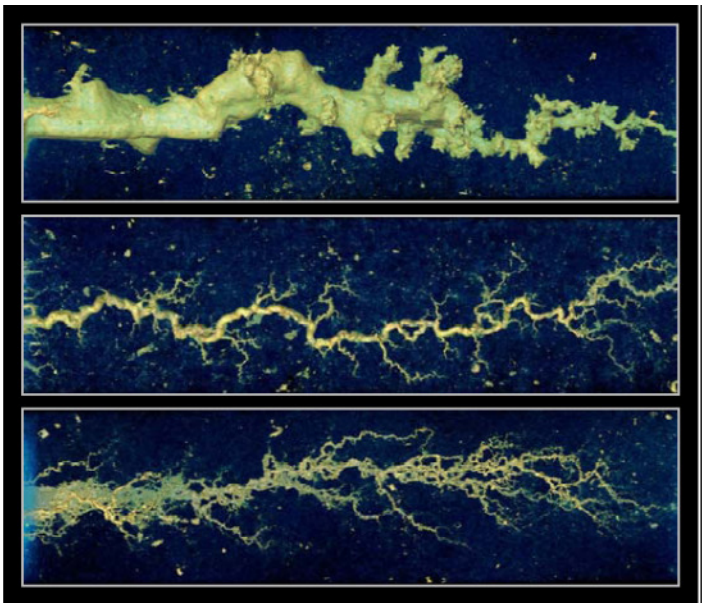

Figure 5 CT Images of Acidized cores at low, optimum and high acid flux [15]

To better visualize the intricacies of wormholes formed, advanced CT imaging is used for select acidized core plugs. High-resolution images of three acidized Indiana limestone core plugs are shown in Fig. 5. The core plugs were selected along the wormholing efficiency curve for Indiana limestone at low, optimum, and high acid flux, respectively.

CHAPTER 3

MATERIALS & METHODS

3.1 Materials

There were three important substance used in this study that includes the core samples, the injection acid and the additives. Apart from these substances, the main equipment used in our study was the coreflood system and CT Scan Machine.

Indiana Limestone Cores: Indiana Limestone was used in all the experiments mainly because of its homogeneous nature. 12 sets each comprising of two 12 inch cores were acquired for this study. The diameter of all the cores was 1.5 inch and the permeability and porosity ranged from 0.9 mD to 7 mD and 13% to 15%, respectively.

Hydrochloric Acid (HCl): 15% HCl solution was prepared from a 37% HCl solution (from Emsure, Merck Chemicals, Germany) by diluting it. For dilution, simple calculations provided the volume of DI water and HCl to be used, and thus 315 ml of DI was taken in a flask and 1 ml of an amine based corrosion inhibitor (**A270)** was added to it. Then 37% HCl solution was poured in to fill up till the 500 ml mark, thereby producing a solution of 15% HCl.

Corrosion Inhibitor: An amine based corrosion inhibitor **A270** is also added to the solution to protect the coreflood system from corrosion.

DCI Dual Coreflood System: The Dual Coreflood System used for the acidizing experiments is a high pressure high temperature core flow test equipment that comprises a fluid delivery pump, four fluid accumulators and two core holders capable of holding 12 inch core each placed in an oven, effluent accumulators and back pressure pumps. The sleeves inside the core holders have four equidistant pressure tappings (2.4 inch apart) connected to pressure transducers. These transducers can thus monitor the pressure difference across a particular section. Consequently the propagation of a wormhole can be recorded as a function of pressure drop in a particular section.

Toshiba Medical CT Scanner: Toshiba Medical CT Scanner was used to run pre-acidizing and post-acidizing CT scans of all the cores. The machine can generate CT data for cores with a minimum slice thickness of 1 mm. Consequently, about 300 images of each core were generated.

Figure 6 DCI Coreflood System

Figure 7 Toshiba CT Scan Machine

3.2 Methodology

This section describes the general plan of work, including the design and methodology that was adopted to carry out the experiments in pursuit of achieving our objectives. A proper framework methodology has been designed which is divided into three distinct phases. The project began with rock characterization, followed by coreflooding and characterization of the cores post acidization. Different tasks pertaining to these phases and respective approaches to achieve the tasks are briefly described below.

3.2.1 Rock Characterization (Phase-1)

Rock characterization is the first phase where petro physical properties of the core samples were determined using suitable equipment.

CT scan: First of all, the fresh dry cores were scanned on the CT scan machine with a slice thickness of 1 mm thus generating about 300 slices of each core. The cross section images of the rocks were obtained by using Voxel Calc software and were used to study the pre acidizing morphology of the rocks. The CT scan will be more important in the post acidizing (coreflooding) analysis where we will visualize the wormhole and study its structure. Moreover, the CT scan images can also be used to validate the values of the petro physical properties earlier measured in the lab.

Saturation of Cores and Porosity Measurement: The cores after the CT Scans were put under vacuum for a few hours and weighed. Then they were saturated with deionized water at a pressure of 2,000 psi for a few hours. After saturation, the samples were weighed again and since the density of DI water is considered to be unity, therefore the difference in the weight of dry and saturated samples simply translated into the pore volume of the rocks.

Permeability: Permeability of the rock samples was measured by flowing DI water across the cores in the coreflood system. Prior to acidizing DI water is flowed across the cores to establish a stabilized core. Since the coreflood system has the capability to record pressure data at every second, this function was used to calculate the permeability of the whole core and those of particular sections using the pressure data for about 100 seconds prior to acid injection. The permeabilities for these 100 points are then averaged to obtain more accurate values.

The complete data of porosity and permeability values for all the 24 cores is presented in the Appendix A in Table 4.

3.2.2 Coreflooding Experiments (Phase-2)

The fresh cores after characterization were placed in the high pressure high temperature coreflood system described in the previous section. A confining pressure of approximately 1,500 psi more than the expected injection pressure was applied to both the cores. The cores were then heated up to the desired temperature of 65°C. Before injecting the acid into the cores, de-ionized water was injected to established stabilized flow in the cores at the desired back pressure at the outlet of the second core. The pressure data from the outlet and inlet of cores at this point was used for the calculation of the initial permeability of the cores. After stabilization, acid was injected from one face of the core (inlet) which created wormholes in the core till they broke through from the other end (outlet). Primarily, back pressure applied was varied and the volume injected for breakthrough was noted against different injection rates and the wormhole thus created was studied. The phase of CO_2 is extremely important and was given consideration in these experiments.

Fig. 8 shows the schematic of the coreflood equipment and its components can be labeled as (1) Injection Pump (2) Accumulators fpr fluid Injection (3) Pressure Tappings (4) Confining Stress (5) Axial Stress (6) Accumulator for Effluent (7) Back Pressure Pump (8) Effluent Drainage

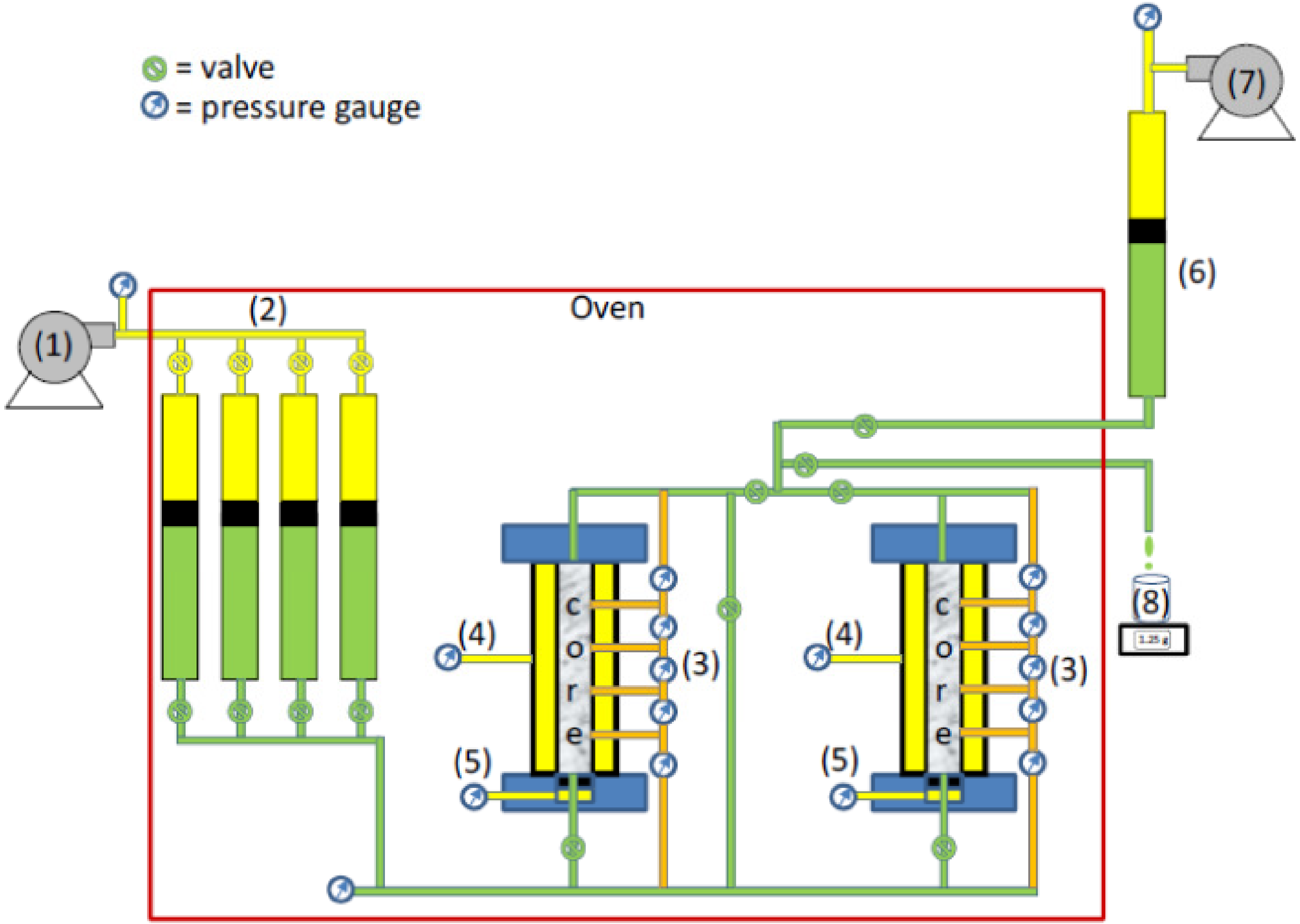

Figure 8 Schematic of Coreflood Equipment [16]

3.2.3 Post Acidizing Characterization (Phase-3)

After acidizing, the cores were unloaded from the coreflood system and kept in an oven at 65°C for over 24 hours to dry. The dry cores were then weighed again and the difference of the weights inherently is the amount of the limestone dissolved. The cores were then CT scanned again. After post acidizing CT Scanning, a few samples were selected to be analyzed on the SEM and for thin section analysis.

Scanning Electron Microscope: Scanning Electron Microscope is used for the qualitative description of mineralogy, grain texture, its size and shape and pore structure. Advanced techniques in this area can be used for the elemental analysis, calculation of different reservoir parameters and rock properties in a short time.

For our purpose we cut 3, 4 mm thick slices from the selected points (from section 2 of both cores in series) of the particular cores. The cores were then plated with gold for about 10 min and then SEM analysis was carried out. The mapping and EDX (by weight and by atomic number) were done, the details of which are given in the next chapter.

Thin Section Analysis: Thin section analysis is the examination under a regular microscope of the composition and pore structure of the rock samples. The slices for thin section were taken from the adjacent slices acquired for SEM. The analysis from the thin sections is also discussed in the next chapter.

3.3 Experimental Plan

A series of experiments was scheduled in which most of the variable parameters were kept constant and mainly the pressure and flow rate were varied as per objectives of the study. In the following, the ranges and values of the varied and fixed parameters have been discussed respectively. Table 3.1 at the end also summarizes the experimental plan with numerical values.

1. **Pressure:** To the best of our knowledge, all the acidizing experiments conducted until now are in the range of 1,000–2,000 psi. In this work, it was aimed to conduct experiments for high pressure reservoirs where the pressure was varied from 1,000 to 5,000 psi. CO_2 is considered to be dissolved at around 1,000 psi but that is not the case. It was believed that this consideration will be found true in when the pressure is increased way above 1,000 psi. Temperature affects both the phase of CO_2 and the rate of the reaction which in turn has its own effects on the structure of wormhole formed. The temperature here was kept constant at 150° F.

2. **Flow Rate:** The flow rate of the acid being injected was varied from 1 cc/min to 10 cc/min.

3. **Length of Core:** Length of core has significant effect on the formation of wormholes as the boundary effects vary with the length of the core. 12 inch cores will be used and two of them will be simultaneously run in series which will give us a total length of 24 inch. The cores used in this work were of the same diameter of 1.5 inch. Here it was assumed that the diameter of the core has no effect on the acidizing process.

It was initially planned that our proposed 12 experiments will be carried out in four sets (each comprising of 3 experiments) in which the flow rate will be kept constant and pressure varied. This continued for the first six experiments but later the plan was altered as per the availability of ready cores prepared for a specific test run. The following Table 1 describes the sequence in which experiments were conducted with most parameters mentioned.

Table 1 Experimental Plan

Experiment No.	Core 1	Core 2	Perm 1 (mD)	Perm 2 (mD)	Flow Rate (cc/min)	Pressure (psi)
1	IL-10	IL-11	1.57	0.98	1	1,000
2	IL-12	IL-13	0.9	1.07	1	3,000
3	IL-15	IL-14	2.53	2.17	1	5,000
4	IL-16	IL-17	2.97	3.87	2	1,000
5	IL-18	IL-19	4.89	3.95	2	3,000
6	IL-20	IL-21	1.99	3.91	2	5,000
7	IL-26	IL-27	4.58	5.1	10	3,000
8	IL-28	IL-29	5.73	5.5	5	3,000
9	IL-22	IL-23	5.66	4.13	5	1,000
10	IL-30	IL-31	6.54	5.72	10	1,000
11	IL-32	IL-33	3.68	2.67	10	5,000
12	IL-45	IL-46	3.1	3.94	5	5,000

CHAPTER 4

RESULTS AND DISCUSSION

4.1 Coreflood Experiments

The series of 12 experiments was completed and the coreflood data was analyzed independently for each of the experiment. Then, all the results were combined to find out how varying parameters affect different aspects of wormholing phenomenon. In all the experiments, first of all the desired temperature of 65°C was achieved and stabilized and then DI water was injected in the core at the planned flow rate for the particular experiment while keeping the back pressure applied at the outlet of the second core in accordance with the plan for a specific experiment. The stable flow was identified by the stable values of pressure at the inlet and outlet of the cores and across all sections as well. The pressure data from these points was also used to calculate the permeability of the cores. The acid is then injected into the core and as it touches the face of the first core and begins to dissolve the carbonate rock, a wormhole is generated and in dictated by pressure drop in the first section. As the wormhole propagates along the length of the core, the pressure differential across each section keeps on coming down to zero and that is when a breakthrough is said to have taken place. The volume of acid consumed by the core is called the breakthrough volume and is reported in terms of pore volumes of acid injected for breakthrough.

4.1.1 Description of Basic Analysis

The data logs for all the experiments include logging time, valve configuration, pressure values at the pumps, confining and triaxial pressures, inlets, outlets, pressure tappings, temperature values at various points etc.

From the valve configuration and the notes kept, the time of injection of acid is determined. Pressure differentials in specific sections are plotted against time of acid injection which show a sharp drop to zero indicating the propagation of wormhole through them. This breakthrough time is visually determined and used for all subsequent calculations.

The following gives a description of the table used for the basic analysis of all the experiments.

Sections: It represents the number of sections within a core.

Lengths: Corresponding to every section we have a length beginning from the inlet of Core 1.

Breakthrough Time (hours): It is the time at which breakthrough occurs in a specific section. Its values are manually entered by observing the pressure drop charts for every section

Apparent Breakthrough Volume: Since the injection rate is constant, the apparent breakthrough volume is calculated by the following formula:

$$Apparent\ Breakthrough\ Volume = \ BreakthroughTime\ \times 60\ \times Flow\ Rate \quad (4.1)$$

Actual Breakthrough Volume (ABV) (cm^3): Actual Breakthrough Volume is calculated by subtracting the dead volumes from the Apparent Breakthrough Volume. Both of these volumes represent volume of acid required to penetrate from the inlet of Core1 to the end of a specific section

Breakthrough Pore Volume Total (PVT_B): Actual Breakthrough Volume is converted in terms of Pore volumes by dividing Actual Breakthrough Volume by the total pore volume of two cores

Pore Volume till Section End: It is assumed that the cores are homogeneous and the void spaces (pore volume) are distributed uniformly across the bulk of the two cores. This assumption is used to calculate the pore volume available from the beginning of Core1 to the end of a specific section. Mathematically, the total pore volume is divided by 10 and is cumulatively calculated by addition

Section Specific Breakthrough Pore Volume (PV_{BT}): It is the most important quantity calculated here as it is used in all later graphical analysis. This quantity is the amount of acid, in terms of pore volumes till section end, required for breakthrough. It is calculated by dividing the Actual Breakthrough Volume by Pore Volume till section end.

The tables of calculation for all the experiments are provided in the Appendix B.

4.1.2 Pressure Profiles and Phase of CO_2

The experiments conducted for this project can be categorized into four sets of experiments carried out at four constant rates in two cores of 12 inch length each connected in series at a temperature of 65°C. Primarily the varying parameter for a specific set of experiments was the back pressure applied at the end of second core. The experiments conducted at a pressure of 1,000 psi lasted for much longer period of time in which the acid could only break through eight sections of the two cores when the injection rate was low and would eventually break through at higher rates. On the other hand, the acid broke through all ten sections of the two cores relatively very quickly when the applied back pressure was 3,000 or 5,000 psi.

The most important feature that distinguishes the wormholing phenomenon under low pressure from those under high pressures is the injection pressure response and the pressure itself at the tip of wormhole being propagated. The injection pressure rises as the wormhole propagates at low pressure because of CO_2 being produced in the gaseous form. This is not only visible in the injection profile but it can be seen that the pressure in the section ahead of the wormhole also rises indicating the presence of CO_2 in the gaseous phase. This phenomenon however diminishes when it comes to the experiments conducted under 3,000 and 5,000 psi which actually shows that most of the CO_2 being produced goes into the solution at higher pressure. It also goes on to indicate that there exists a pressure above which the phases of the products behave similarly even if the pressure is further increased.

The injection pressure profile for all these experiments shows that at high pressures of 3,000 and 5,000 psi, the injection pressure drops from its stabilized value when the acid begins to penetrate and falls down to the back pressure value when the breakthrough is achieved whereas in the case of tests conducted at 1,000 psi the injection pressure keeps on increasing as CO_2 is generated in the gaseous form (especially in the case of low rates when the breakthrough is not achieved).

Effect of mass transfer is also an important aspect in the comparison of the high pressure and low pressure tests considering the CO_2 effect. The presence of gaseous phase CO_2 at low pressure increases the movement of hydrogen ions from the solution to the surface of wormhole which allows the acid to react and dissolve the rock along its walls with fresh acid instead of moving forward. By the time this acid is reaches the wormhole tip, it is largely spent, decreasing the pace of propagation. This leads to more “face dissolution” type of propagation and fatter but smaller wormholes.

At elevated pressures CO_2 is more soluble in the aqueous solution, and tends to buffer diffusion of hydrogen ions from the bulk to the rock surface leading to a lower reaction rate. Subsequently the acid available at the tip of the wormhole is far less spent than in lower pressure experiments, leading to faster tip propagation. Fig. 9 to Fig. 14 show the injection pressure profile and pressure differentials in all sections during experiments conducted at 1,000, 3,000 and 5,000 psi, respectively.

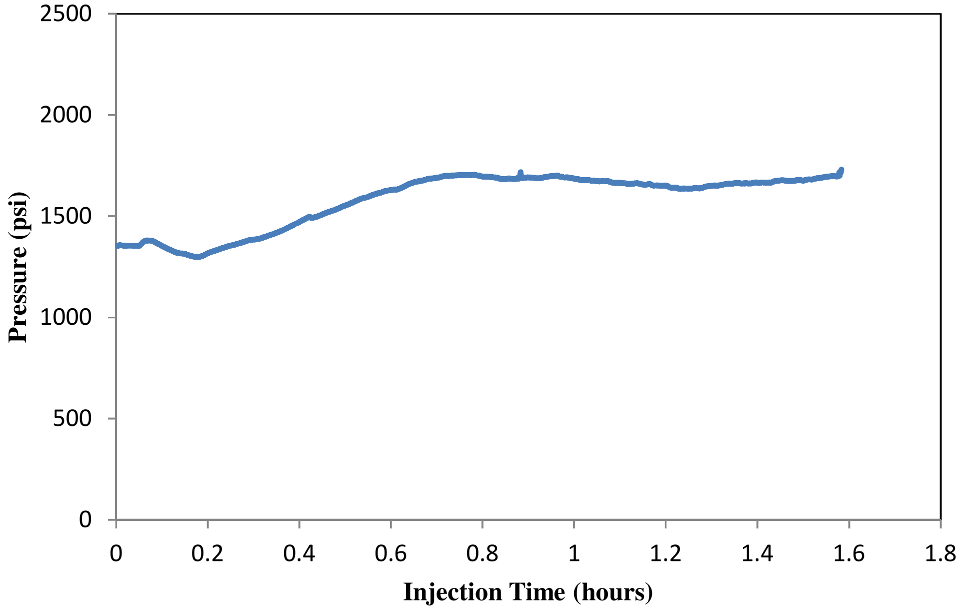

Figure 9 Injection Profile at Core 1 for Experiment at 1,000 psi and 2 cc/min

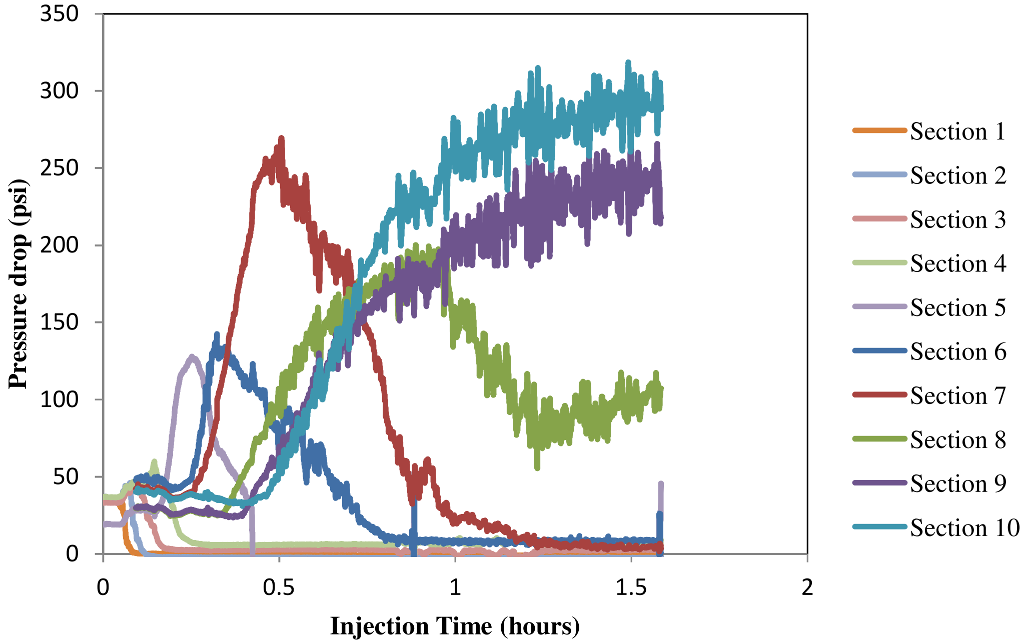

Figure 10 Pressure Differentials Profile for Experiment at 1,000 psi and 2 cc/min

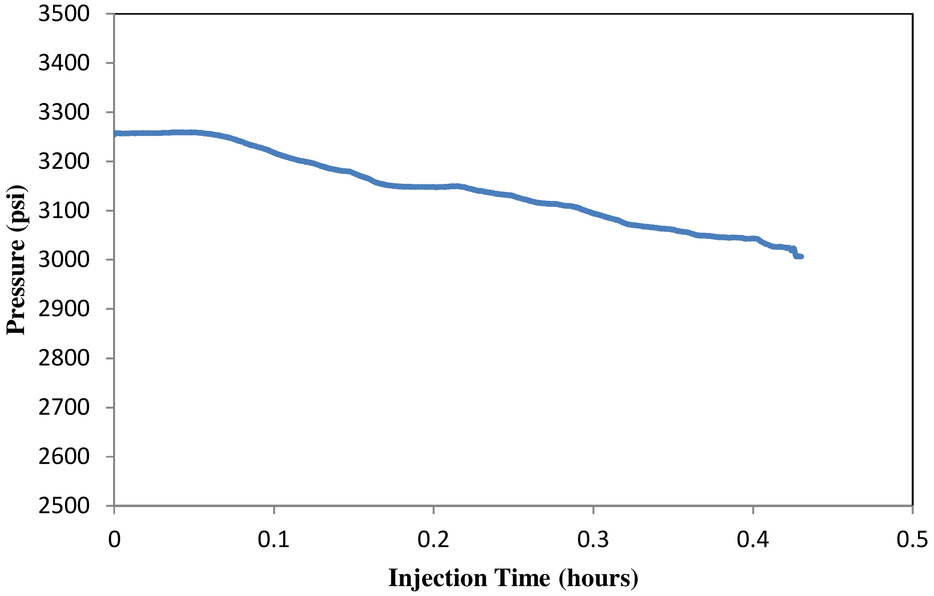

Figure 11 Injection Profile for Experiment at 3,000 psi and 2 cc/min

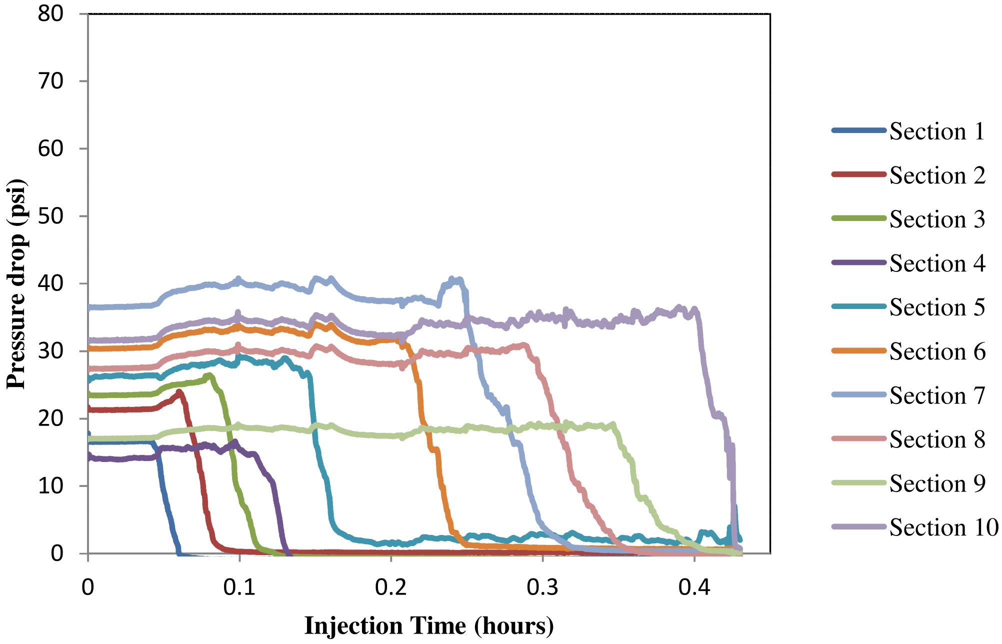

Figure 12 Pressure Differentials Profile for Experiment at 3,000 psi and 2 cc/min

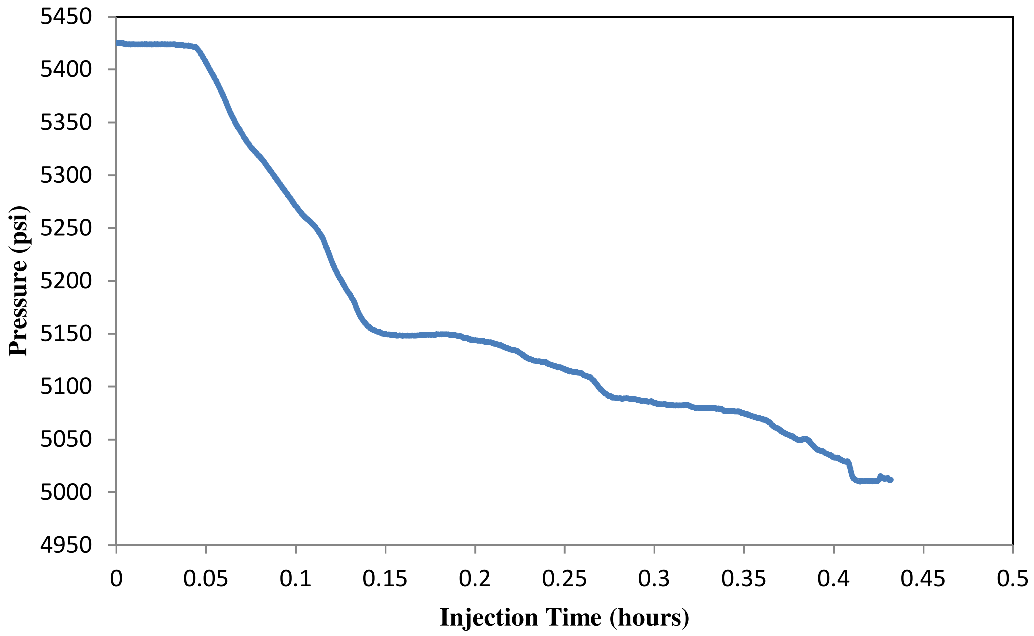

Figure 13 Injection Profile at Core 1 for Experiment at 5,000 psi and 2 cc/min

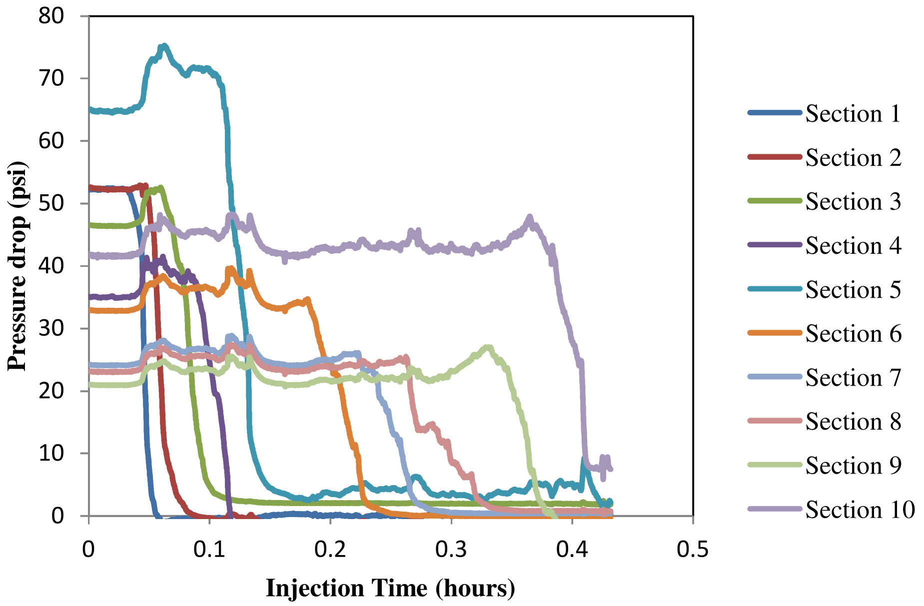

Figure 14 Pressure Differentials Profile for Experiment at 5,000 psi, 2 cc/min

4.1.3 Effect of Pressure and Flow Rate

This section will report the effects of change in pressure and flow rate by plotting the pore volume to breakthrough in two ways. Firstly, we plotted the pore volume to breakthrough for each section against the length of that section for various pressures while keeping the flow rate constant. In other words, we can see the effect of pressure at a specific rate for a particular section.

From Fig. 15 to Fig. 18, it can be seen that at lower rates, the effect of pressure is very much dominant as compared to higher rates. At lower rates (1 cc/min & 2 cc/min), the pore volume to breakthrough for low pressure cores (1,000 psi) is much higher as compared to high pressure cores (3,000 and 5,000 psi). Along with different reaction kinetics at different pressures, the main factor that accounts for this difference is the different phase of CO_2. At 1,000 psi, it is proposed that CO_2 is in gaseous phase as indicated by the pressure drop response. This gaseous CO_2 forces the hydrogen ions from the bulk of the solution to the walls of the wormhole causing the diameter in the hole to increase and thereby increasing the required number of pore volumes of acid to be injected for breakthrough. This phenomenon keeps on growing as the wormhole moves ahead along the length of the core but the effect of length will be discussed in the next section in detail. On the other hand, at 3,000 and 5,000 psi, more or less all CO_2 is considered to be in solution which assists in smooth propagation of the wormhole. CO_2 dissolved in the acid solution can help to keep the wormhole go straight.

But at higher rates (5 cc/min and 10 cc/min) we see that the effect of pressures diminishes and is not so obvious. We see that more or less similar volumes of acid are required for breakthrough at 1,000 psi and 3,000 psi. This is because of the fact that for experiments at 1,000 psi, with increased flow rate, the phenomenon of rock dissolution gradually begins to change from a mass transfer limited process to a reaction rate limited process. In this way lesser amount of CO_2 is generated and this much amount can be kept dissolved in the solution, which eventually causes a smooth propagation of wormhole even at 1,000 psi with high flow rates. But still it can be inferred from the plots that in general higher pressures are favorable for wormhole propagation and require less pore volumes to breakthrough. The plots are presented below.

It must be noted that pressure or flow rate alone cannot determine the structure of the wormhole or the volume required for breakthrough. It is rather the combination of both that determines it. If the breakthrough volumes are plotted against length while keeping the pressure constant we can observe the effect of changing the flow rates at a certain value of reservoir pressure.

The major inference from the following plots is that the PV_{BT} is quite sensitive to the change of flow rate at a pressure of 1,000 psi but as the pressure increases, the sensitivity to flow rate decreases.

The CO_2 effect is also visible in Fig. 19 representing the experiments carried out at 1,000 psi whereas the effect diminishes in other Fig. 20 and Fig. 21.

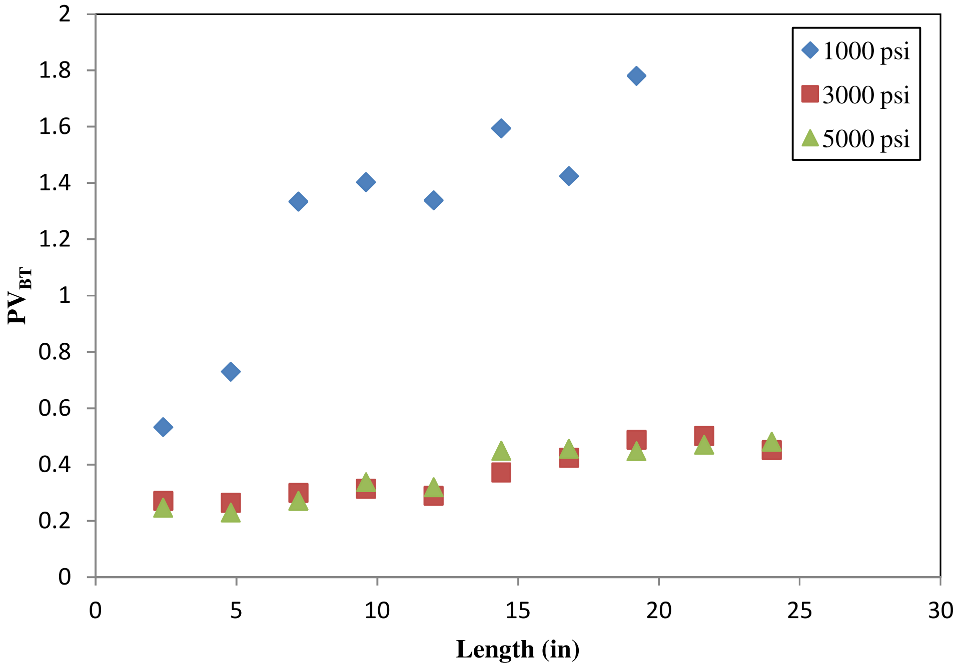

Figure 15 Effect of Pressure on PV_{BT} at 1 cc/min

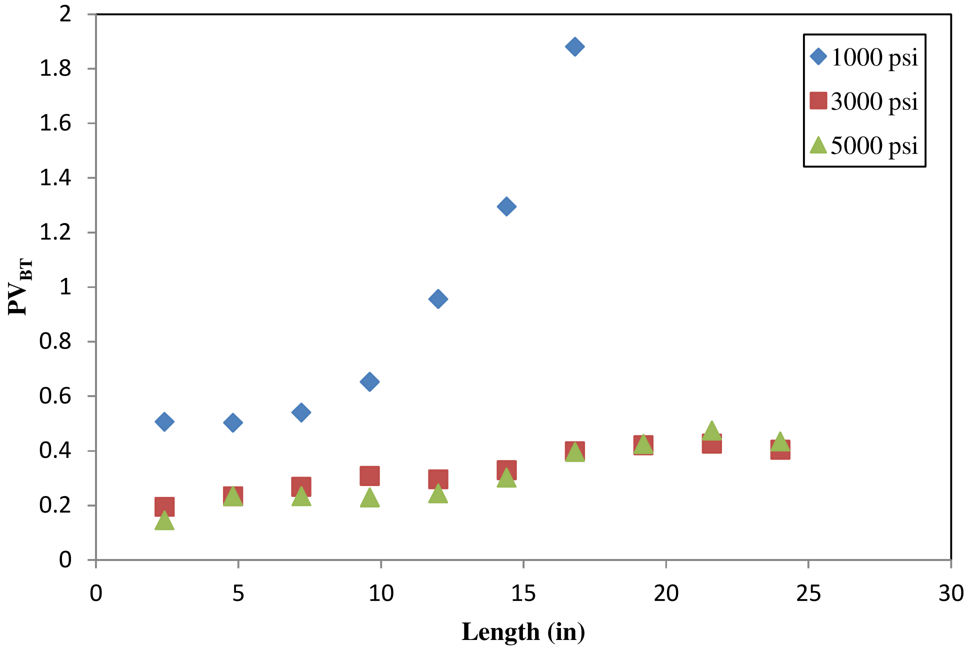

Figure 16 Effect of Pressure on PV_{BT} at 2 cc/min

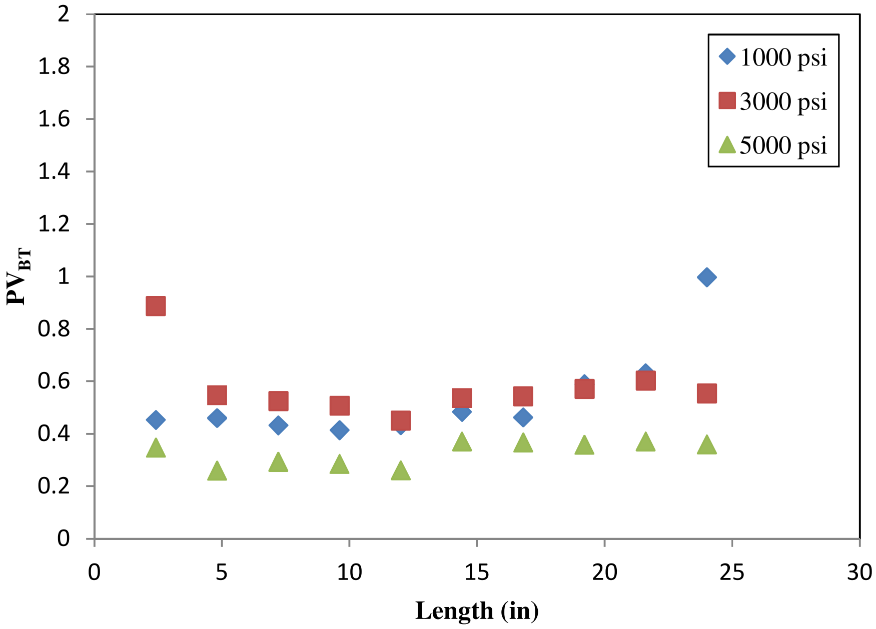

Figure 17 Effect of Pressure on PV_{BT} at 5 cc/min

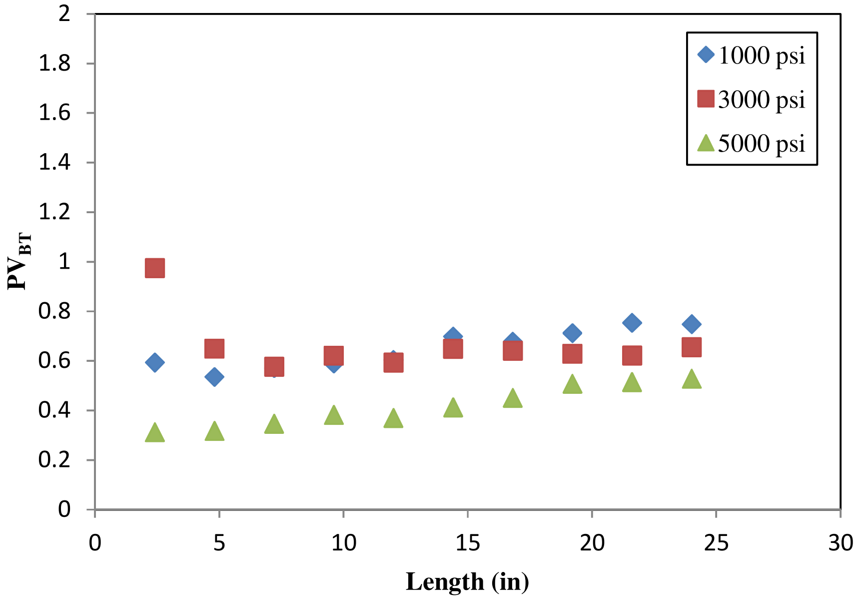

Figure 18 Effect of Pressure on PV_{BT} at 10 cc/min

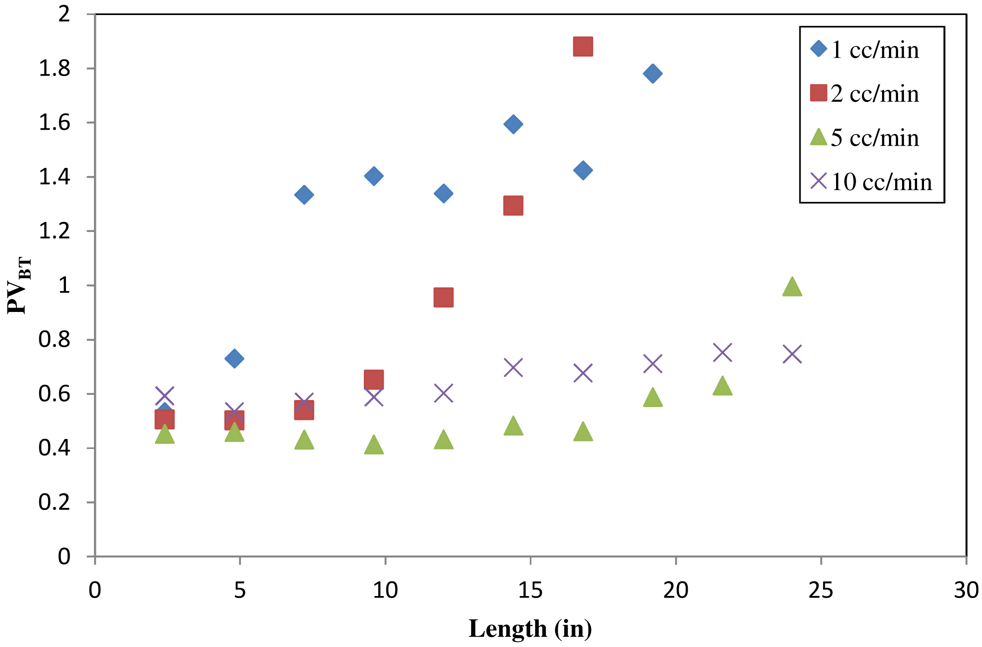

Figure 19 Effect of Flow Rate on PV_{BT} at 1,000 psi

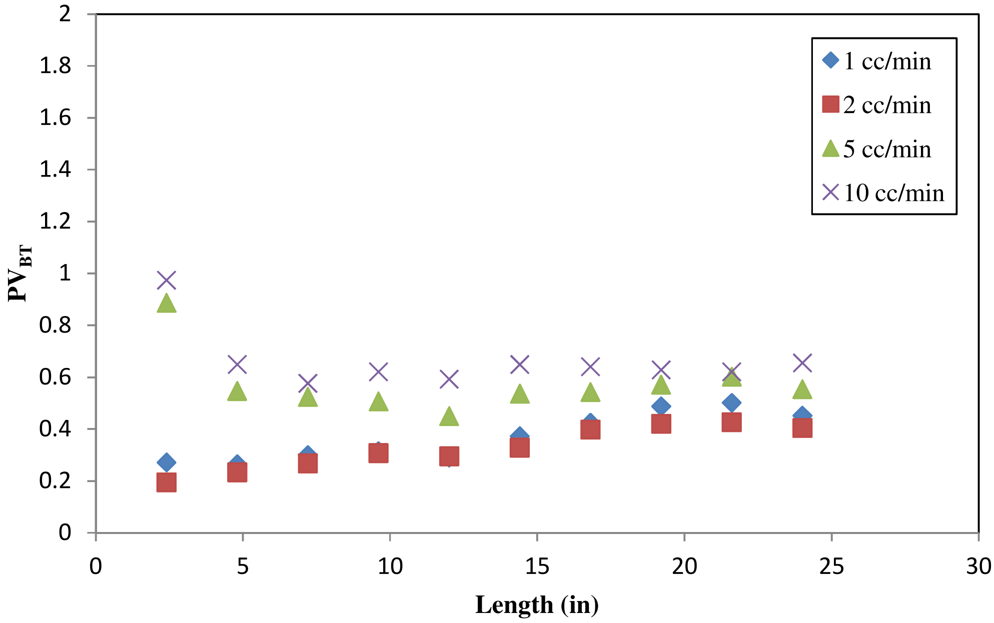

Figure 20 Effect of Flow Rate on PV_{BT} at 3,000 psi

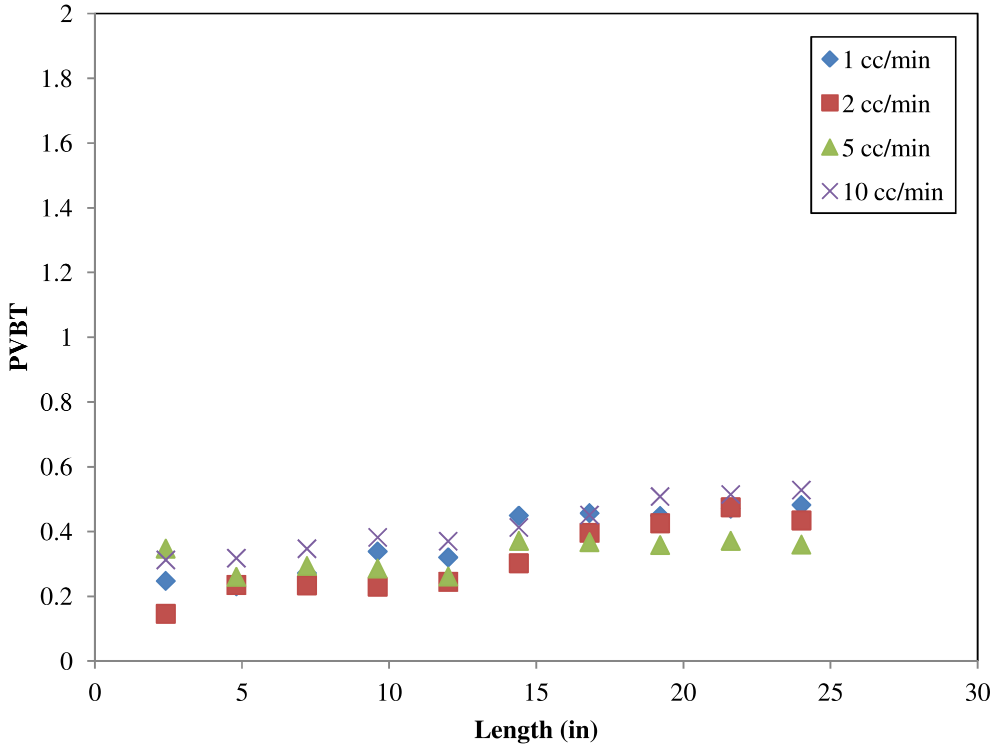

Figure 21 Effect of Flow Rate on PV_{BT} at 5,000 psi

4.1.4 Effect of Core Length

Investigating the effect of length on the propagation of wormhole was one of main objectives of this study. To study this effect, the pore volume to breakthrough was plotted against the interstitial velocity for all the sections while keeping the pressure constant. It was noted that more pore volumes of acid were required as the length of core was increased. It should be kept in mind that more volume of acid being required for the breakthrough is obvious but an increased pore volume means that the amount of acid required for longer cores is more than what simple law of direct proportionality would suggest. The increase in PVBT is higher for experiments conducted at 1,000 psi with increasing length however this impact reduces as we move from low injection rates to high injection rates.

It is seen that for higher pressures of 3,000 psi, the impact of length is visible but diminishes and is almost unnoticeable in the case of 5,000 psi. These observations are in accordance with the inferences regarding the phase of CO_2 discussed previously and the smooth propagation of wormholes at higher pressures described later. The plots can be seen in the Fig. 22 to Fig. 24.

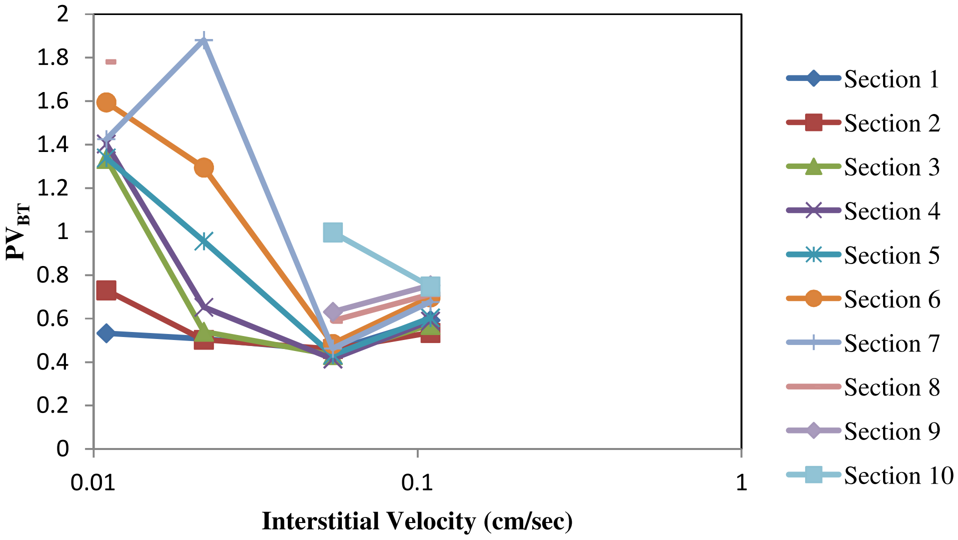

Figure 22 Effect of Length on PV_{BT} at 1,000 psi

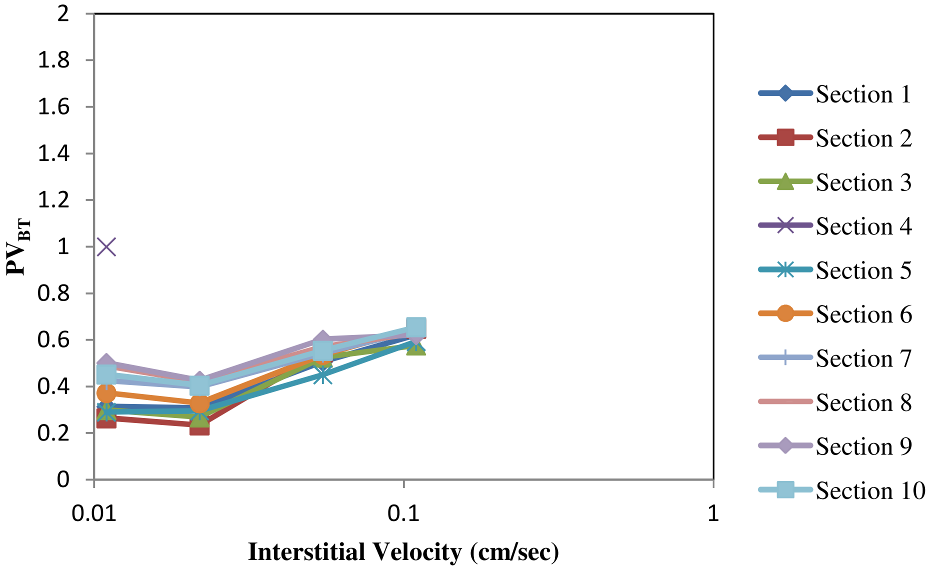

Figure 23 Effect of Length on PV_{BT} at 3,000 psi

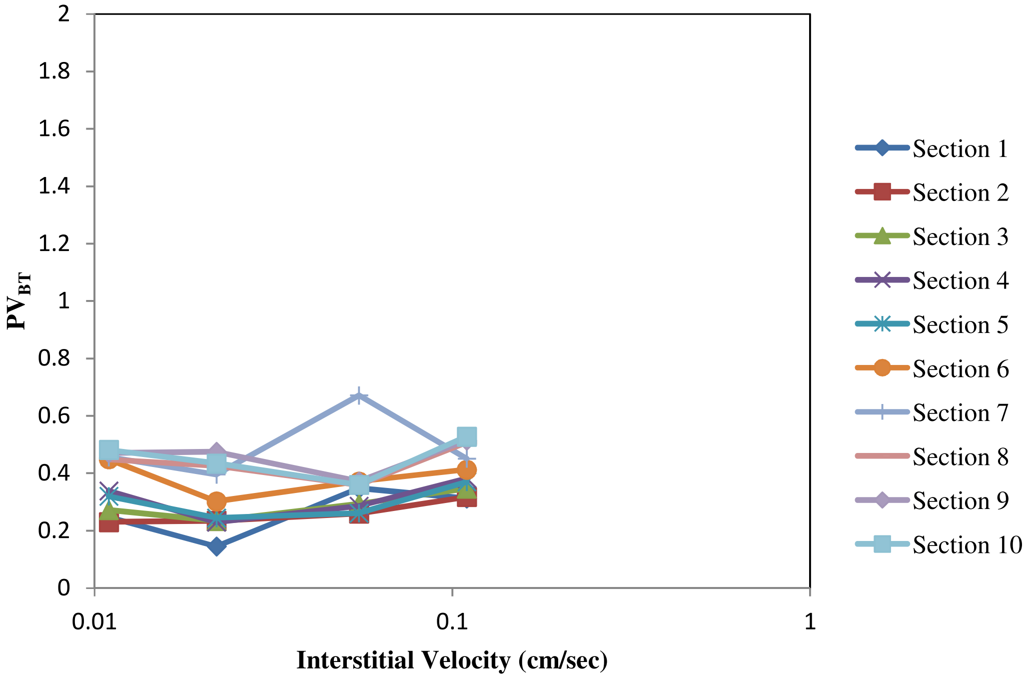

Figure 24 Effect of Length on PV_{BT} at 5,000 psi

4.1.5 Optimum Flow Rate

The optimum flow rate for acidizing is the flow rate at which the least amount of acid (calculated in terms of pore volumes) injection to achieve the breakthrough. For our study, as mentioned before, acid was injected at four different rates under pressures of 1,000, 3,000 and 5,000 psi. The pore volumes required for breakthrough were plotted against the rates of injection. This is a typical and conventional plot which gives a curvy u-shaped plot, the lowest point on which being the optimum rate of injection under a specific pressure and length of the core.

This conventional plot can be described on the basis of the nature of wormhole it creates. At extremely low rates, since the reaction rate is very fast and the mass transfer of hydrogen ions a limited phenomenon, the acid is consumed on the face of the core and instead of propagating forward. A dominant single hole is created if the injection rate is kept at it optimum. As the injection rate is further increased, though the volume required for breakthrough does not increase much but the structure of the dissolution pattern changes to unfavorable ramified structures instead of a single dominant hole.

The optimum flow rate is actually a function of a number of factors including the type of acid, its concentration, temperature, pressure, length of core, type of rock and its heterogeneities. Because most parameters are kept constant in our experiments and only flow rate and pressure are varied, the optimum flow rate can be studied as a function of the pressure and since we have pressure tappings along the length of the two cores being acidized, the optimum flow rate can also be studied as a function of core length.

Cumulative Analysis: The experiments conducted at 1,000 psi show a marked difference from the ones conducted at high pressures of 3,000 and 5,000 psi. For these experiments large volumes of acid were required to achieve the breakthrough as CO_2 in gaseous phase hindered the smooth propagation of the wormhole. It is seen that for most of the sections the optimum rate of injection comes out to be 5 cc/min which means that at rates lower than 5 cc/min, the acid is being more utilized in enhancing the wormhole size instead of propagation and at rates higher than 5 cc/min more volume is being consumed to create more or less the similar time of wormholes. Ramification is the phenomenon which is supposed to take at rates higher than optimum but it actually happens when the rates are increased to a great extent. A small increment does not make a big difference.

At high pressures, the optimum flow rate was found to be much lower (2 cc/min for most cases irrespective of length) than the ones at low pressure. It has been proposed that the major factor that governs this change is the difference of phase of CO_2 in both the cases. At lower pressure of 1,000 psi, CO_2 that is evolved from the reaction between HCl and carbonate rock is in the gaseous phase as discussed in the previous section, it actually forces the hydrogen ions to the walls of the wormhole and hinders its propagation. On the other hand, at higher pressures, more CO_2 is dissolved in the solution which helps in smooth propagation of the wormhole.

It can be seen that for the case of experiments at 5,000 psi, for wormhole of larger lengths, that is 16.8 in to 24.0 in, the optimum rate is higher and is about 5 cc/min but that is most probably due to lower permeability of the cores used as compared to the experiments at 3,000 psi at similar rates.

Below are presented all the plots (Fig. 25 to Fig. 34) for all the sections showing cumulative Breakthrough Pore Volume at different rates. The optimum values found from these plots are tabulated and follow these plots.

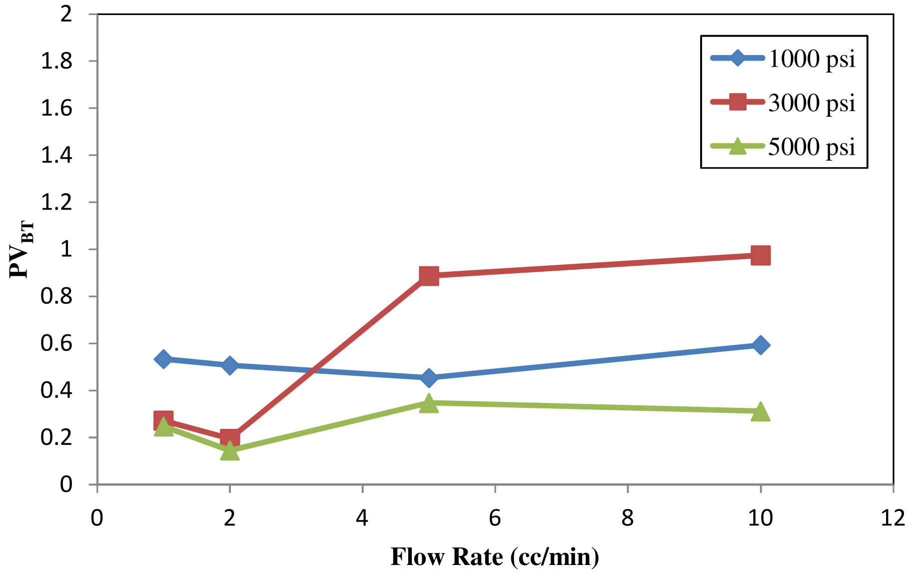

Figure 25 Selection of Optimum Flow Rate for Section 1

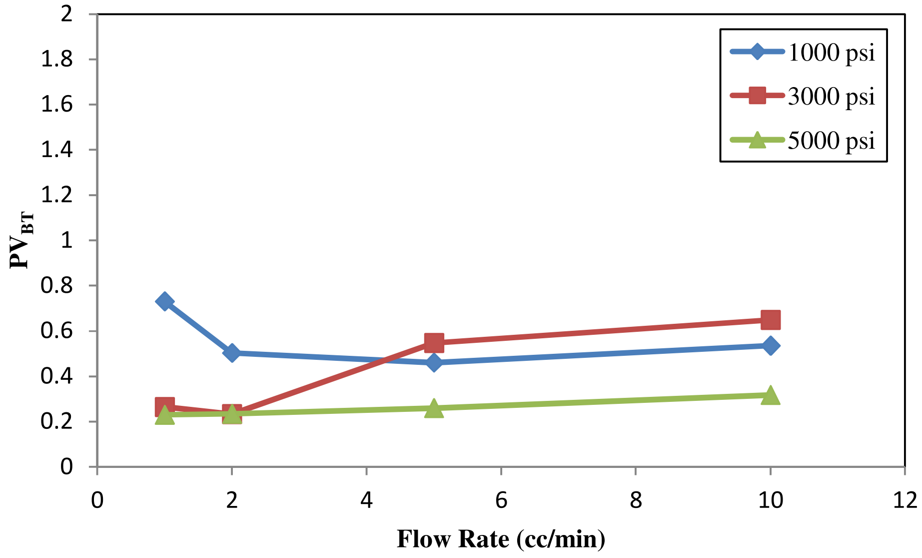

Figure 26 Selection of Optimum Flow Rate for Section 2

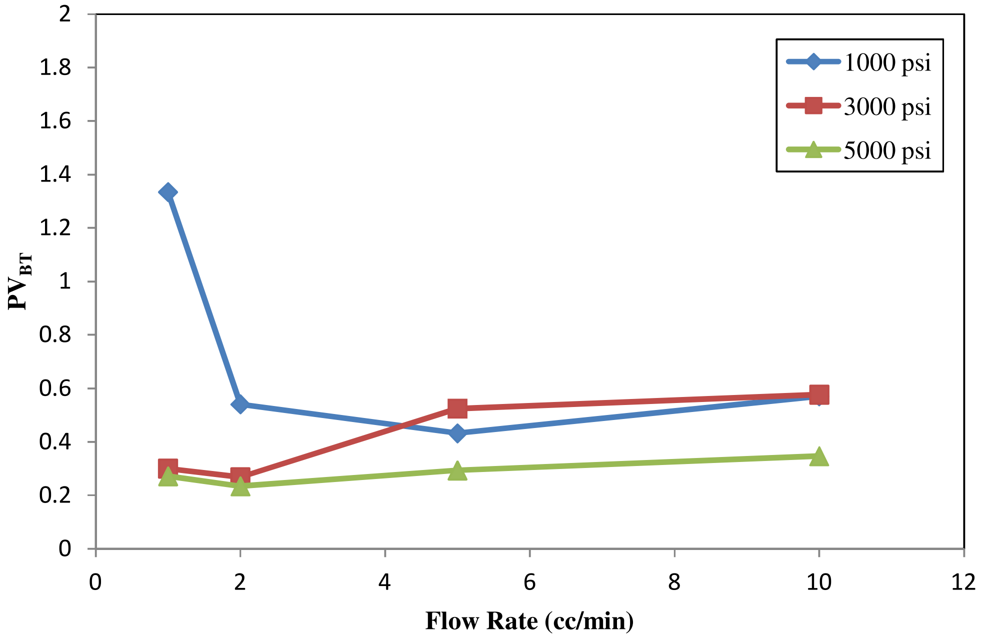

Figure 27 Selection of Optimum Flow Rate for Section 3

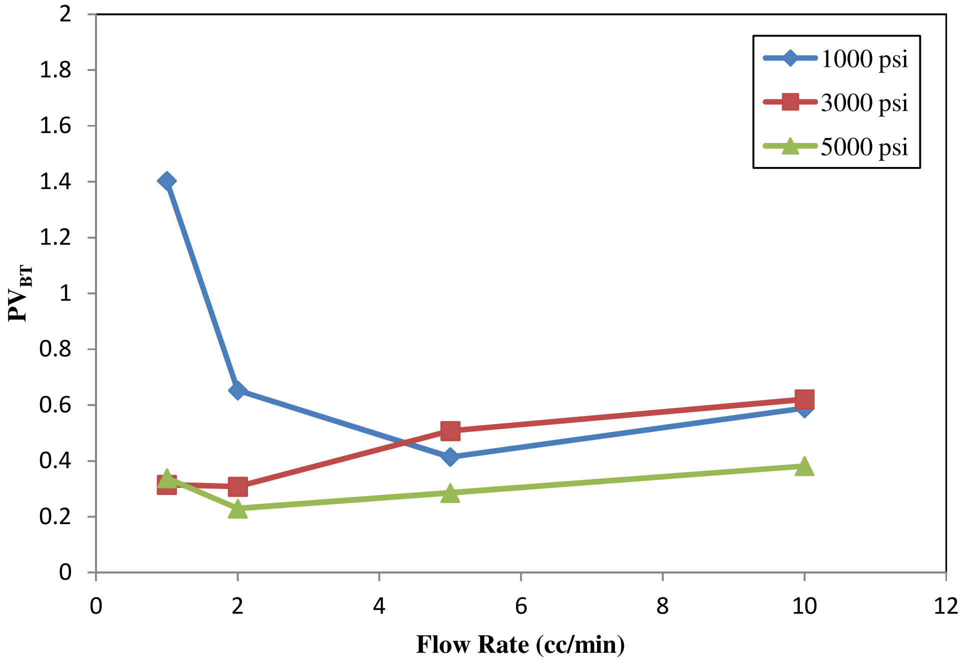

Figure 28 Selection of Optimum Flow Rate for Section 4

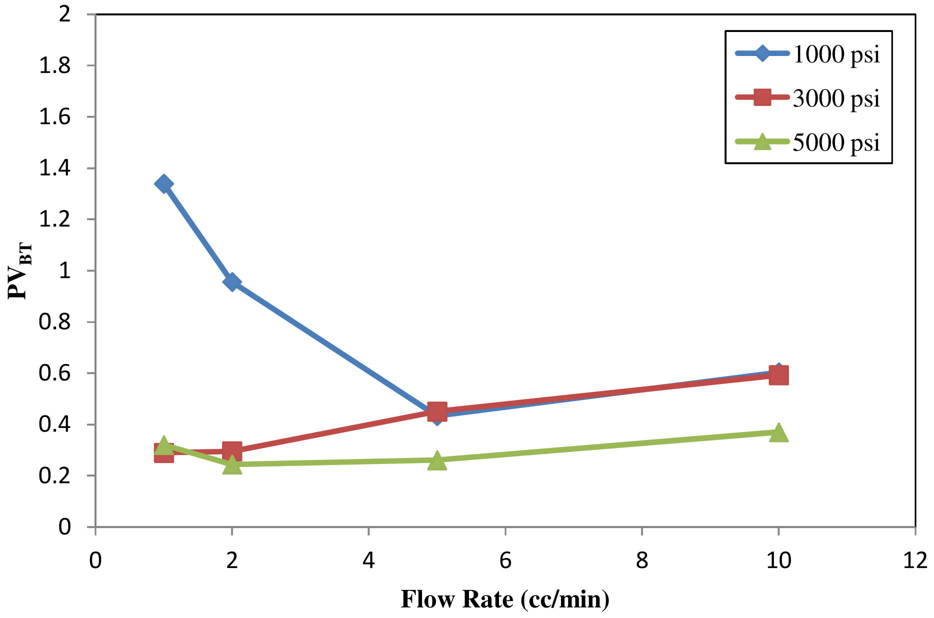

Figure 29 Selection of Optimum Flow Rate for Section 5

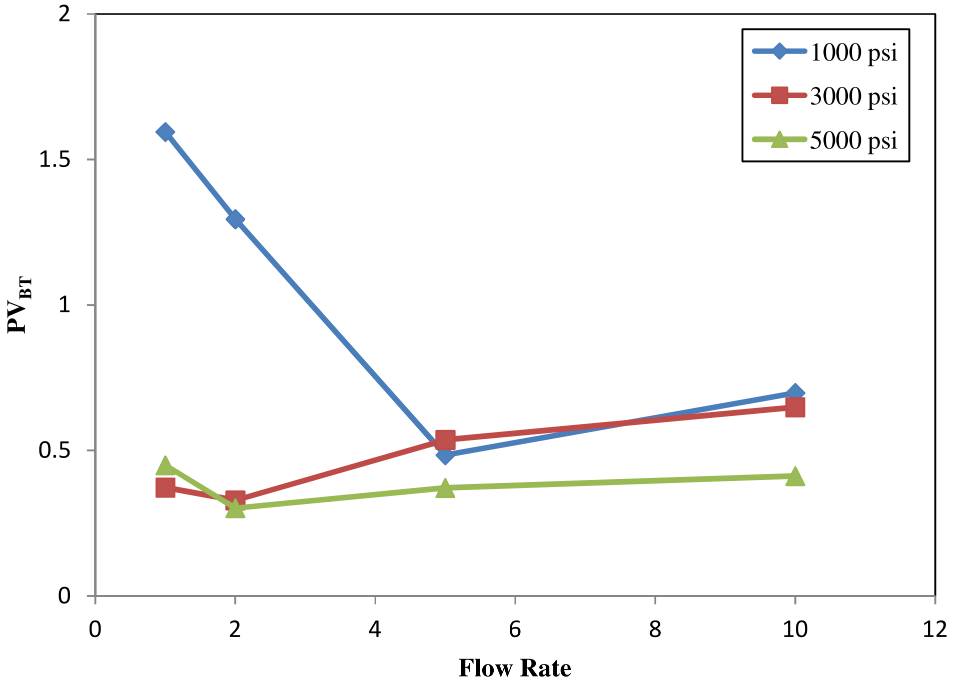

Figure 30 Selection of Optimum Flow Rate for Section 6

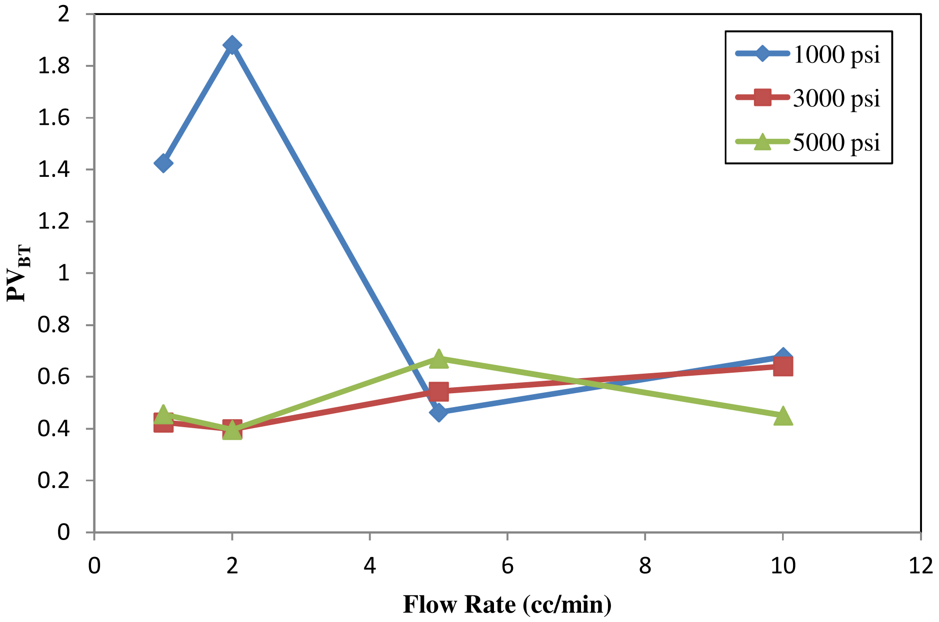

Figure 31 Selection of Optimum Flow Rate for Section 7

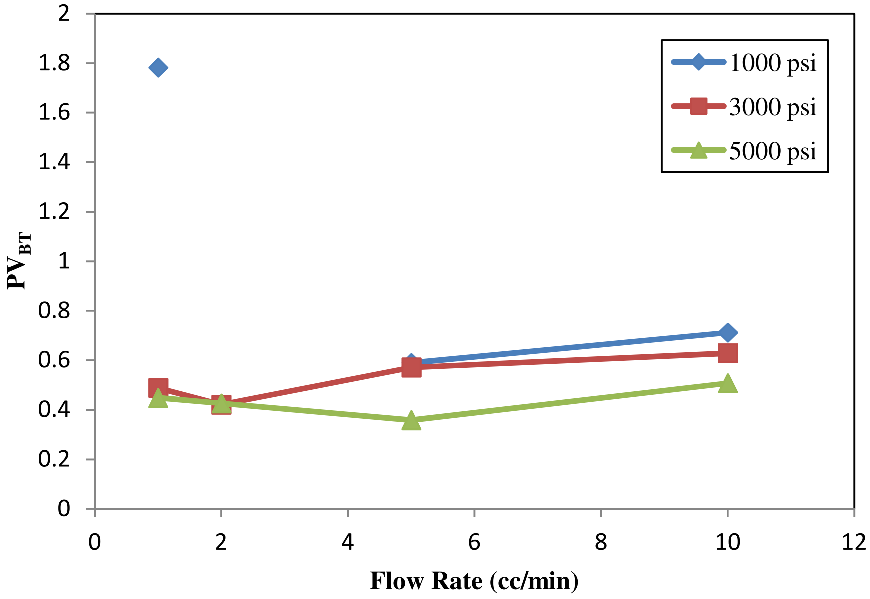

Figure 32 Selection of Optimum Flow Rate for Section 8

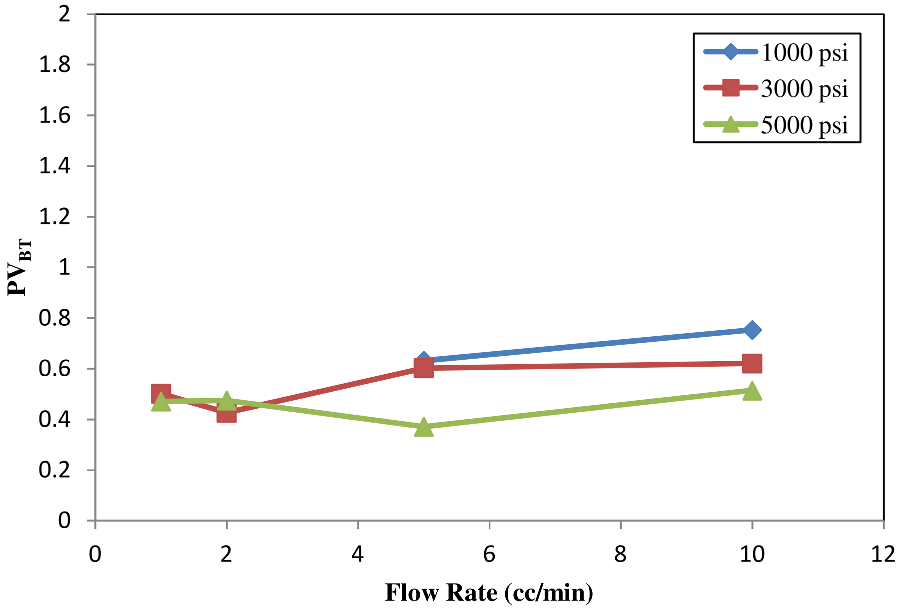

Figure 33 Selection of Optimum Flow Rate for Section 9

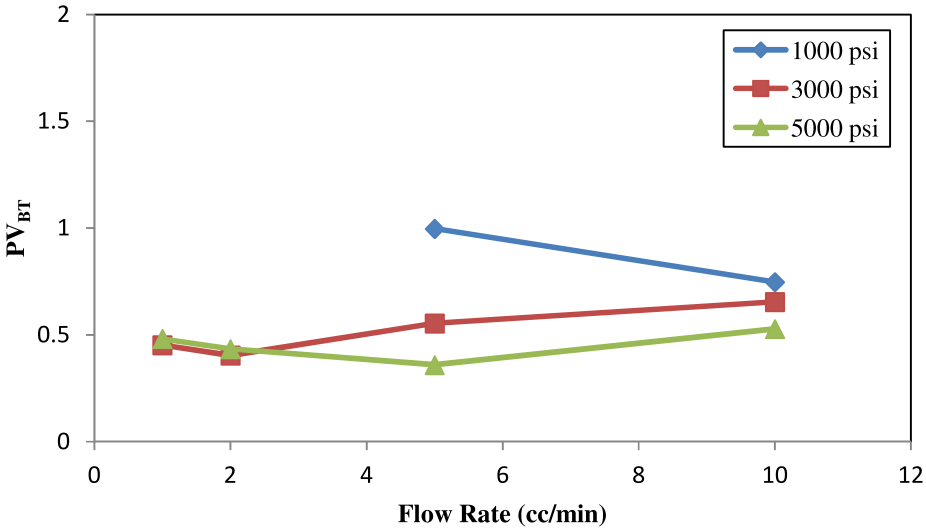

Figure 34 Selection of Optimum Flow Rate for Section 10

Table 2 Optimum Rates for Different Pressures

Optimum Flow Rate (cc/min) Observations			
Sections	**1,000 psi**	**3,000 psi**	**5,000 psi**
Section 1	5	2	2
Section 2	5	2	2
Section 3	5	2	2
Section 4	5	2	2
Section 5	5	2	2
Section 6	5	2	2
Section 7	5	2	2
Section 8	5	2	5
Section 9	5	2	5
Section 10	10	2	5

Section by section analysis roughly reflects the same characteristics as that of the cumulative analysis but it represents more scattered data because of the heterogeneities. For cumulative analysis, the effect of any abrupt data point gets suppressed whereas in the case of section by section analysis it remains as it is, causing the scatter.

The general trend is that more volume of acid is required for breakthrough of sections that fall late in the series as compared to earlier ones. The simple logic is that as the wormhole goes lengthier and fatter in size, more volume of acid is required for the next section because some of the acid is consumed on the walls of the wormholes.

It should be noted that Section No. 6 shows somewhat peculiar behavior as compared to all other sections for any specific test. The reason behind it seems like the end effect because Section 6 is the first section that comes after the tubing connecting the two cores so it seems as if the acid takes more time than it should to pass through the dead volume space and thus the volume required to breakthrough section 6 apparently goes higher especially in the case of experiments conducted at low flow rates.

The same aspect of CO_2 effect is obviously noticeable in the case of section by section analysis as the experiments conducted at 1,000 psi show greater volumes being required for acid penetration as compared to the ones at 3,000 psi and 5,000 psi, reason again being the fact that it dissolves more rock at 1,000 psi due to CO_2 being in gaseous phase.

The table representing the volume of acid required for a specific section is presented in the following.

Table 3 Section by Section Analysis for Volume to Breakthrough

Pressure (psi)	Flow Rate (cc/min)	Section 1	Section 2	Section 3	Section 4	Section 5	Section 6	Section 7	Section 8	Section 9	Section 10
1,000	1	4.8960	8.5146	23.3257	14.7772	9.9308	26.3557	3.7317	39.2313	NR	NR
1,000	2	4.8996	4.8294	5.9486	9.5672	20.9882	28.8840	52.1723	NR	NR	NR
1,000	5	4.6710	4.8126	3.8799	3.7152	5.2284	7.6103	3.4530	15.2001	9.9498	44.1603
1,000	10	5.4456	4.3794	5.8914	5.9022	6.0750	10.7408	5.0778	8.7552	9.9540	6.3960
3,000	1	2.4921	2.3589	3.4035	3.2824	1.7577	7.2187	6.7379	8.5444	5.6076	0.0335
3,000	2	2.0178	2.8192	3.4987	4.4088	2.5562	5.1095	8.4494	5.9521	4.9226	2.1198
3,000	5	4.1799	2.1984	5.0622	4.8057	2.3607	6.1004	6.1605	8.0988	9.0267	1.2723
3,000	10	5.0700	3.4164	4.542	7.9368	5.0634	5.6594	6.2370	5.7294	5.9038	10.1216
5,000	1	2.3870	2.0606	3.4256	5.2001	2.3805	10.5663	4.8299	3.7652	6.2978	5.5958
5,000	2	1.4899	3.3089	2.3809	2.2250	3.1016	6.0350	9.8205	6.4628	8.8810	0.7051
5,000	5	3.5751	1.7697	3.7146	2.6916	1.6851	9.4751	3.5421	3.0324	4.8828	2.6244
5,000	10	3.2520	3.3630	4.2204	5.0748	3.3630	6.5108	7.0998	9.4362	5.9130	6.7536

NR: Data was not reported because breakthrough did not reach these sections

4.1.6 Wormhole Speed

For all the experiments, wormhole speed is the average pace of propagation of wormhole and was calculated by dividing the length of the core (from inlet face of core 1 to the end of a specific section) by the time taken to breakthrough till the end of this section.

Obviously wormhole speed is directly proportional to the flow rate with which the acid is injected into the core. We see that at low injection rates the wormhole speed is not influenced by the pressure and remains constant at low values. However, with the increase in flow rate, as the wormhole speed increases, pressure also begins to play role and we see that at higher pressure hole propagation is faster, especially in the beginning. But the average speed for 3,000 and 5,000 psi experiments drops down to almost same values when the complete breakthrough is achieved at 24 in length. Following figures explain the wormhole propagation pace along the length.

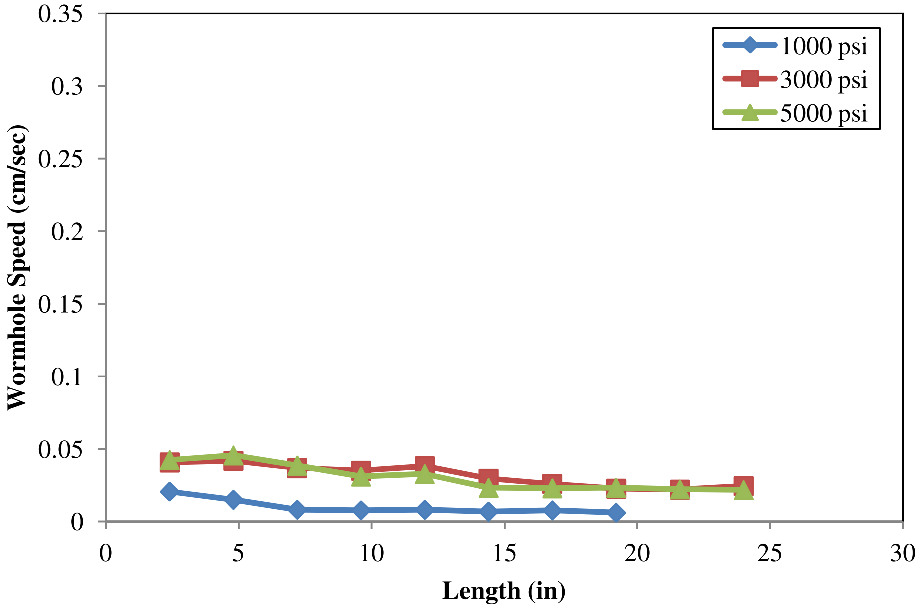

Figure 35 Wormhole Speed at Injection Rate of 1 cc/min

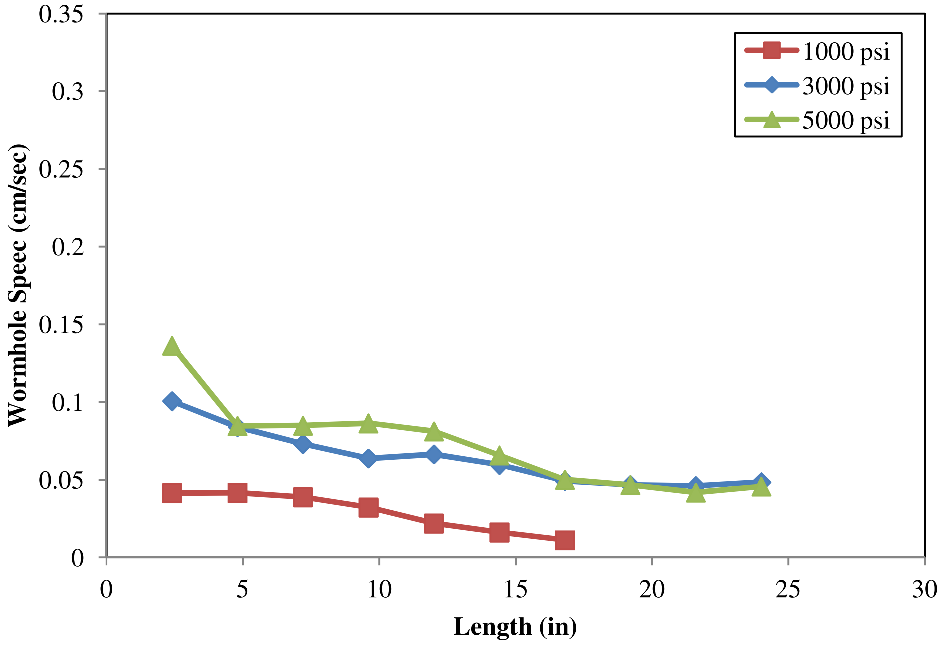

Figure 36 Wormhole Speed at Injection Rate of 2 cc/min

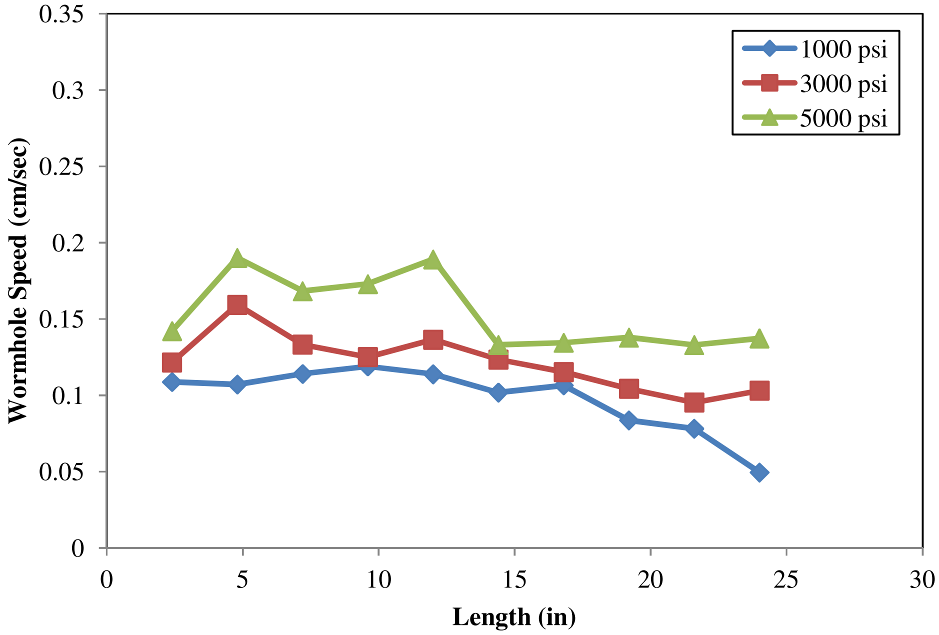

Figure 37 Wormhole Speed at Injection Rate of 5 cc/min

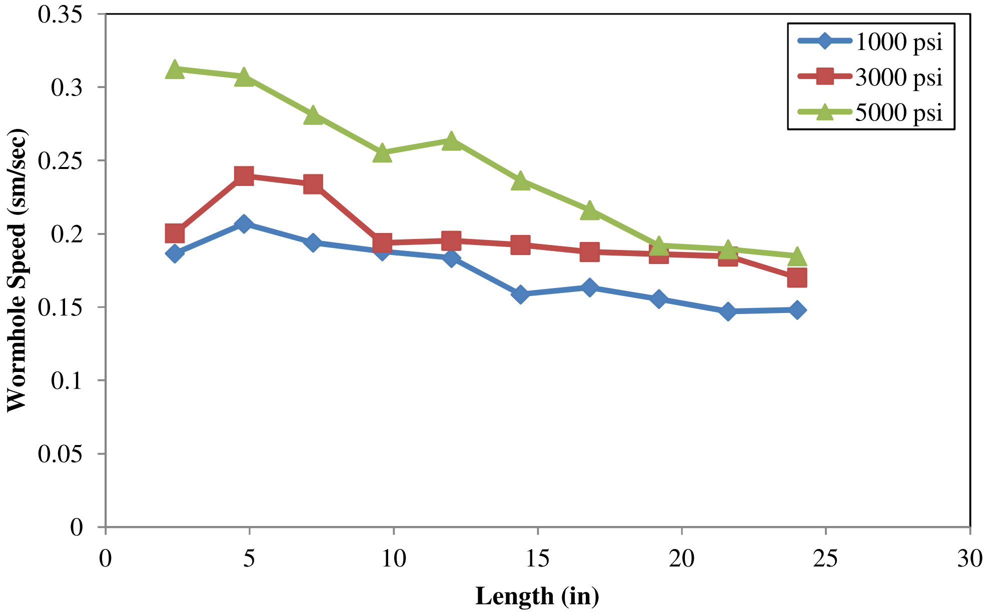

Figure 38 Wormhole Speed at Injection Rate of 10 cc/min

4.2 CT Scan Analysis and Images of Cores

As mentioned in the methodology of the project, after the coreflooding experiments were completed, the cores were dried at a temperature of 65°C in an oven for about 24 hours. The cores were then taken to the Research Institute, KFUPM for X-Ray CT Analysis.

4.2.1 CT Scan Parameters

All the cores were scanned under same room conditions and using same exam plan. The scan plan adopted applied 130 kV of voltage, 150 mA of current, 3.0 sec of scanning time, 12 sec of scan time interval and 1 mm slice thickness. In this way about 300 images were created for every single core, providing enormous CT data. The way the wormhole propagates with its tortuous path can be easily monitored from these CT data. The thickness of the wormhole is also observed and discussed in the following sub-section. Fig. 39 to Fig. 44 shows six processed CT images from Experiment No. 3 are being presented. The first three are from IL-15 and the other three from IL-14, showing how the wormhole propagated from face of one core to the end of the other. Hole-size towards the end of the first core and the beginning of core 2 comfortably match each other, showing smooth propagation of wormholes from the end of one core to the other.

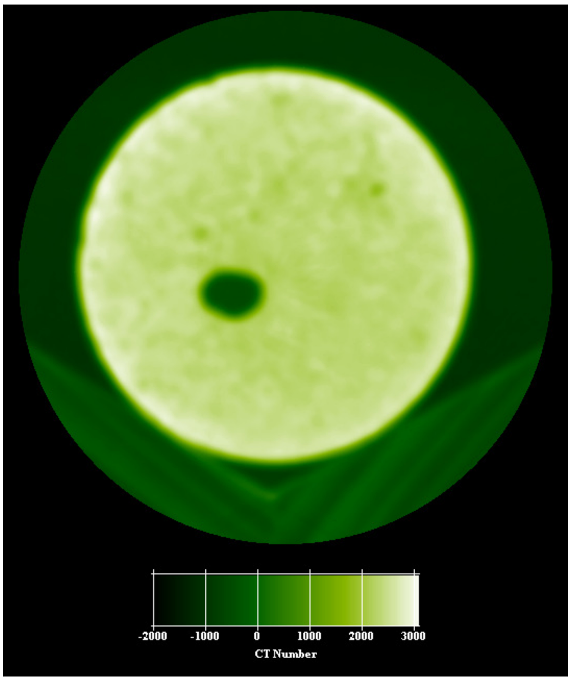

Figure 39 CT Image of IL-15 at the beginning (IL-15002)

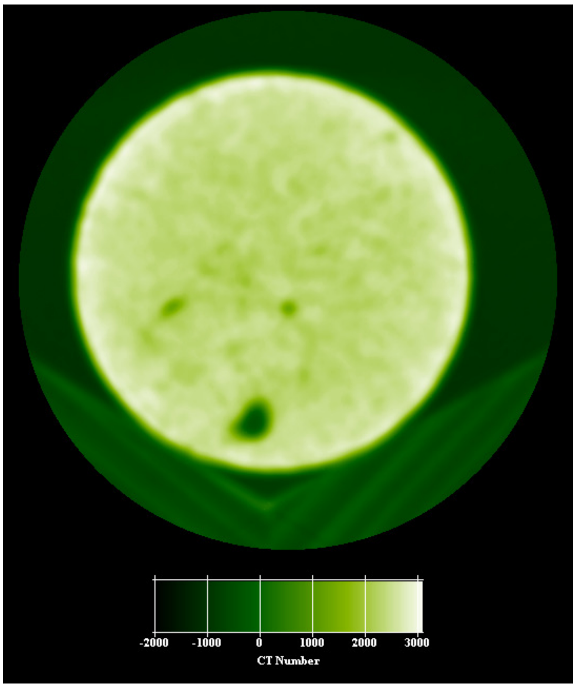

Figure 40 CT Image of IL-15 at the middle (IL-15150)

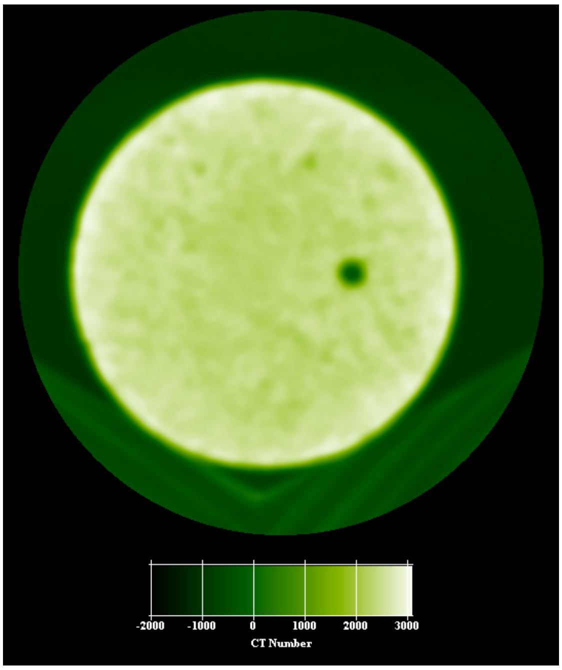

Figure 41 CT Image of IL-15 at the end (IL-15298)

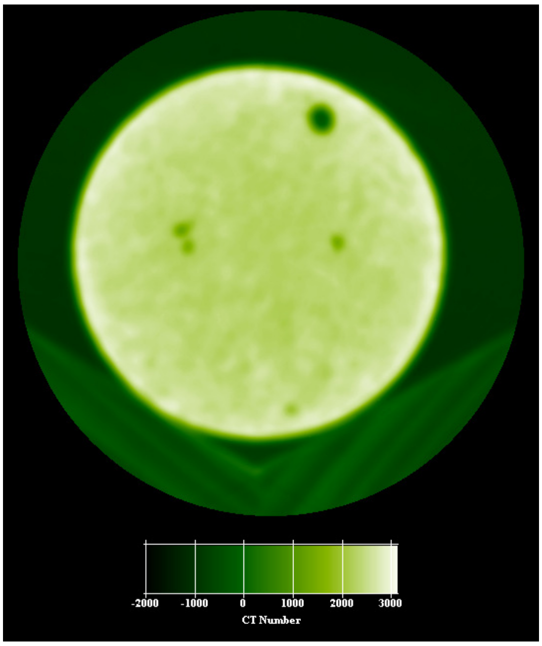

Figure 42 CT Image of IL-14 at the beginning (IL-14003)

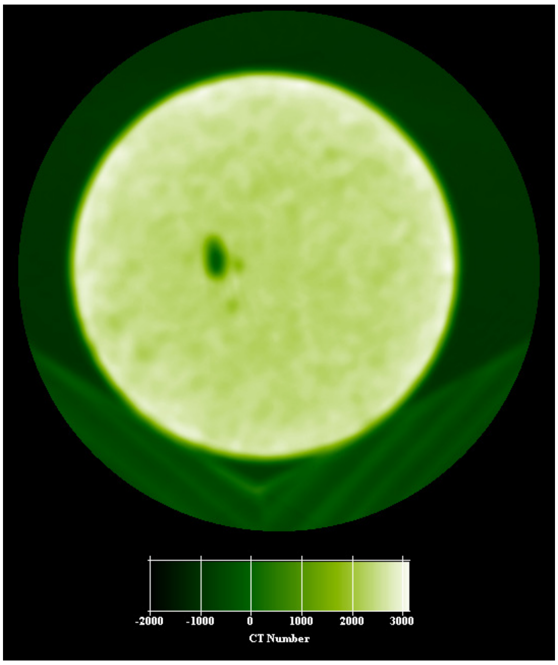

Figure 43 CT Image of IL-14 in the middle (IL-14149)

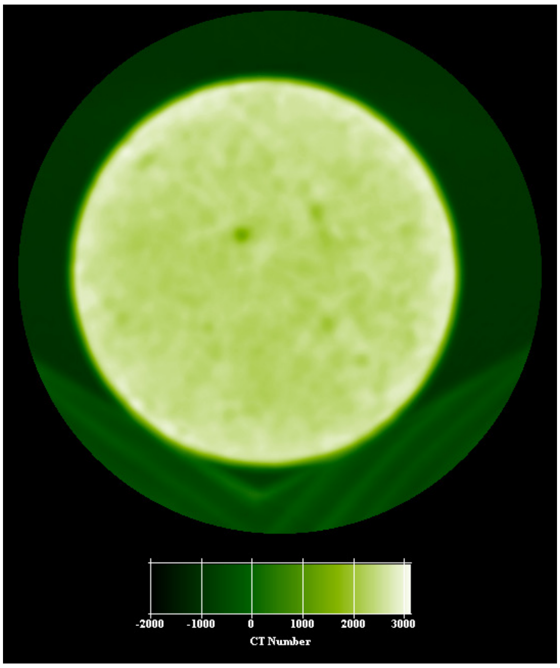

Figure 44 CT Image of IL-14 at the end (IL-14293)

In the following, Fig. 45 to Fig. 48, all slices for Experiment No. 3 after acidizing are being shown. As compared to previous images where we looked at one single image, these figures summarize one complete experiment. This experiment was conducted with a back pressure of 5,000 psi and a flow rate of 1 cc/min. In these slices the propagation can be very clearly tracked. The tortuosity of the wormhole and varying diameter can also be very closely seen. Here it can be seen that the wormhole in this case is pretty much a single dominant hole. At some points it can be seen that there are small branches coming out but they do not prolong. The points where an oval shaped hole is seen, the hole is changing its path there. Towards the end of the experiment, in Core IL-14 (Fig. 48), it can be seen that the wormhole almost disappears. This is because it is so slim there that it cannot be clearly identified from the CT images. However, almost same wormhole diameters at the end of Core IL-15 and the beginning of Core IL-14 can be seen in Fig. 45 and Fig. 46, respectively. All the CT data generated was used to prepare such images but only one case has been presented.

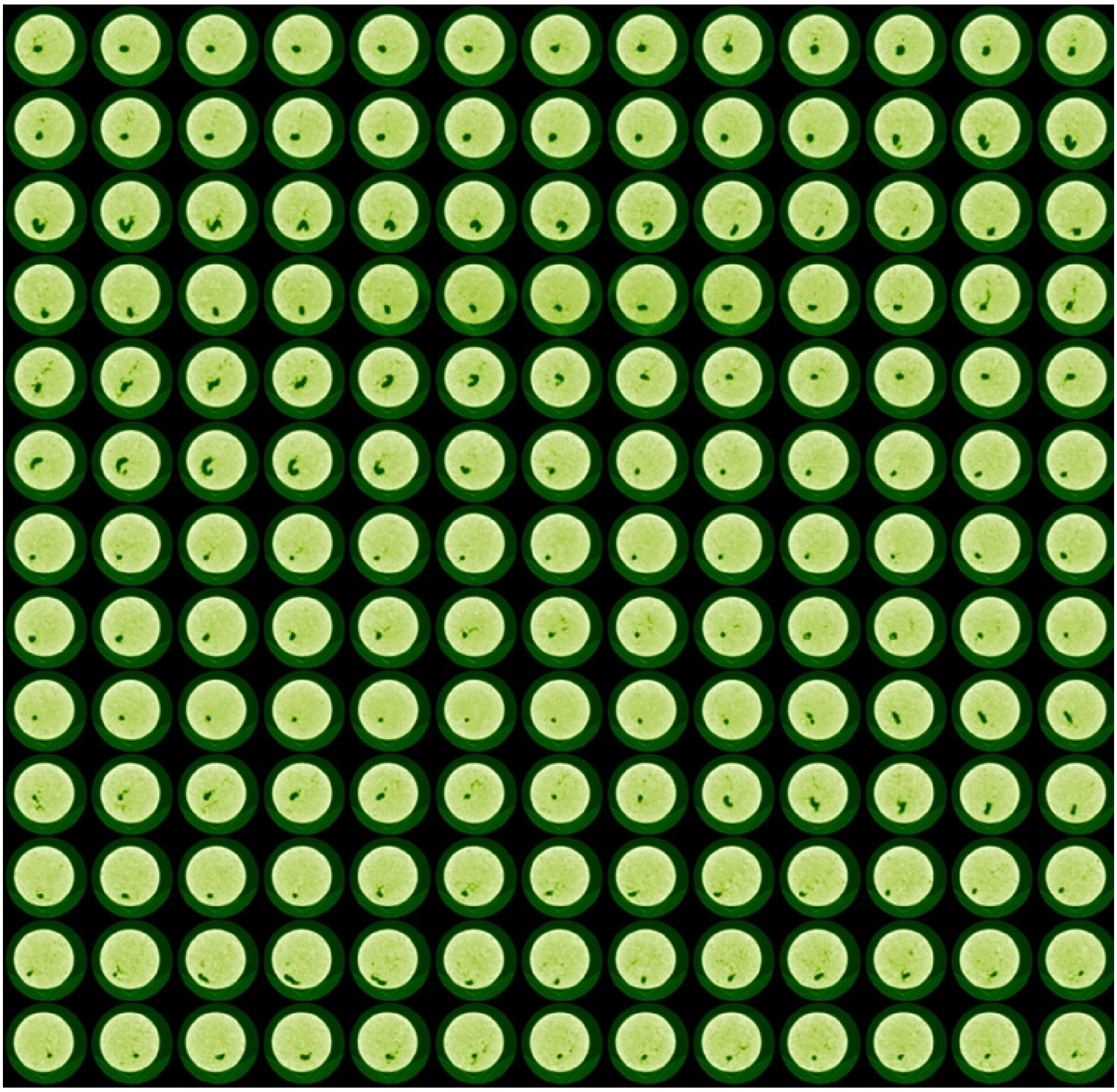

Figure 45 Images of acidized IL-15 - I

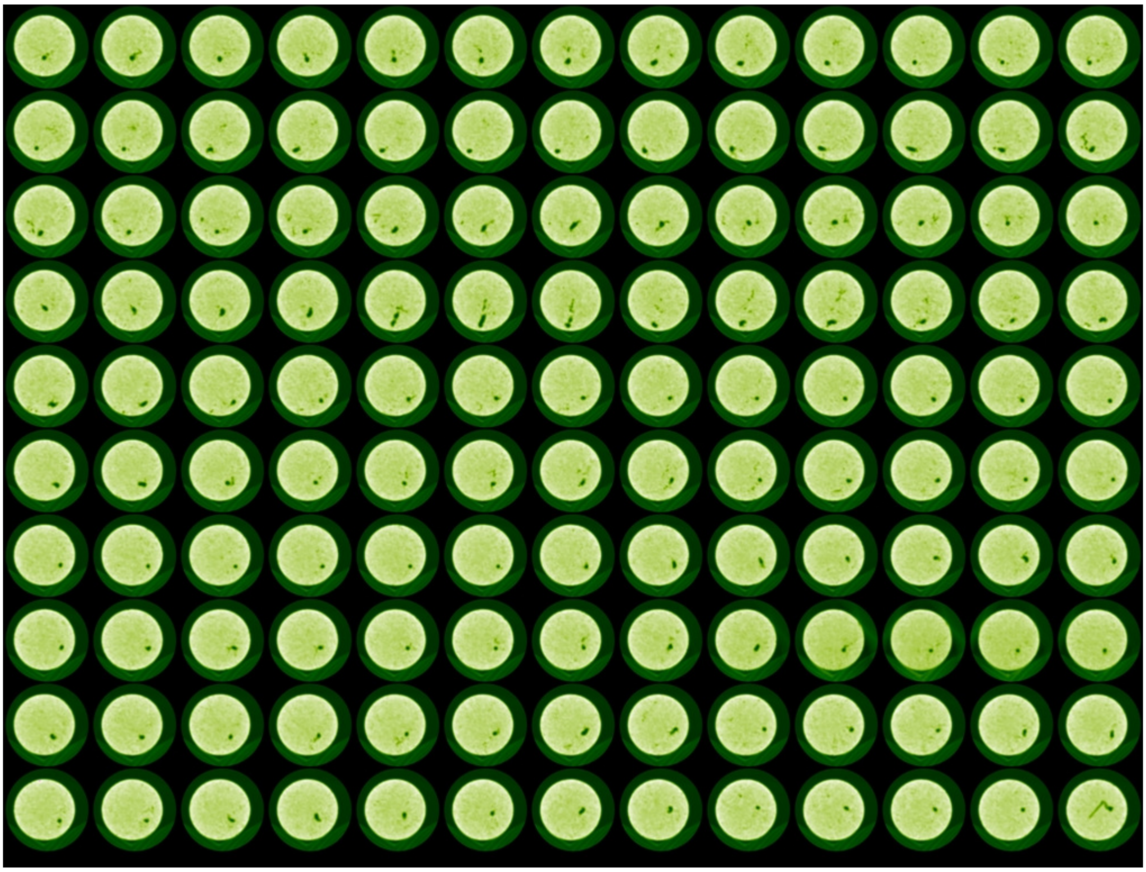

Figure 46 Images of acidized IL-15 - II

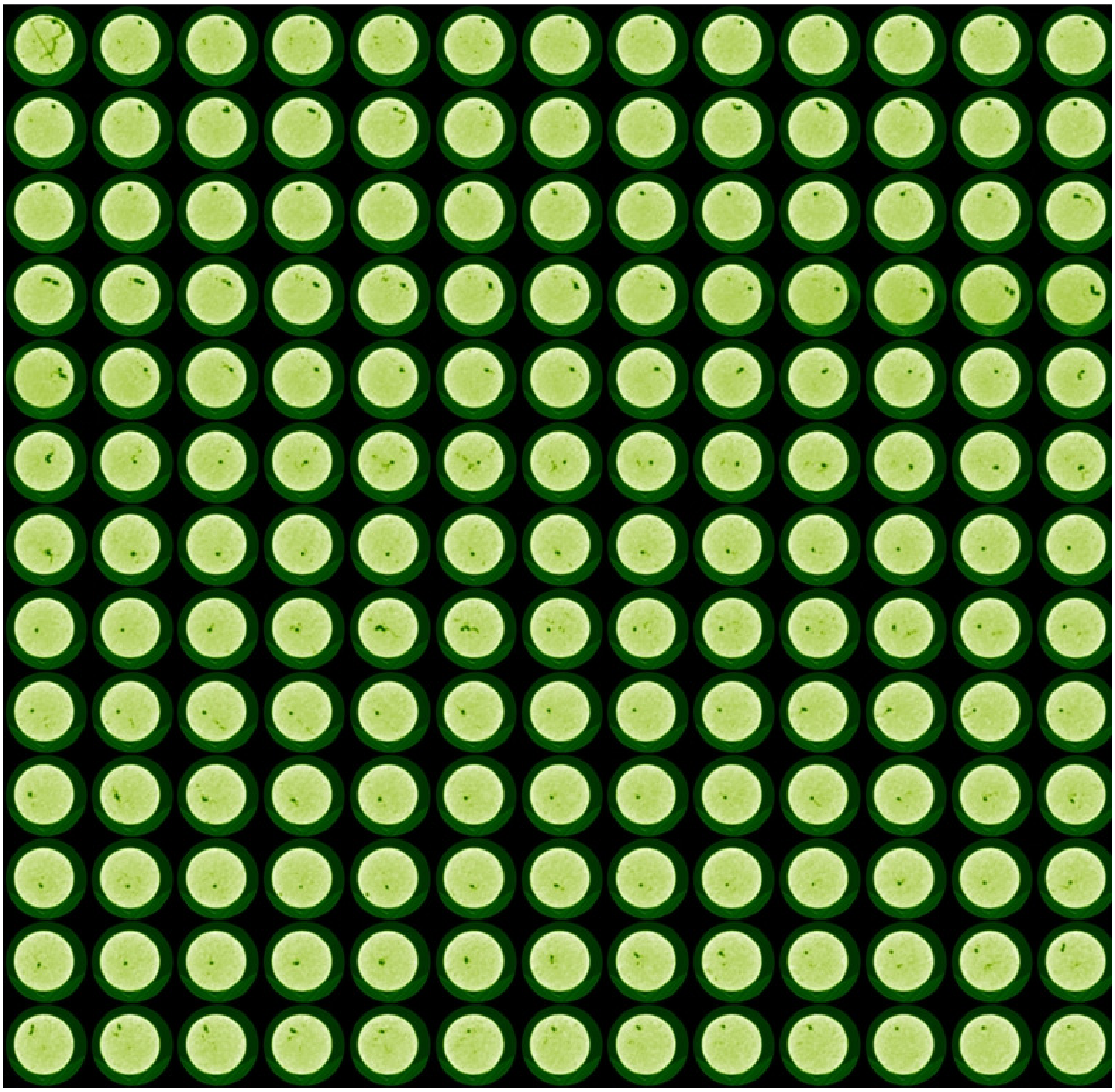

Figure 47 Images of acidized IL-14 - I

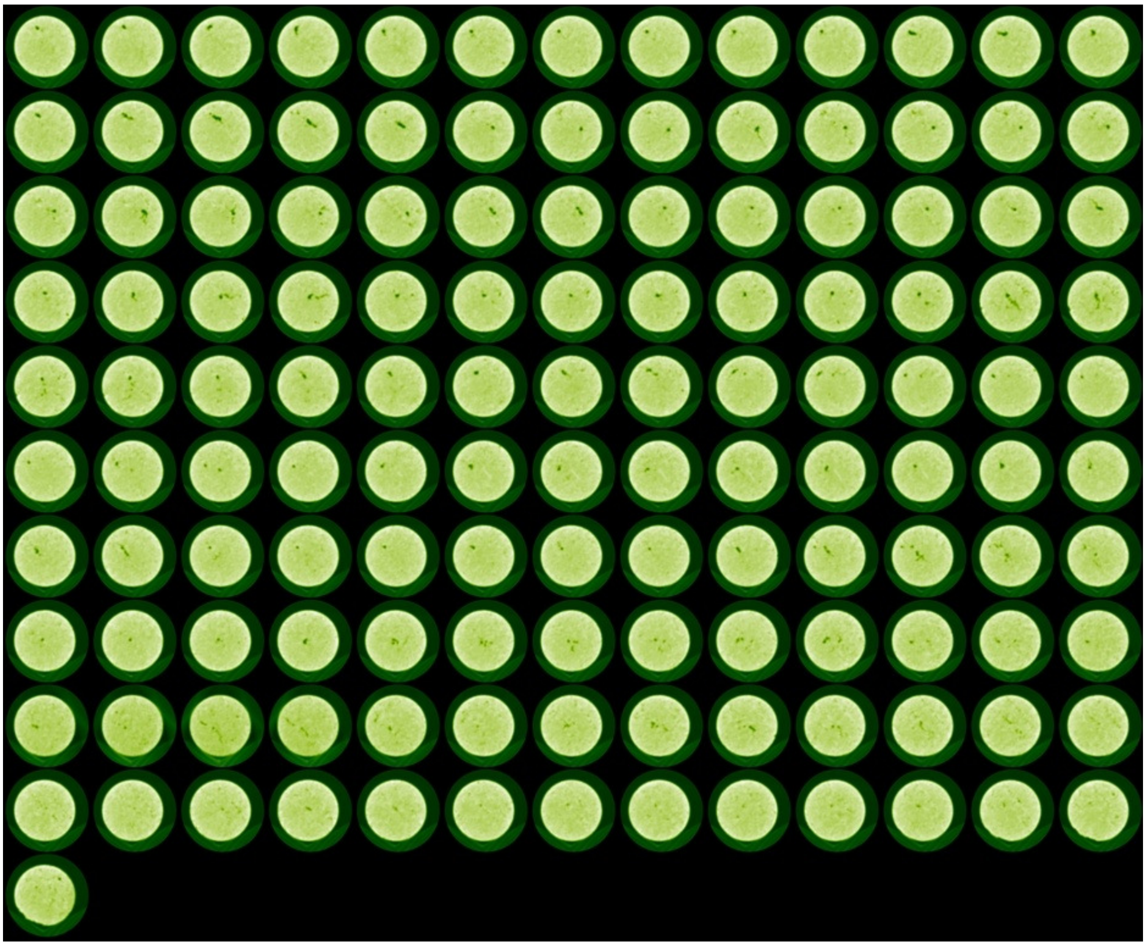

Figure 48 Images of acidized IL-14 - II

4.2.2 Wormhole Diameter Profile

The wormhole diameter profile was generated by using the Voxel Calc software which has the ability to process the CT data and produce its images. The distance between any two marked points can be read by the software. This feature was used to measure the wormhole at six points; two faces and four pressure tappings.

It was found out that in general the diameter of the whole obviously reduced as the wormhole propagated but the diameter of the wormhole was largely consistent in the cases of 3,000 and 5,000 psi whereas it was more of a cone shaped structure in the case of experiments conducted at 1,000 psi.

The wormhole diameter seems to be oppositely affected by the flow rate of the acid in the case of high and low pressure experiments. At low pressure (Fig. 49), low rate produces larger holes in the beginning and the high rate produces relatively smaller holes. On the other hand, high rates produced marginally bigger holes than low rates when the experiments were conducted at high pressure of 3,000 and 5,000 psi (Fig. 50 and Fig. 51).

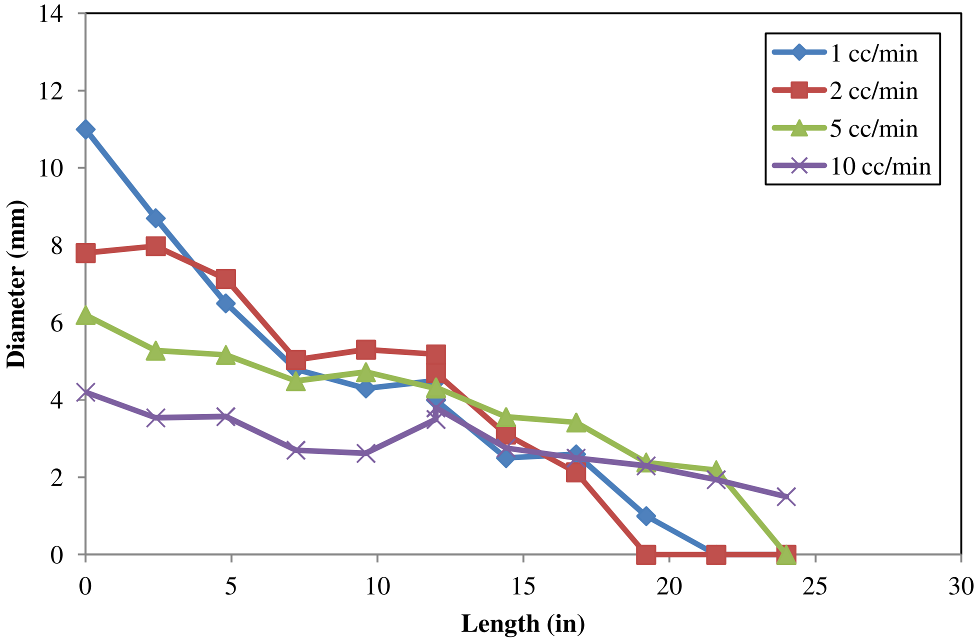

Figure 49 Wormhole Diameter Profile at 1,000 psi

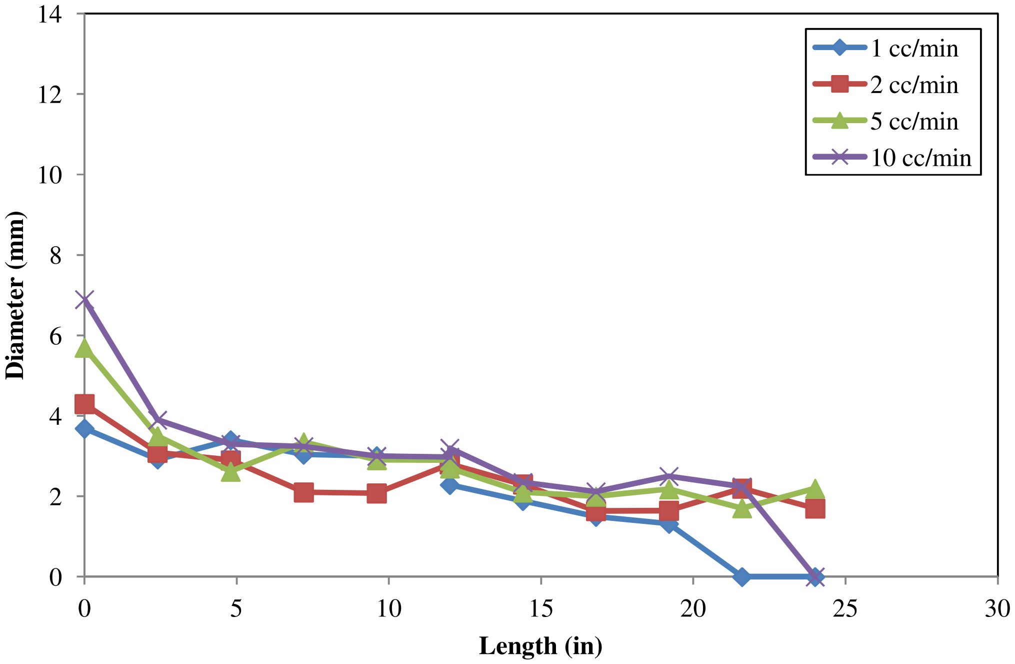

Figure 50 Wormhole Diameter Profile at 3,000 psi

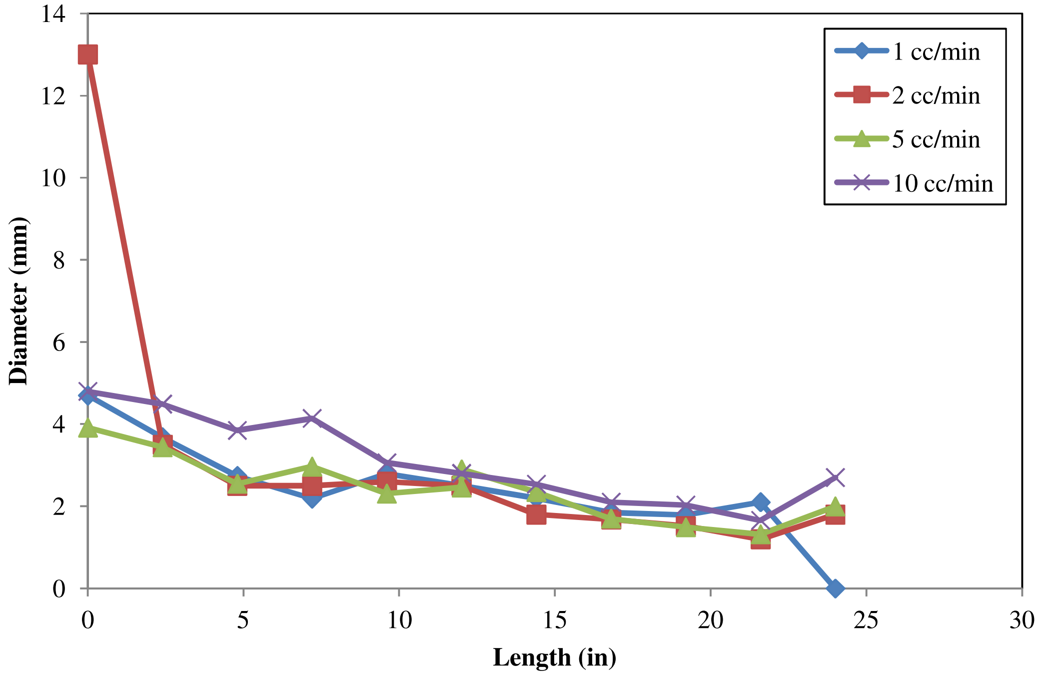

Figure 51 Wormhole Diameter Profile at 5,000 psi

4.3 Comparison with previous coreflood studies

The coreflood data from the experiments conducted in this work is compared with previous coreflood studies in literature in this section. The purpose of the comparison is to see how the new experimental conditions influence the value of PV_{BT}.

The first comparison is with Fredd's [7] work where he conducted acidizing experiments on 4 in cores with a back pressure of 2,200 psi at different temperatures. The acid used was 0.5 M HCl. In Fig. 52, the data of PV_{BT} and flow rate from three of his experiments conducted at 80°C, 50°C and 22°C was plotted along with the experiments of this project conducted at 65°C with back pressures of 1,000 and 3,000 psi. To have comparable core lengths, the data for 2 sections which correspond to 4.8 in of length was used. It can be clearly seen that the required volume for breakthrough in our experiments is much lower than Fredd's work. The primary reason is the difference in the acid concentration because the acid used in our experiments is 15% HCl which corresponds to about 4.33 M HCl so the acid reaction is much faster and hence lesser amount of acid was required.

In Fig. 53, a comparison is made between data published in the work of Buijse, Fredd [17] and this project. Fredd had used 4 in cores for acidizing cores by acetic acid at 20 °C with a back pressure of 2,200 psig. Buijse used 1.5 M HCl to acidize his 2 in cores at 25 °C and 60 °C. The data from our study for this comparison has been that of section 1 which corresponds to 2.4 in. The acid as mentioned earlier is 4.33 M HCl at 65 °C with back pressures of 1,000 psi and 3,000 psi

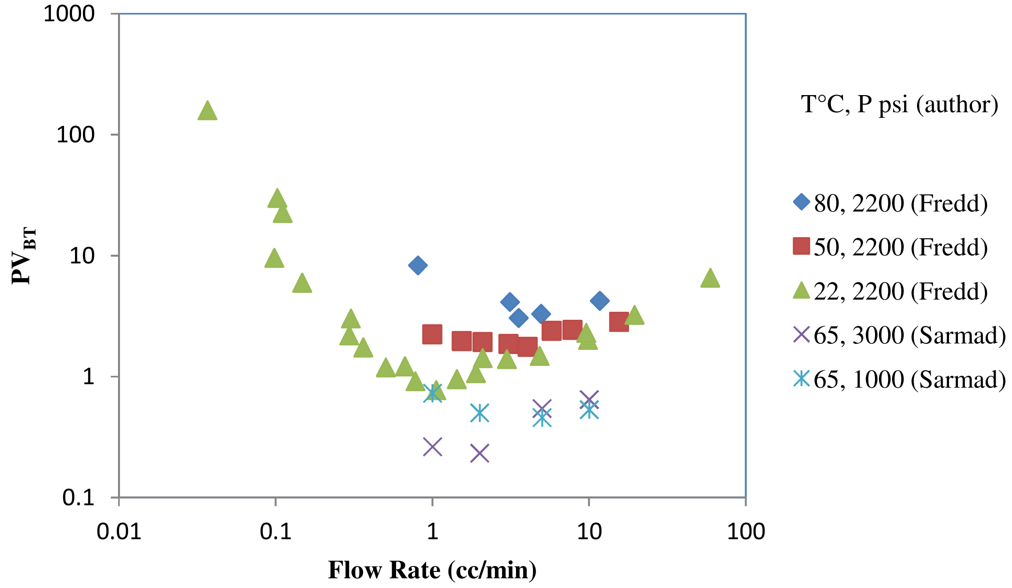

Figure 52 Comparison of PV_{BT} with Fredd's work

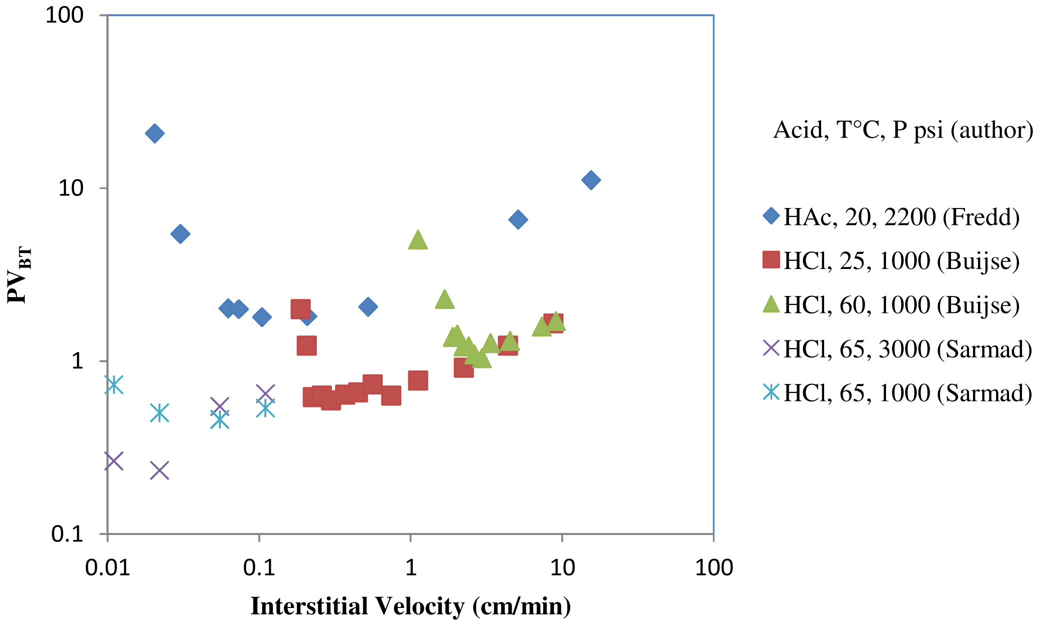

Figure 53 Effect of interstitial velocity on PV_{BT}

The optimum flow rate is a function of many parameters and this fact can be prominently observed in Fig. 53. The weak acetic acid is very slow to react and causes face dissolution that is why it requires high volumes to be injected before the breakthrough is achieved. The acid used by Buijse is weaker in concentration as compared to this study so it also needs higher amounts than our experiment. He used 1.5 M HCl solution whereas in this project the acid strength was 15% HCl by volume which corresponds to 4.33 M HCl. It can also be noticed that all experiments conducted with HCl appear to be converging on the same straight line at higher flow rates than the optimum.

There are very few articles in literature that describe the effect of core length on wormholing phenomenon. Mahmoud [18] conducted experiments with cores of varying length and studied the length effect at 1,000 psi. The value of flow rates for his experiments ranged from 0.1 cc/min to 1.0 cc/min and four different core sizes were used (3 in, 6 in, 10 in, 20 in). This data is compared in Fig. 54 with our experiments conducted at 1,000 psi. The flow rate for our experiments ranged from 1 cc/min to 10 cc/min. The pressure transducers on the coreflood system allowed us extract data for breakthrough at different lengths and four different lengths, comparable to the lengths used by Mahmoud were selected for this comparison (2.4 in, 7.2 in, 9.6 in and 19.2 in). But it must be noted that the two studies have been done at different temperatures; Mahmoud at room temperature and Sarnad at 65°C.

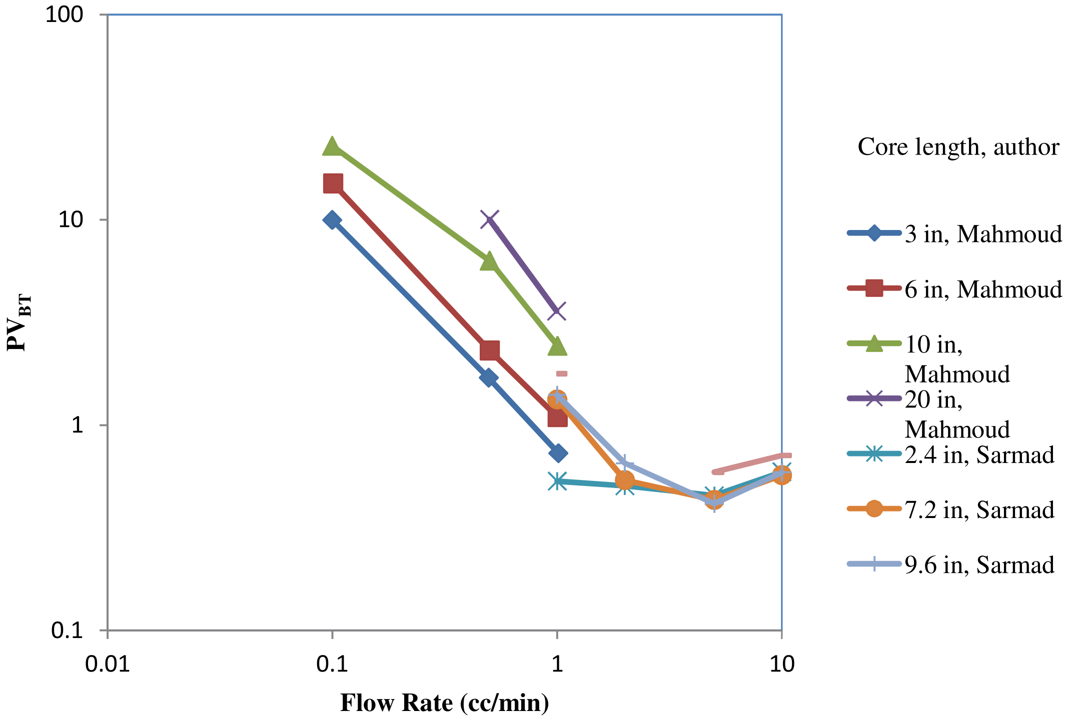

Figure 54 Effect of flow rate on PV$_{BT}$

It can be seen that at 1 cc/min both the studies fall acceptably close to each other. This work can be considered as the extension of the optimum flow rate curve produced by Mahmoud. The optimum rate does not seem to have been achieved in Mahmoud's experiments whereas it is achieved at the values of 5 cc/min in most cases (of different lengths) in our study. As discussed in a previous section, the effect of length is prominent before the optimum is reached but diminishes at higher values of flow rate.

4.4 Think Section Analysis

Five thin sections were prepared from the acidized cores of different experiments. In the following, the detailed petrographic studies of these samples are presented which consist of primary carbonate particles, the depositional and digenetic fabrics, and porosity types. It can be noted in that brownish color represents the grain particles whereas the bluish green color represents the porous region and the wormholes (channel produced by acidizing)

Sample from Core 1 (Section 2) of Experiment conducted at 1,000 psi with 2 cc/min

Fig. 55 shows the image of the thin section prepared from Core IL-16 and can be described as fine-to medium-grained, well sorted, rounded, compressed grains, micritized peloids, echinoderms, crinoids, forams, brachiopods, bryozoans, mainly reduced interparticle porosities, minor amounts of moldic and intraparticle porosities, pores reduced by syntaxial calcite overgrowths and blocky calcite cement, 20% porosity, pore size 50-1,300 micron.

Sample from Core 1 (Section 2) of Experiment conducted at 5,000 psi with 2 cc/min

Fig. 56 shows the image of the thin section prepared from Core IL-20 and can be described as fine-to medium-grained, well sorted, rounded, borings, compressed grains, micritized peloids, echinoderms, crinoids, forams, brachiopods, bryozoans, mainly reduced interparticle porosities, minor amounts of moldic and intraparticle porosities, pores reduced by syntaxial calcite overgrowths and blocky calcite cement, 25% porosity, pore size 50-3,500 micron.

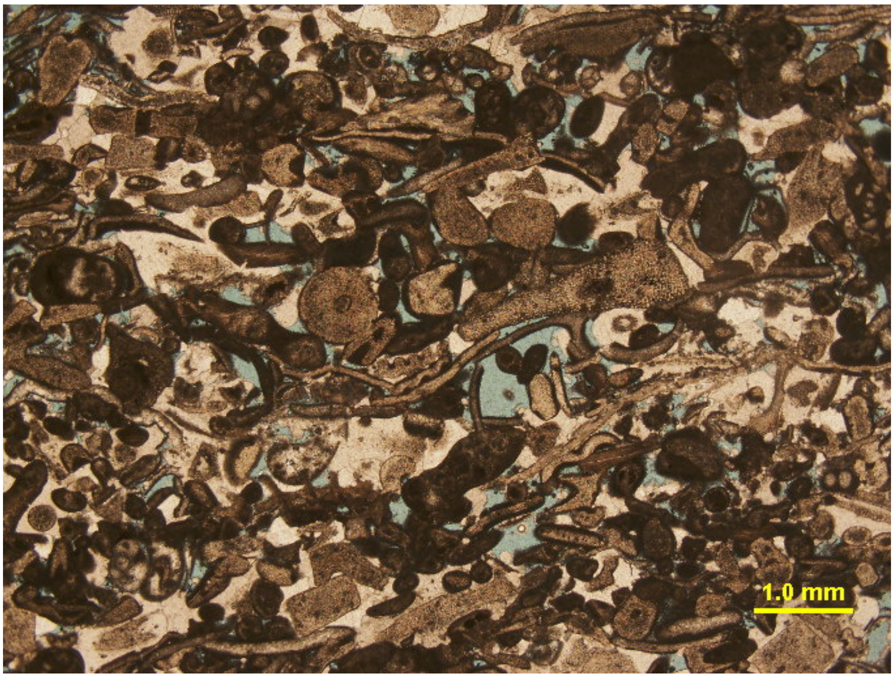

Figure 55 Thin Section Image of Core IL-16 at Section 2

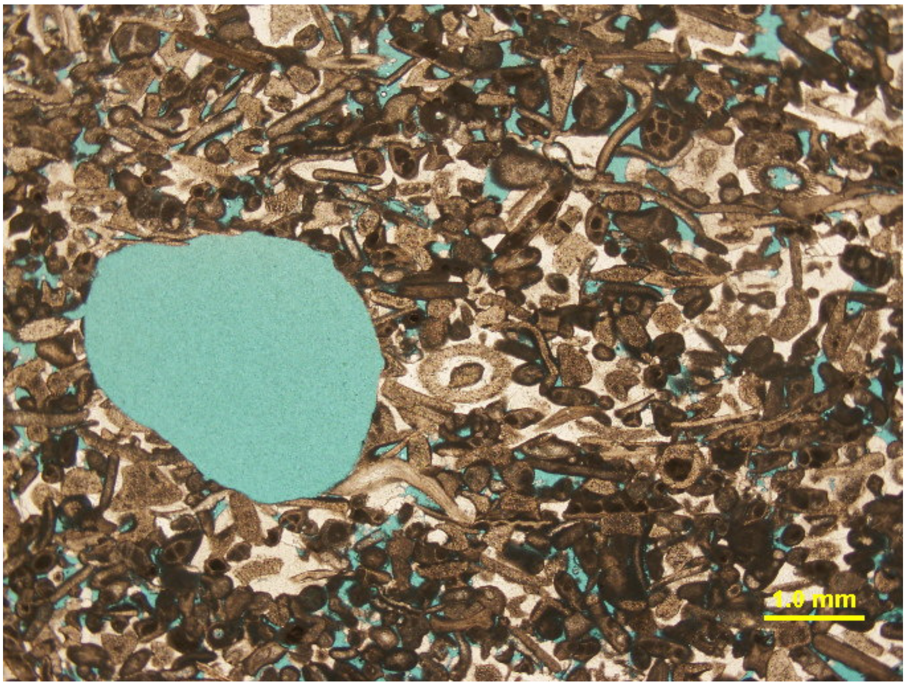

Figure 56 Thin Section Image of Core IL-20 at Section 2

Sample from Core 2 (Section 7) of Experiment conducted at 5,000 psi with 2 cc/min

Fig. 57 shows the image of the thin section prepared from Core IL-21 and can be described as fine-to medium-grained, well sorted, rounded, borings, compressed grains, micritized peloids, echinoderms, crinoids, forams, brachiopods, bryozoans, mainly reduced interparticle porosities, minor amounts of moldic and intraparticle porosities, pores reduced by syntaxial calcite overgrowths and blocky calcite cement, 25% porosity, pore size 50-3,300 micron.

Sample from Core 1 (Section 2) of Experiment conducted at 1,000 psi with 10 cc/min

Fig. 58 shows the image of the thin section prepared from Core IL-30 and can be described as f Fine-to medium-grained, well sorted, rounded, borings, compressed grains, micritized peloids, echinoderms, crinoids, forams, brachiopods, bryozoans, mainly reduced interparticle porosities, minor amounts of moldic and intraparticle porosities, pores reduced by syntaxial calcite overgrowths and blocky calcite cement, 30% porosity, pore size 50-4,000 micron.

Sample from Core 1 (Section 2) of Experiment conducted at 5,000 psi with 10 cc/min

Fig. 59 shows the image of the thin section prepared from Core IL-32 and can be described as f Fine-to medium-grained, well sorted, rounded, borings, compressed grains, micritized peloids, echinoderms, crinoids, forams, brachiopods, bryozoans, mainly reduced interparticle porosities, minor amounts of moldic and intraparticle porosities, pores reduced by syntaxial calcite overgrowths and blocky calcite cement, 30% porosity, pore size 50-6,000 micron.

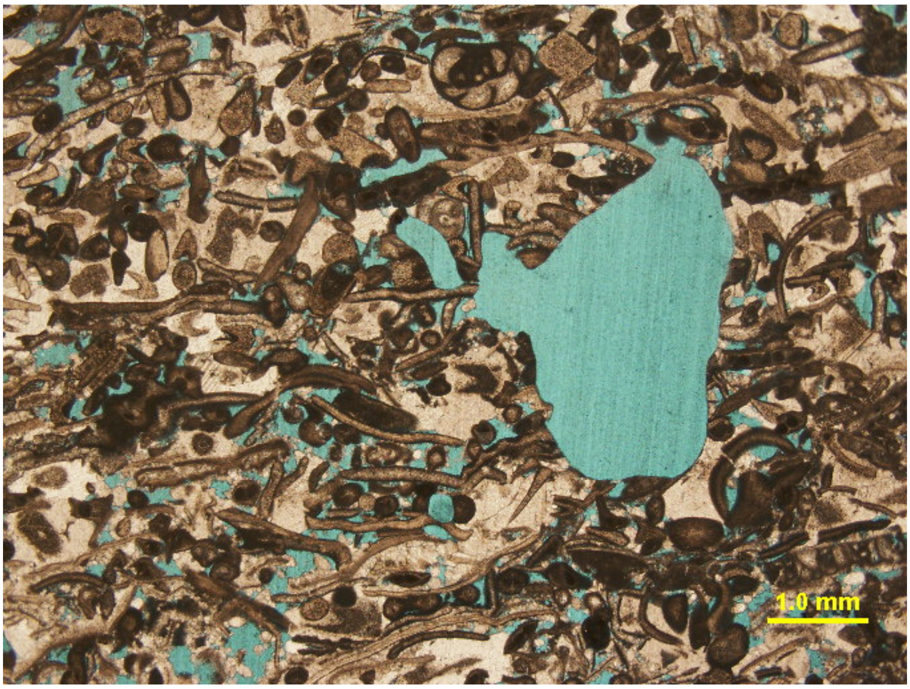

Figure 57 Thin Section Image of Core IL-21 at Section 7

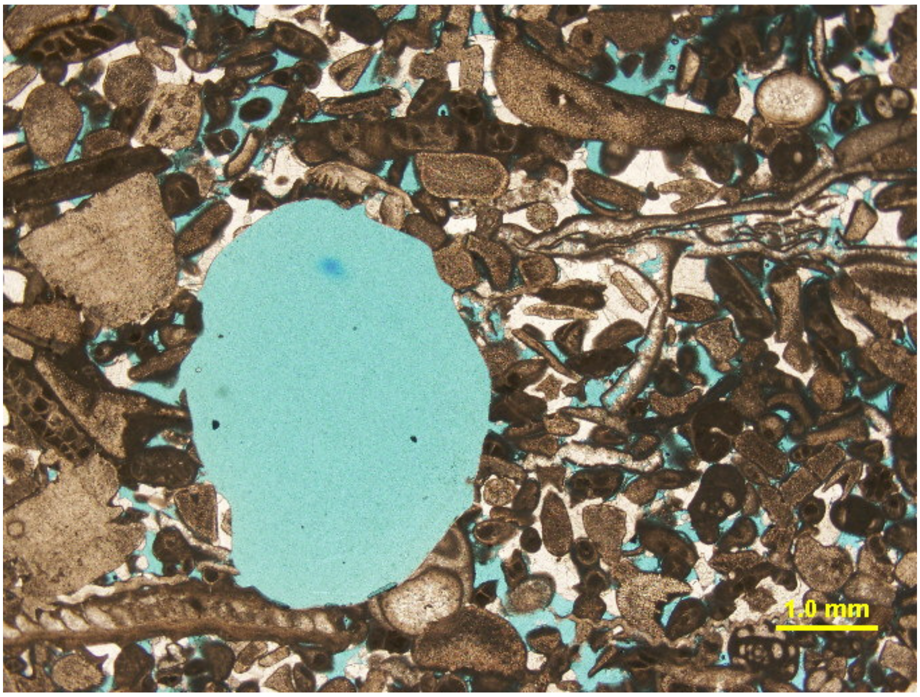

Figure 58 Thin Section Image of Core IL-30 at Section 2

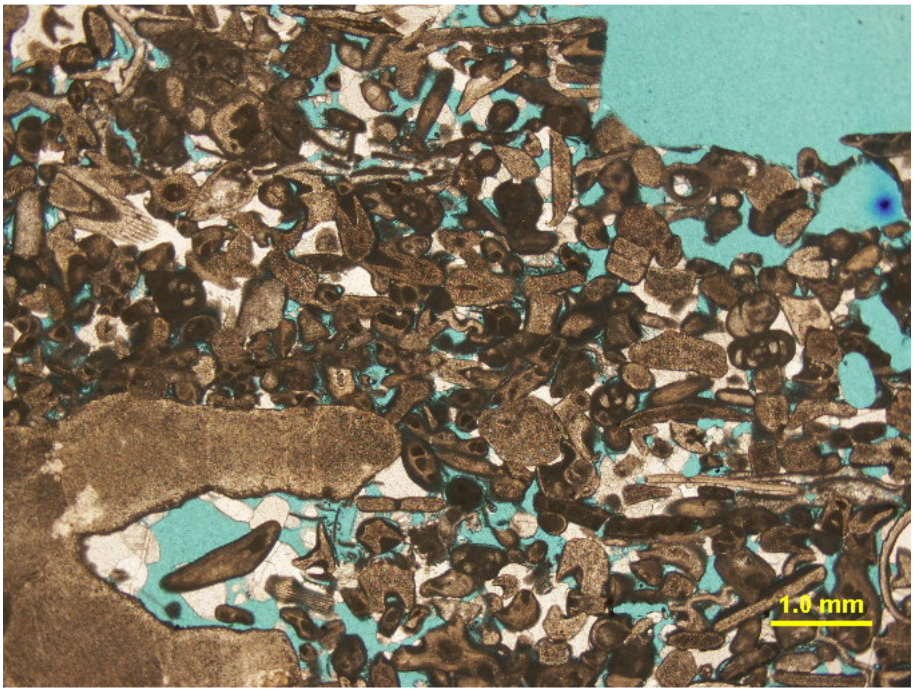

Figure 59 Thin Section Image of Core IL-32 at Section 2

4.5 Scanning Electron Microscope (SEM) Analysis

Four samples from the acidized cores of different experiments were collected to be analyzed on SEM. The samples were selected mostly from section 2 and section 7. This was done so that the end effects can be overseen. One untreated sample from one of these cores was also analyzed. Mapping, EDX Spectrum and Imaging are presented here.

4.5.1 Mapping of Samples

The mapping of these samples indicate presence of four elements which are Calcium, Carbon, Oxygen and Chlorine. out of which three are from the rock itself. Initially it was believed that Carbon, Oxygen and Calcium belong to Calcium carbonate whereas Chlorine is either from the acid or from the reaction product $CaCl_2$ solution. So a hypothesis was made to track the concentration of chlorine across the surface of the wormhole into the rock and some vague inferences regarding the transfer of Calcium Chloride were made. But when an untreated sample was analyzed it also showed some traces of Chlorine thereby negating the hypothesis because if the original rock has traces of chlorides present, then it cannot be used as an indicator of acid or Calcium chloride migration. In the following, the mapping of samples from IL-16, IL-17 and IL-21(untreated) are presented.

4.5.2 Spectrum of Samples

For the EDX spectra, a few points are chosen on the surface of the sample which are then used to generate the spectra using an electron beam and receiving the reflected response. The purpose of this analysis is to identify the presence of different elements in the sample, not their quantity. However rough analysis of the numbers so obtained on the EDX is also important. The detailed spectra of all the elements so examined is given in the appendix however two of them are being discussed here.

Fig. 60 shows the image of section 2 on which six points were selected. The mean values for the existing elements are tabulated in Table 4. The details in the appendix show that the points are pretty much in agreement with each other. Since the three elements Calcium, Carbon and Oxygen come from the rock itself so no major change was expected in its values. Chlorine has two sources; from the acid and from the rock but the varying magnitude is not sufficient to make any strong conclusion.

Fig. 61 shows the zoomed image of IL-17, section 7. It can be seen that points selected for this analysis are very close to the wormhole and therefore the spectrum also shows significant variations for almost all elements but the data is too small to make a strong inference.

Table 4 Mean values of elements from SEM

Spectrum	Carbon (%)	Oxygen (%)	Chlorine (%)	Calcium (%)
IL-16 Section 2	**32.7**	**48.07**	**0.1**	**19.12**
IL-17 Section 7	**22.8**	**56.37**	**1.09**	**19.77**

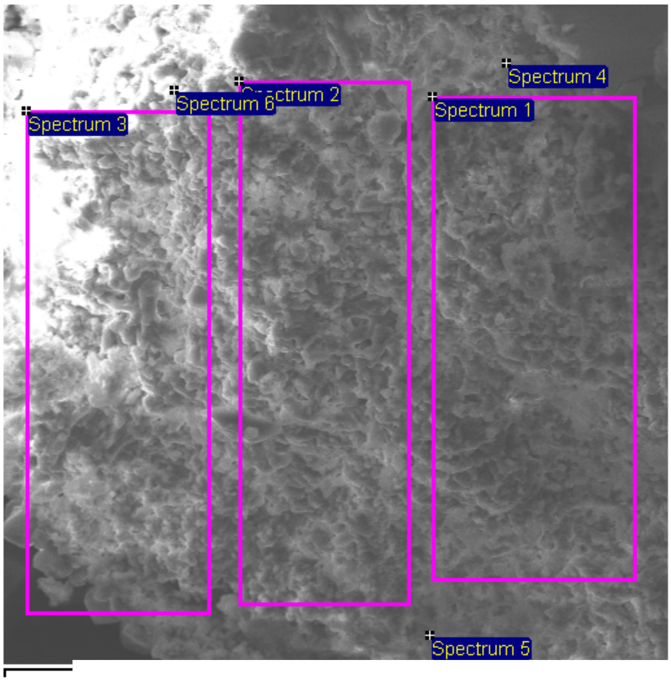

Figure 60 Zoomed in Electron Image of Section 2 Core IL-16

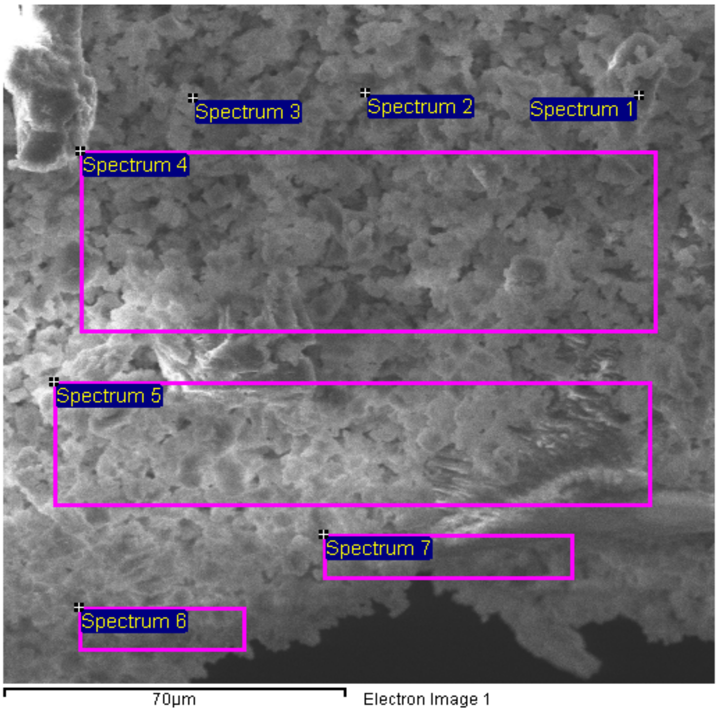

Figure 61 Zoomed in Electron Image of Section 7 Core IL-17

4.5.3 SEM Imaging

In the following, several images provide excellent insight into the texture, pore and grain size of the samples. Fig. 62 to Fig. 65 show the same location on the slice (IL-16) with ascending magnification beginning from a resolution of 20 µm to 1 µm. The location is quite close to the actual wormhole and the visible region has been affected by the incoming acid. The size and structure of the pores can very clearly seen specially at higher resolution in Fig. 65.

Fig. 65 to Fig. 68 show an undamaged zone of the core IL-16. This region is far away from the wormhole can be considered representative of the original rock sample. Here again the images have been presented in ascending order of magnification. The magnification begins at 100 µm and goes high up to 1 µm. The grain and pore sizes can be very easily identified. The sample looks homogeneous. The image to the left in these photos is the electron image and to the right is the back scattered image.

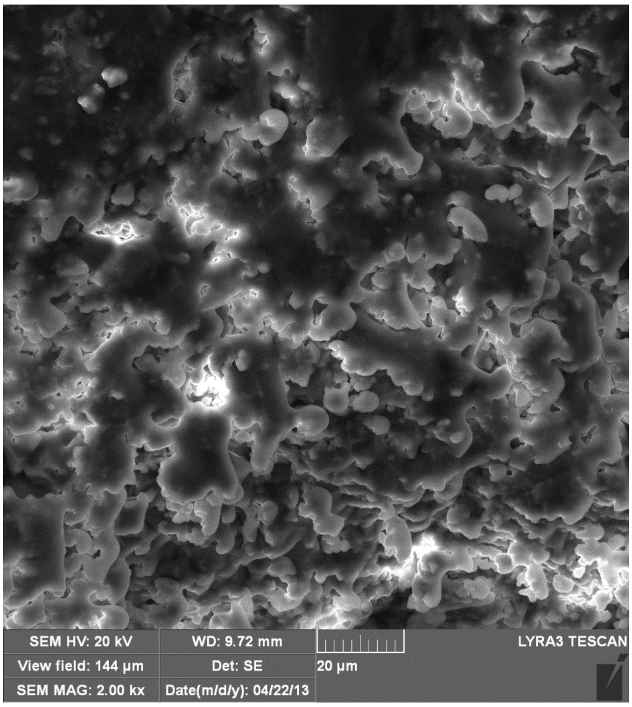

Figure 62 IL-16 Close to wormhole with 20 µm resolution

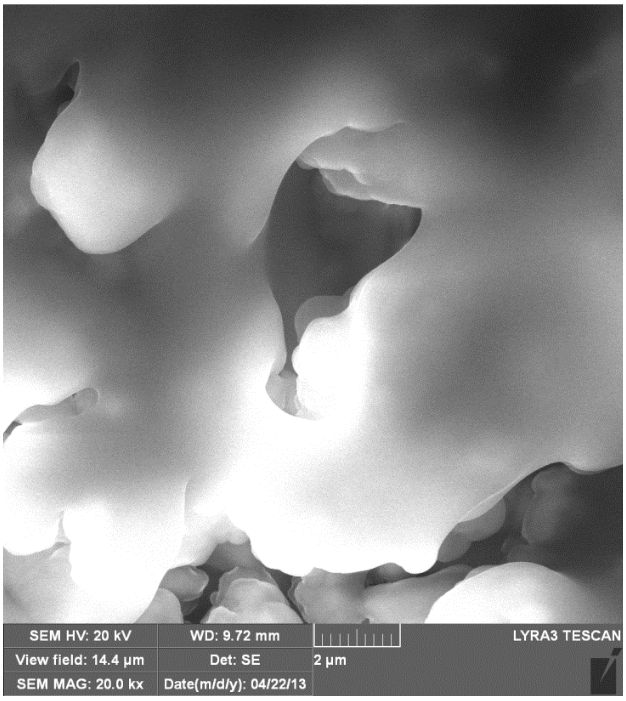

Figure 63 IL-16 Close to wormhole with 2 µm resolution

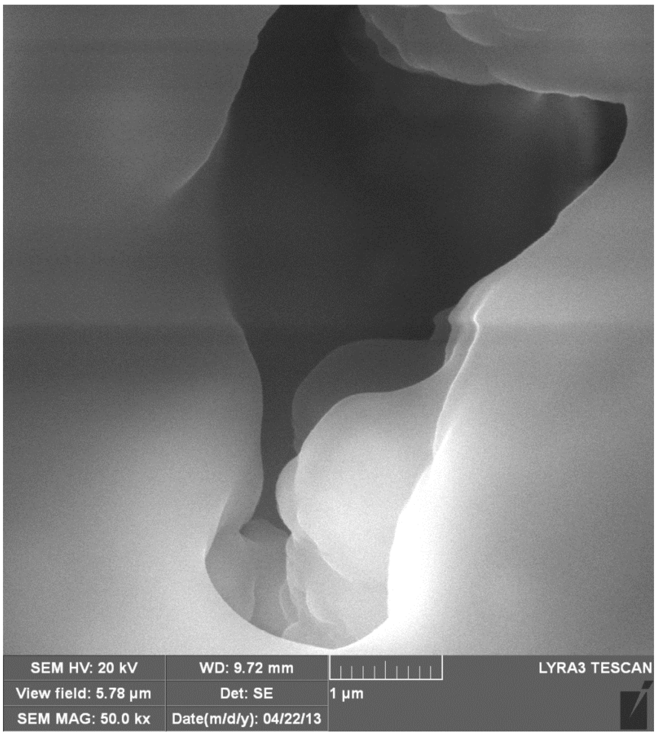

Figure 64 IL-16 Close to wormhole with 1 µm resolution

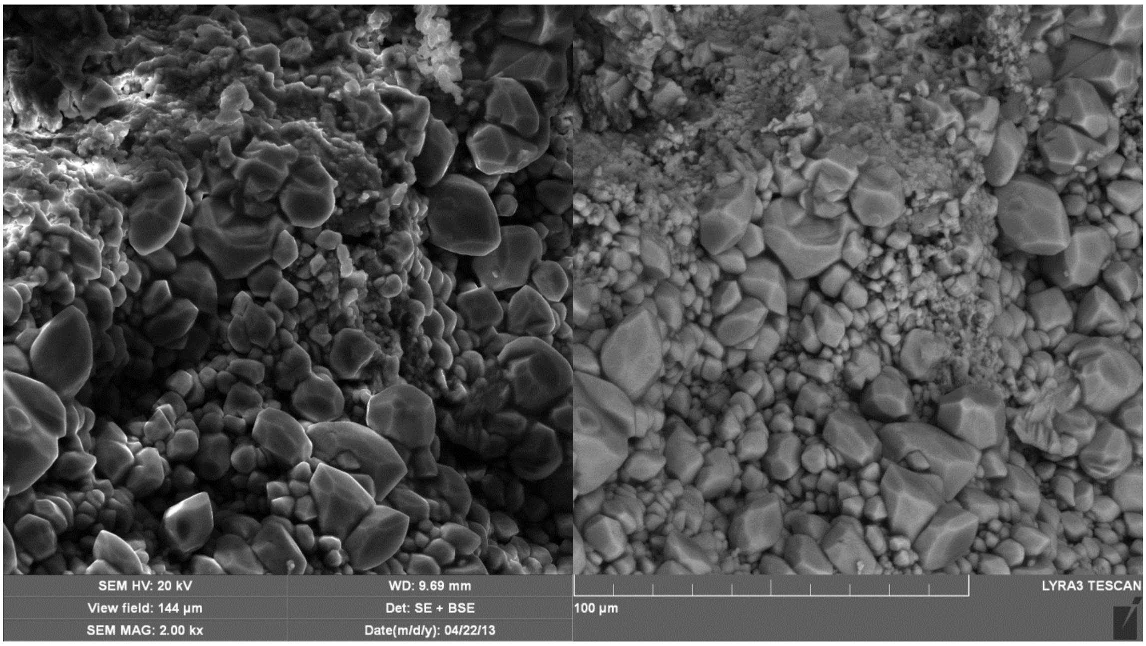

Figure 65 IL-16 Undamaged Zone with 100 µm resolution

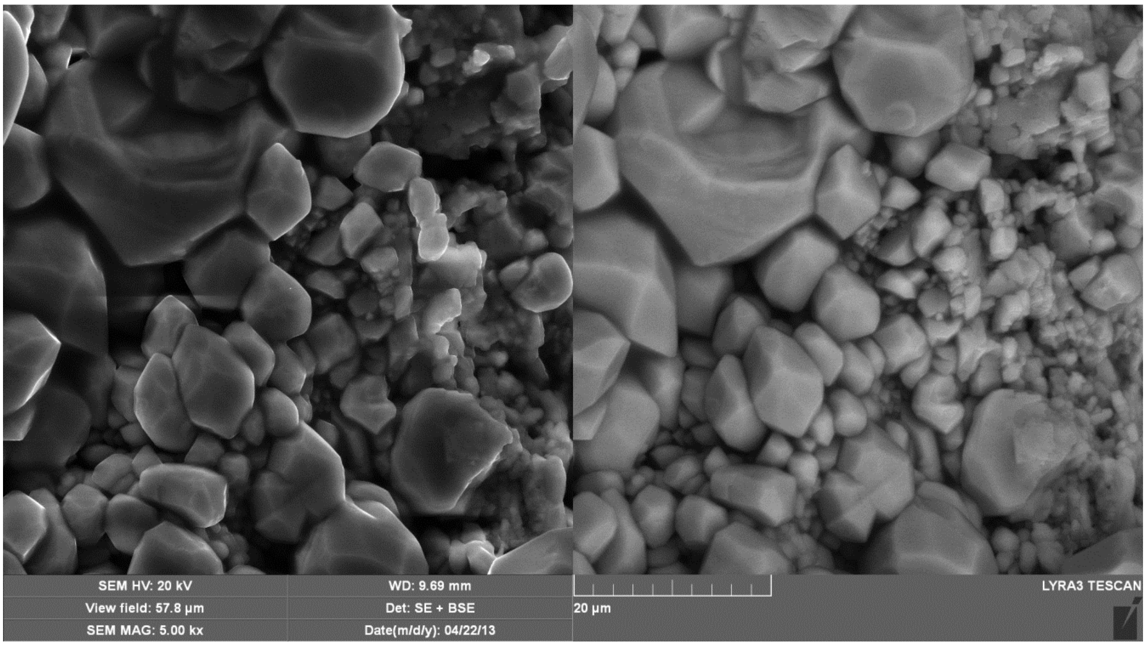

Figure 66 IL-16 Undamaged Zone with 50 µm resolution

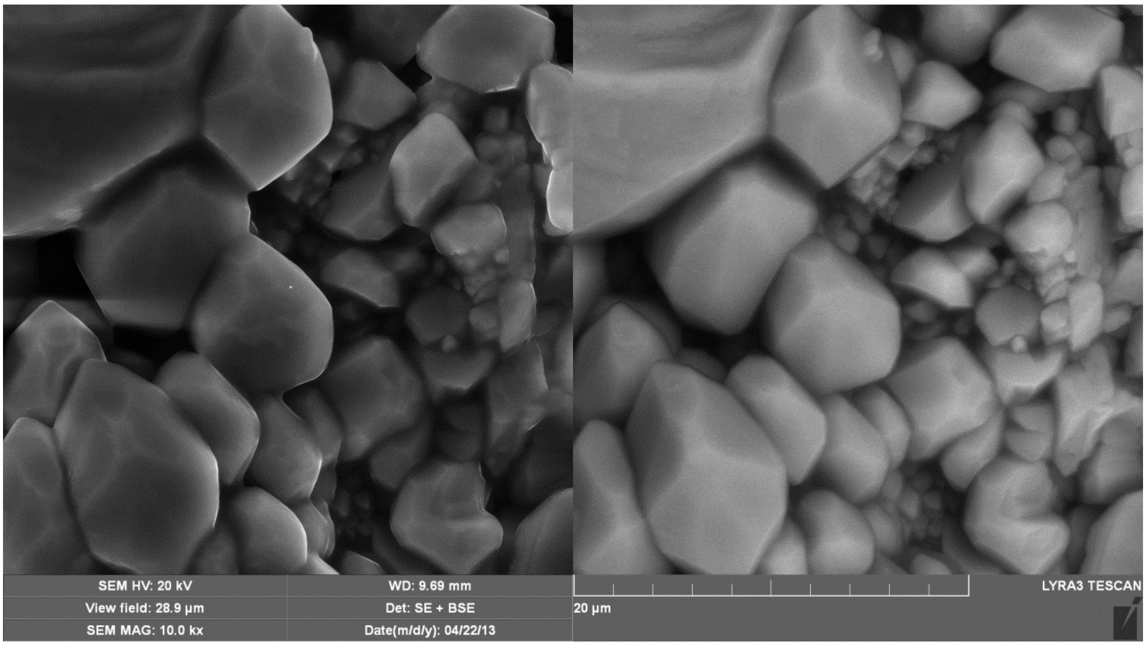

Figure 67 IL-16 Undamaged Zone with 20 µm resolution

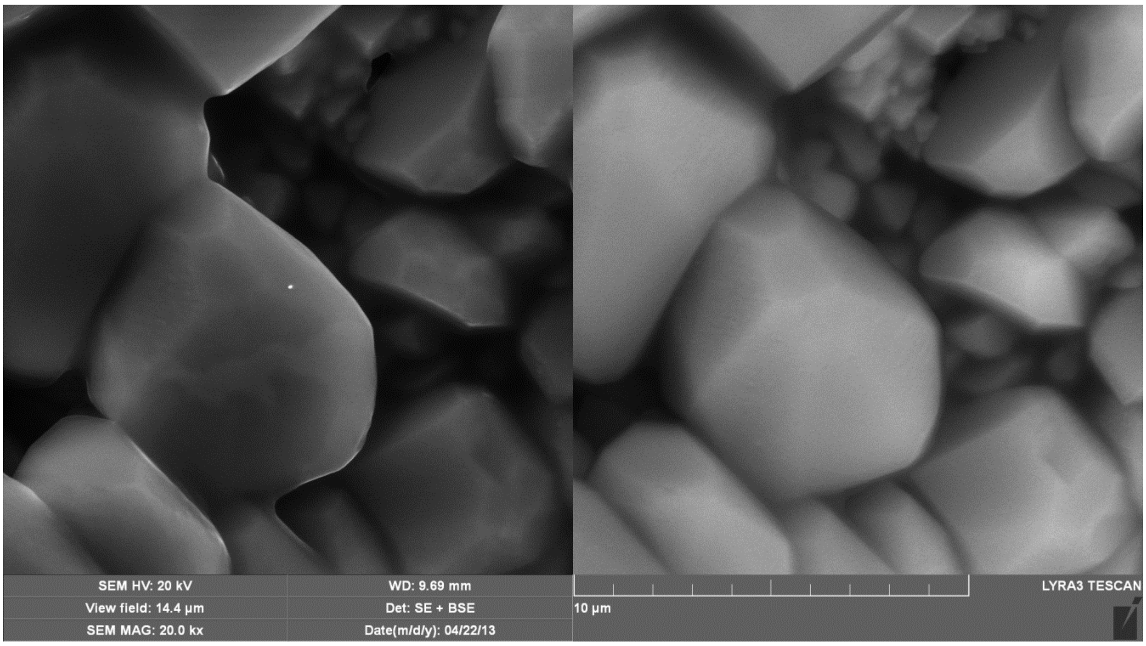

Figure 68 IL-16 Undamaged Zone with 10 µm resolution

Fig. 69 to Fig. 73 show IL-17 which was the second core in series when the experiment with a back pressure of 5,000 psi and a flow rate of 1 cc/min was carried out. The resolution in these figures begins from 200 µm which show the entire wormhole at this section and in the next figures the area in the vicinity is zoomed in to see how the acid has altered the pore structure. The resolution in Fig. 68 goes up to 500 nm. The pores and grains can be very clearly identified.

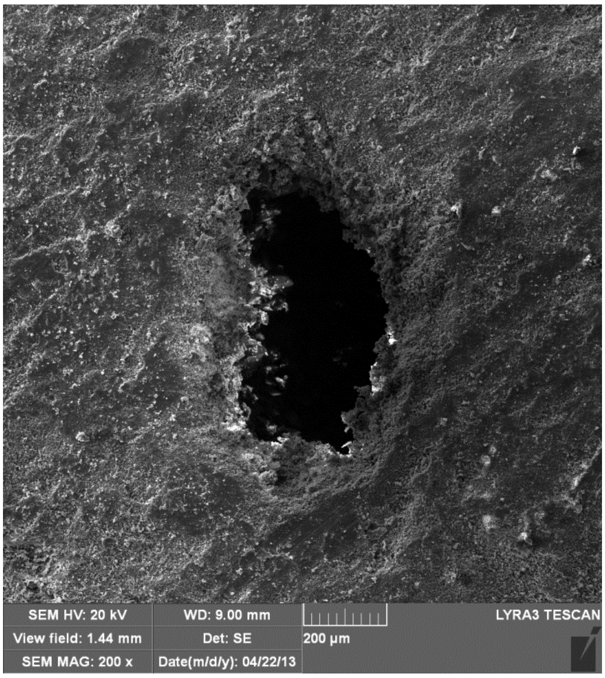

Figure 69 IL-17 Wormhole with 200 µm resolution

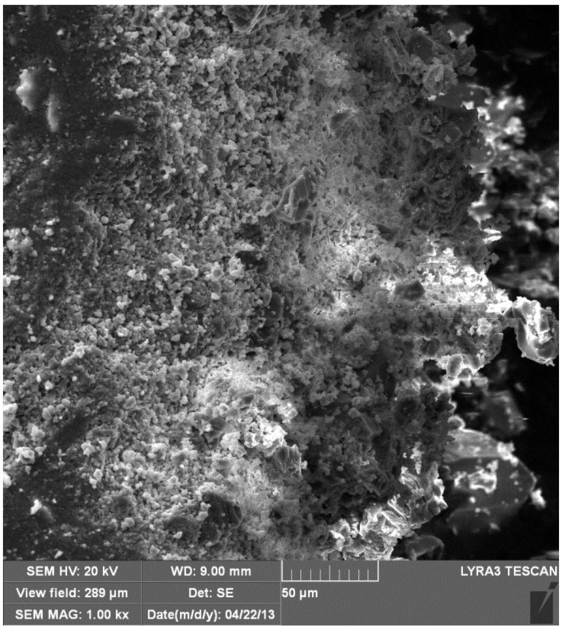

Figure 70 IL-17 Close to wormhole with 50 µm resolution

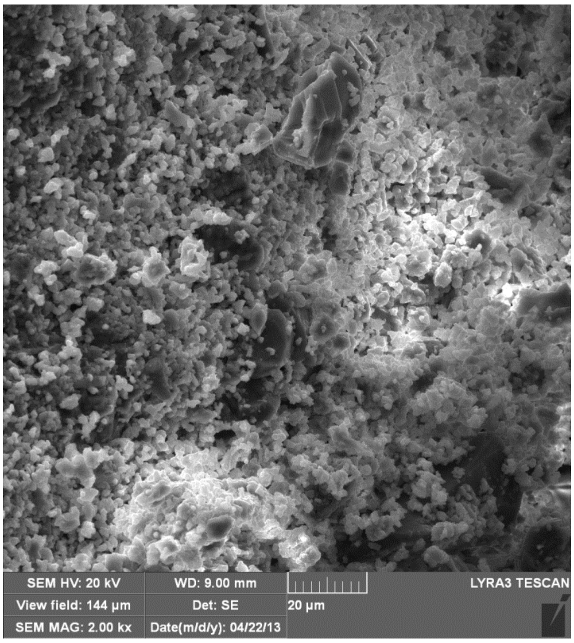

Figure 71 IL-17 Close to wormhole with 20 µm resolution

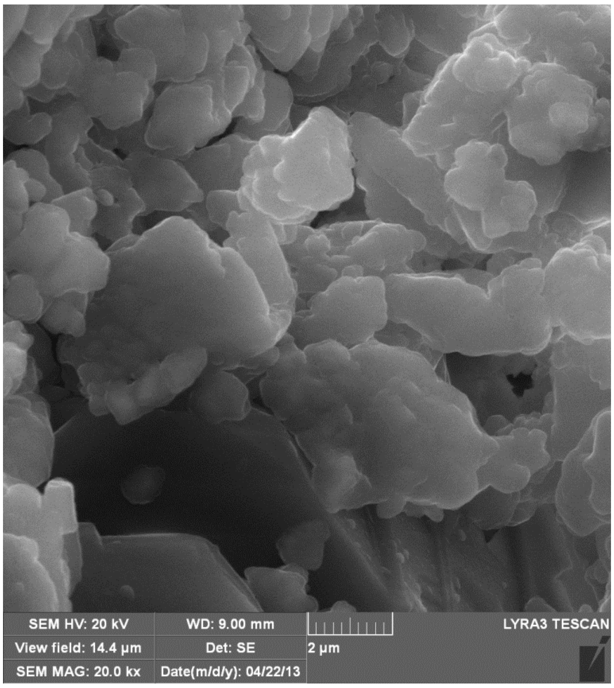

Figure 72 IL-17 Close to wormhole with 2 µm resolution

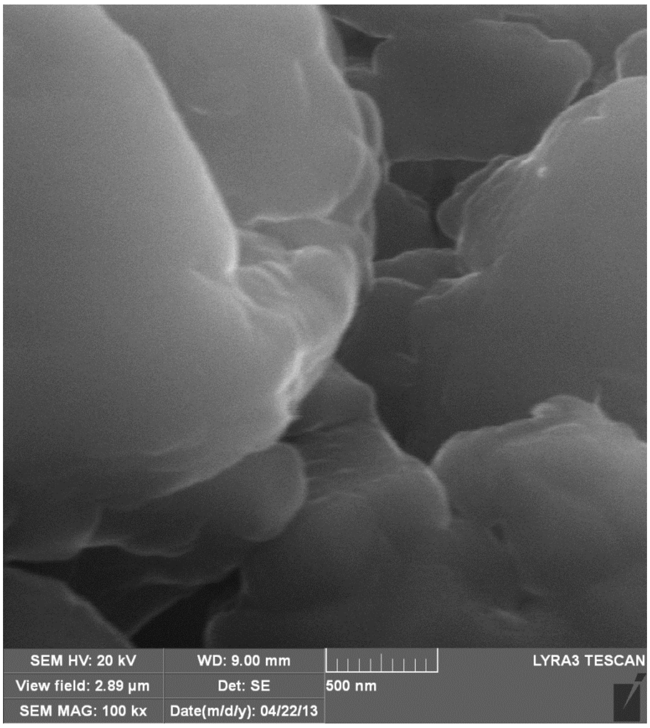

Figure 73 IL-17 Close to wormhole with 500 nm resolution

Fig. 74 to Fig. 77 present a comparison of two sample taken from IL-21; one of them before acidization and the other after it was treated with the acid at 5,000 psi with a flow rate of 2 cc/min. Fig. 74 and Fig.76 are the images from the untreated samples whereas Fig. 75 and Fig. 77 are from the treated sample at the same and corresponding resolutions. The images of the treated sample were taken from a little bit inside of the core and hence it can be seen that most geological features are preserved and are not altered by the acidizing process. The images from the acidized samples are relatively blurred because the coating is not smooth as compared to the untreated sample.

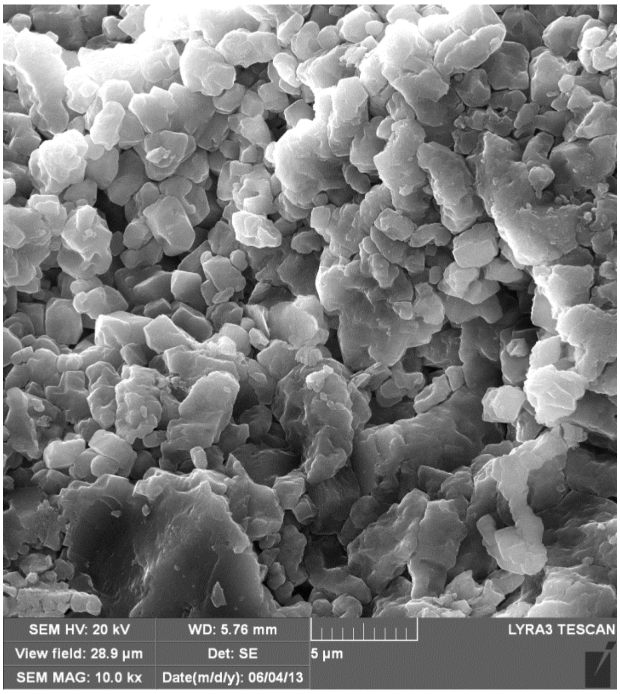

Figure 74 IL-21 Untreated sample with 5 µm resolution

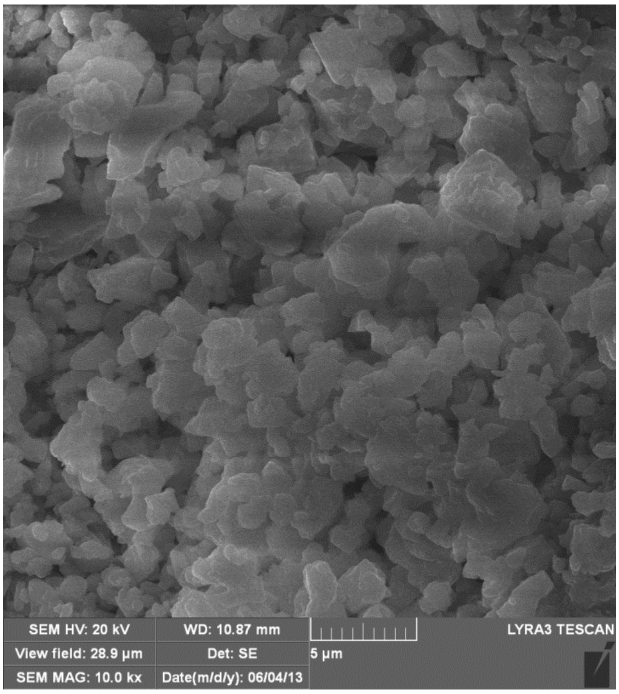

Figure 75 IL-21 Acidized sample with 5 µm resolution

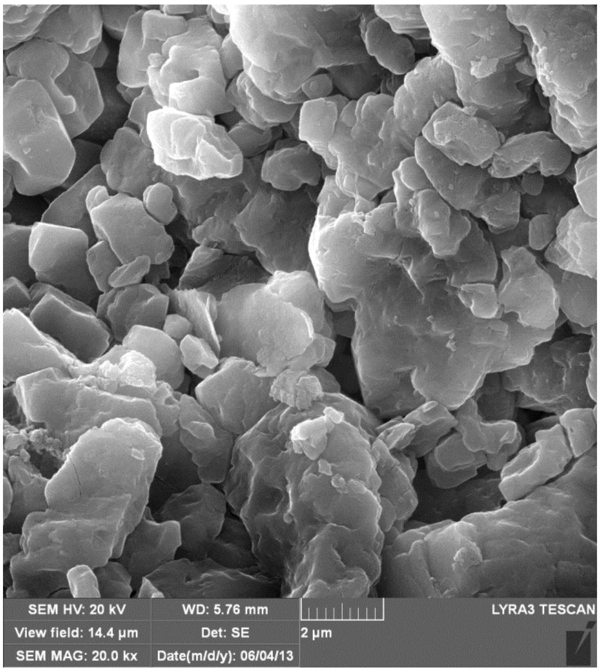

Figure 76 IL-21 Untreated sample with 2 µm resolution

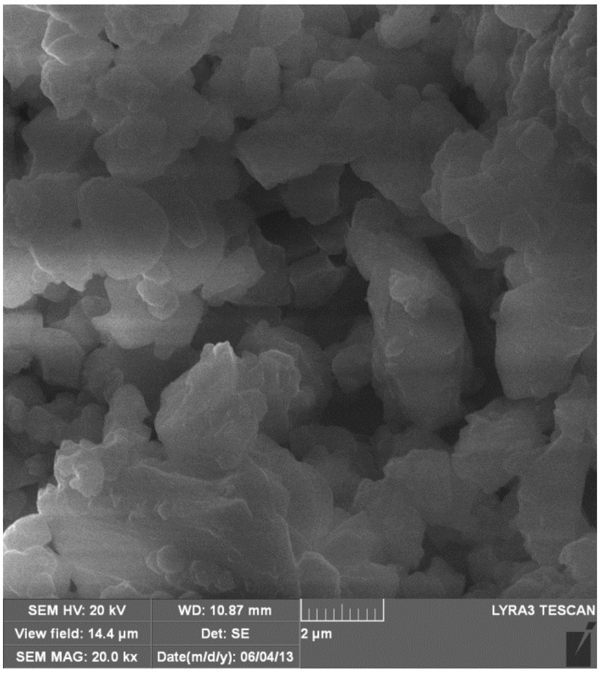

Figure 77 IL-21 Treated sample with 2 µm resolution

CHAPTER 5

CONCLUSIONS AND RECOMMENDATIONS

Following conclusions can be inferred from this project

1. The phase of CO_2 is critically important. It was observed that at pressures around 1,000 psi, it is largely in gaseous phase and as the pressure increases solubility of CO_2 in the spent acid also increases and almost all CO_2 is consumed at elevated pressures.

2. The gaseous phase of CO_2 appears to enhance the mass transfer phenomenon which slows propagation of wormhole, reduces its potential length and produces a fatter hole.

3. Pressure and flow rate effects on wormhole are interdependent. At low flow rates, more PV_{BT} are required for low pressures reservoirs than high pressure reservoirs. At high flow rates, the effect of pressure diminishes.

4. At low pressures, PV_{BT} is quite sensitive to the flow rate but at high pressures it is not the case and we do not have a clear optimum.

5. The PV_{BT} is directly proportional to the length of the core, especially if the pressures are low.

6. The optimum flow rate is also affected by the phase of CO_2. Optimum flow rate is high when the pressures are low.

7. At low flow rates, the speed is similar for all pressures. At higher rates, the speed is higher for high pressures.

8. At low pressure, low rate produces larger holes in the beginning and the high rate produces relatively smaller holes. However, the effect is quite opposite when the experiments were conducted at high pressures.

Recommendations and Future Work

1. Matrix acidizing is an old subject yet a diverse one. In this study, the experimental limits were stretched by using high back pressures and two cores of 12 inch length in series. The data generated here is essential to future studies. This work can be extended on a lot of lines.
2. More experiments with different flow rates can provide more data points which will be helpful in understanding the phase of CO_2 at different pressures. Optimum flow rate can also be adjusted if more data points are available.
3. The CT scan images generated can be used for more detailed study with respect to wormhole propagation and conditions applied.
4. The coreflood data generated, together with the CT scan data can be very effectively used to improve the existing models.
5. The coreflood study can be coupled with Rotating Disk Experiment to understand the kinetics aspects of the phenomenon.
6. The acidized cores are still available and very few samples were taken for SEM and thin section analysis. Study of more representative samples can add a lot to our understanding.

NOMENCLATURE

A270	corrosion inhibitor
ABV	Actual Breakthrough Volume
CO	initial acid concentration
$CaCl_2$	Calcium Chloride
$CaCO_3$	Calcium Carbonate
CO_2	Carbon Oxide
CT	Computed Topography
D	Diffusion Coefficient
DI	de-Ionized
EDX	Energy Dispersive X-ray Spectroscopy
E_f	rate of reaction
HCl	Hydrochloric acid
H_2O	Water
HEDTA	hydroxyl-ethylene-diamine-triacetic acid
GLDA	L-glutamic acid –N, N-diacetic acid
IL	Indiana Limestone
L_e	cylindrical length of wormhole
m	order of reaction
N_{DA}	Damkohler Number
OLI	Schlumberger software for thermodynamic simulations
PV_{BT}	Pore Volume to Breakthrough
PVT_{BT}	Breakthrough Pore Volume Total
q_e	flow rate at the tip of wormhole

q_T	optimum flow rate
r_{wh}	radius of wormhole
SEM	Scanning Electron Microscope
u_e	acid flux at the tip of wormhole
Γ	Dimensionless kinetic parameter

APPENDIX A: Physical Properties of Cores

Table 5 Physical Properties of cores

Core ID	Diameter (mm)	Average diameter (mm)	Length (mm)	Average Length (mm)	Volume (cc)	Dry Weight (gm)	Saturated weight (gm)	Pore Volume (cc)	Porosity (%)	Dry Weight Post Acidizing (gm)
IL 10	38.02	38.07	301.27	301.302	342.797	794.18	839.9	45.72	13.3373	770.1
	37.98		301.11							
	38.14		301.54							
	38.13		301.46							
	38.08		301.13							
IL 11	38.08	38.166	301.44	301.378	344.615	792.84	838.88	46.04	13.3598	790.2
	38.04		301.74							
	38.12		301.12							
	38.13		300.99							
	38.46		301.6							
IL 12	38.18	38.08	301.47	301.386	343.073	794.22	839.58	45.36	13.2217	787.9
	38.05		301.48							
	38.13		301.32							
	38.02		301.32							
	38.02		301.34							
IL 13	38.08	38.138	301.33	301.336	344.062	792.78	839.1	46.32	13.4627	793.1
	38.13		301.36							
	38.29		301.5							

	38.11		301.34							
	38.08		301.15							
IL 14	37.01	37.08	300.97	300.94	324.81	741.86	789.28	47.42	14.5993	742.1
	37.12		300.96							
	37.19		300.97							
	37.07		300.9							
	37.01		300.9							
IL 15	37.23	37.146	300.27	300.25	325.22	734.48	783.55	49.07	15.0883	727.6
	37.07		300.3							
	37.04		300.34							
	37.25		300.21							
	37.14		300.13							
IL 16	37.14	37.134	299.81	299.91	324.642	734.7	782.85	48.15	14.8317	706.1
	37.17		299.68							
	37.1		299.77							
	37.18		299.93							
	37.08		300.36							
IL 17	37.13	37.17	301.82	301.83	327.354	740.32	788.85	48.53	14.8249	746.5
	37.29		301.85							
	37.05		301.62							
	37.18		301.78							
	37.2		302.08							
IL 18	37.02	37.1	301.73	301.73	326.014	724.32	777.57	53.25	16.3337	718.6
	37.06		301.79							
	37.21		301.77							
	37.14		301.63							
	37.07		301.73							

IL 19	37.16	37.054	301.36	301.348	324.794	729.16	779.36	50.2	15.4559	727.6
	37.02		301.3							
	37.16		301.37							
	36.92		301.43							
	37.01		301.28							
IL 20	37.02	37.128	302.21	302.182	326.995	735.82	786.53	50.71	15.5079	727.6
	37.26		302.2							
	37.12		302.14							
	37.1		302.14							
	37.14		302.22							
IL 21	37.21	37.058	301.77	301.738	325.285	728.27	779.78	51.51	15.8354	728
	36.91		301.79							
	37.11		301.75							
	36.95		301.7							
	37.11		301.68							
IL 22	37.04	37.11	301.46	301.438	325.874	725.6	777.07	51.47	15.7945	705.3
	37.23		301.53							
	36.91		301.48							
	37.15		301.35							
	37.22		301.37							
IL 23	37.28	37.206	301.52	301.544	327.677	742.52	789.93	47.41	14.4685	738.6
	37.03		301.55							
	37.19		301.65							
	37.25		301.61							
	37.28		301.39							
IL 26	37.13	37.174	301.07	301.066	326.595	724.21	776.48	52.27	16.0045	721.8
	37.21		300.97							

	37.07		300.98							
	37.21		301.15							
	37.25		301.16							
IL 27	37.46	37.274	301.25	301.256	328.562	726.72	779.75	53.03	16.14	733.6
	37.23		301.23							
	37.13		301.33							
	37.2		301.28							
	37.35		301.19							
IL 28	37.35	37.31	300.94	300.918	328.828	732.12	785.17	53.05	16.1331	724.9
	37.25		301							
	37.27		300.95							
	37.47		300.85							
	37.21		300.85							
IL 29	37.33	37.21	301.4	301.26	327.439	729.08	781.66	52.58	16.058	728.2
	37.01		301.6							
	37.17		301.31							
	37.2		300.75							
	37.34		301.24							
IL 30	37.67	37.356	300.77	300.566	329.253	723.46	775.81	52.35	15.8996	714.4
	37.35		300.8							
	37.19		300.35							
	37.17		300.26							
	37.4		300.65							
IL 31	36.97	37.214	300.95	300.942	327.164	723.99	775.19	51.2	15.6497	722.2
	37.16		300.97							
	37.04		301.17							
	37.85		300.85							

	37.05		300.77							
IL 32	37.25	37.212	300.74	300.766	326.937	723.8	776.25	52.45	16.0428	714.3
	36.81		300.65							
	37.39		300.79							
	37.28		300.84							
	37.33		300.81							
IL 33	37.35	37.23	301.07	301.076	327.591	723.15	774.81	51.66	15.7697	720.1
	37.19		301.16							
	37.42		301.39							
	37.13		301.04							
	37.06		300.72							
IL 45	37.59	37.62	300.65	300.636	334.001	750.91	803.77	52.86	15.8263	746.2
	37.59		300.28							
	37.58		300.66							
	37.62		300.97							
	37.72		300.62							
IL 46	37.69	37.606	300.84	300.812	333.948	757.47	807.4	49.93	14.9514	756.7
	37.56		300.89							
	37.56		300.85							
	37.54		300.76							
	37.68		300.72							

APPENDIX B: Data Analysis of Coreflood Experiments

Table 6 Basic Analysis of Experiment 1 for PV_{BT}

Experiment 1; 1,000 psi, 1 cc/min							
Sections	**Lengths (in)**	**Breakthrough time (hours)**	**Apparent Breakthrough volume (cc)**	**Actual Breakthrough Volume (cc)**	**Breakthrough Pore Volume (total)**	**Pore Volume till section end**	**Breakthrough Pore Volume from face till section end**
1	**2.4**	0.1681	10.0860	4.8960	0.0533	9.1759	0.5336
2	**4.8**	0.3100	18.6006	13.4106	0.1461	18.3519	0.7307
3	**7.2**	0.6987	41.9263	36.7363	0.4003	27.5279	1.3345
4	**9.6**	0.9450	56.7035	51.5135	0.5614	36.7039	1.4035
5	**12**	1.1105	66.6343	61.4443	0.6696	45.8799	1.3392
6	**14.4**	1.6185	97.1100	87.8000	0.9568	55.0559	1.5947
7	**16.8**	1.6806	100.8417	91.5317	0.9975	64.2319	1.4250
8	**19.2**	2.3345	140.0730	130.7630	1.4250	73.4079	1.7814
9	**21.6**					82.5839	
10	**24**					91.7599	

Table 7 Basic Analysis of Experiment 2 for PV_{BT}

Experiment 2; 3,000 psi, 1 cc/min							
Sections	**Lengths (in)**	**Breakthrough time (hours)**	**Apparent Breakthrough volume (cc)**	**Actual Breakthrough Volume (cc)**	**Breakthrough Pore Volume (total)**	**Pore Volume till section end**	**Breakthrough Pore Volume from face till section end**
1	**2.4**	0.1280	7.6821	2.4921	0.0271	9.1680	0.2718
2	**4.8**	0.1673	10.041	4.8510	0.0529	18.3360	0.2646
3	**7.2**	0.2241	13.4445	8.2545	0.0900	27.5040	0.3001
4	**9.6**	0.2788	16.7269	11.5369	0.1258	36.6720	0.3146
5	**12**	0.3081	18.4846	13.2946	0.1450	45.8400	0.2900
6	**14.4**	0.4970	29.8233	20.5133	0.2237	55.0080	0.3729
7	**16.8**	0.6094	36.5612	27.2512	0.2972	64.1760	0.4246
8	**19.2**	0.7518	45.1056	35.7957	0.3904	73.3440	0.4880
9	**21.6**	0.8452	50.7133	41.4032	0.4516	82.5120	0.5018
10	**24**	0.8458	50.7467	41.4367	0.4520	91.6800	0.4520

Table 8 Basic Analysis of Experiment 3 for PV_{BT}

Experiment 3; 5,000 psi, 1 cc/min							
Sections	**Lengths (in)**	**Breakthrough time (hours)**	**Apparent Breakthrough volume (cc)**	**Actual Breakthrough Volume (cc)**	**Breakthrough Pore Volume (total)**	**Pore Volume till section end**	**Breakthrough Pore Volume from face till section end**
1	**2.4**	0.1263	7.5770	2.3870	0.0247	9.6490	0.2473
2	**4.8**	0.1606	9.6376	4.4476	0.0461	19.2980	0.2305
3	**7.2**	0.2177	13.0632	7.8732	0.0816	28.9470	0.2720
4	**9.6**	0.3044	18.2633	13.0733	0.1355	38.5960	0.3387
5	**12**	0.3441	20.6438	15.4538	0.1602	48.2450	0.3203
6	**14.4**	0.5888	35.3301	26.0201	0.2697	57.8940	0.4494
7	**16.8**	0.6693	40.1600	30.8500	0.3197	67.5430	0.4567
8	**19.2**	0.7321	43.9253	34.6153	0.3587	77.1920	0.4484
9	**21.6**	0.8370	50.2231+	40.9131	0.4240	86.8410	0.4711
10	**24**	0.9303	55.8189	46.5089	0.4820	96.4900	0.4820

Table 9 Basic Analysis of Experiment 4 for PV_{BT}

Experiment 4; 1,000 psi, 2 cc/min							
Sections	**Lengths (in)**	**Breakthrough time (hours)**	**Apparent Breakthrough volume (cc)**	**Actual Breakthrough Volume (cc)**	**Breakthrough Pore Volume (total)**	**Pore Volume till section end**	**Breakthrough Pore Volume from face till section end**
1	**2.4**	0.0841	10.0896	4.8996	0.0507	9.6680	0.5068
2	**4.8**	0.1243	14.9190	9.7290	0.1006	19.3360	0.5031
3	**7.2**	0.1739	20.8676	15.6776	0.1627	29.0040	0.5405
4	**9.6**	0.2536	30.4349	25.2449	0.2611	38.6720	0.6528
5	**12**	0.4285	51.4231	46.2331	0.4782	48.3400	0.9564
6	**14.4**	0.7035	84.4271	75.1171	0.7770	58.0080	1.2949
7	**16.8**	1.1383	136.5994	127.2894	1.3166	67.6760	1.8808
8	**19.2**					77.3440	
9	**21.6**					87.0120	
10	**24**					96.6800	

Table 10 Basic Analysis of Experiment 5 for PV_{BT}

Experiment 5; 3,000 psi, 2 cc/min							
Sections	**Lengths (in)**	**Breakthrough time (hours)**	**Apparent Breakthrough volume (cc)**	**Actual Breakthrough Volume (cc)**	**Breakthrough Pore Volume (total)**	**Pore Volume till section end**	**Breakthrough Pore Volume from face till section end**
1	**2.4**	0.0601	7.2078	2.0178	0.0195	10.3450	0.1950
2	**4.8**	0.0836	10.0270	4.8370	0.0468	20.6900	0.2338
3	**7.2**	0.1127	13.5257	8.3357	0.0806	31.0350	0.2686
4	**9.6**	0.1494	17.9345	12.7445	0.1232	41.3800	0.3080
5	**12**	0.1708	20.4907	15.3007	0.1479	51.7250	0.2958
6	**14.4**	0.2482	29.7902	20.4102	0.1973	62.0700	0.3288
7	**16.8**	0.3187	38.2397	28.8597	0.2790	72.4150	0.3985
8	**19.2**	0.3683	44.1918	34.8118	0.3365	82.7600	0.4206
9	**21.6**	0.4093	49.1144	39.7344	0.3841	93.1050	0.4268
10	**24**	0.4270	51.2342	41.8542	0.4046	103.4500	0.4046

Table 11 Basic Analysis of Experiment 6 for PV_{BT}

Experiment 6; 5,000 psi, 2 cc/min							
Sections	**Lengths (in)**	**Breakthrough time (hours)**	**Apparent Breakthrough volume (cc)**	**Actual Breakthrough Volume (cc)**	**Breakthrough Pore Volume (total)**	**Pore Volume till section end**	**Breakthrough Pore Volume from face till section end**
1	**2.4**	0.0556	6.6799	1.4899	0.0146	10.2220	0.1458
2	**4.8**	0.0832	9.9888	4.7988	0.0469	20.4440	0.2347
3	**7.2**	0.1031	12.3697	7.1797	0.0702	30.6660	0.2341
4	**9.6**	0.1216	14.5948	9.4048	0.0920	40.8880	0.2300
5	**12**	0.1475	17.6964	12.5064	0.1223	51.1100	0.2447
6	**14.4**	0.2327	27.9215	18.5415	0.1814	61.3320	0.3023
7	**16.8**	0.2796	33.5520	28.3620	0.2775	71.5540	0.3964
8	**19.2**	0.3334	40.0148	34.8248	0.3407	81.7760	0.4258
9	**21.6**	0.4075	48.8958	43.7058	0.4276	91.9980	0.4751
10	**24**	0.4133	49.6009	44.4109	0.4345	102.2200	0.4345

Table 12 Basic Analysis of Experiment 7 for PV_{BT}

Experiment 7; 3,000 psi, 10 cc/min							
Sections	**Lengths (in)**	**Breakthrough time (hours)**	**Apparent Breakthrough volume (cc)**	**Actual Breakthrough Volume (cc)**	**Breakthrough Pore Volume (total)**	**Pore Volume till section end**	**Breakthrough Pore Volume from face till section end**
1	**2.4**	0.0171	10.2600	5.0700	0.0481	10.5300	0.9743
2	**4.8**	0.0228	13.6764	8.4864	0.0806	21.0600	0.6494
3	**7.2**	0.0304	18.2184	13.0284	0.1237	31.5900	0.5767
4	**9.6**	0.0436	26.1552	20.9652	0.1991	42.1200	0.6210
5	**12**	0.0520	31.2186	26.0286	0.2472	52.6500	0.5929
6	**14.4**	0.0683	40.9980	31.6880	0.3009	63.1800	0.6489
7	**16.8**	0.0787	47.2350	37.9250	0.3602	73.7100	0.6408
8	**19.2**	0.0883	52.9644	43.6544	0.4146	84.2400	0.6287
9	**21.6**	0.0981	58.8682	49.5581	0.4706	94.7700	0.6210
10	**24**	0.1150	68.9898	59.6798	0.5668	105.300	0.6552

Table 13 Basic Analysis of Experiment 8 for PV_{BT}

Experiment 8; 3,000 psi, 5 cc/min							
Sections	**Lengths (in)**	**Breakthrough time (hours)**	**Apparent Breakthrough volume (cc)**	**Actual Breakthrough Volume (cc)**	**Breakthrough Pore Volume (total)**	**Pore Volume till section end**	**Breakthrough Pore Volume from face till section end**
1	**2.4**	0.0312	9.3699	4.1799	0.0396	10.5630	0.8870
2	**4.8**	0.0386	11.5683	6.3783	0.0604	21.1260	0.5476
3	**7.2**	0.0554	16.6305	11.4405	0.1083	31.6890	0.5248
4	**9.6**	0.0714	21.4362	16.2462	0.1538	42.2520	0.5073
5	**12**	0.0793	23.7969	18.6069	0.1762	52.8150	0.4506
6	**14.4**	0.1134	34.0173	24.7073	0.2339	63.3780	0.5367
7	**16.8**	0.1339	40.1778	30.8678	0.2922	73.9410	0.5434
8	**19.2**	0.1609	48.2766	38.9666	0.3689	84.5040	0.5713
9	**21.6**	0.1910	57.3033	47.9933	0.4543	95.0670	0.6028
10	**24**	0.1952	58.5756	49.2656	0.4664	105.6300	0.5545

Table 14 Basic Analysis of Experiment 9 for PV_{BT}

Experiment 9; 1,000 psi 5 cc/min							
Sections	**Lengths (in)**	**Breakthrough time (hours)**	**Apparent Breakthrough volume (cc)**	**Actual Breakthrough Volume (cc)**	**Breakthrough Pore Volume (total)**	**Pore Volume till section end**	**Breakthrough Pore Volume from face till section end**
1	**2.4**	0.0328	9.8610	4.6710	0.0454	10.2980	0.4536
2	**4.8**	0.0489	14.6736	9.4836	0.0921	20.5960	0.4604
3	**7.2**	0.0618	18.5535	13.3635	0.1298	30.8940	0.4326
4	**9.6**	0.0742	22.2687	17.0787	0.1658	41.1920	0.4146
5	**12**	0.0916	27.4971	22.3071	0.2166	51.4900	0.4332
6	**14.4**	0.1308	39.2274	29.9174	0.2905	61.7880	0.4842
7	**16.8**	0.1423	42.6804	33.3704	0.3240	72.0860	0.4629
8	**19.2**	0.1929	57.8805	48.5705	0.4716	82.3840	0.5896
9	**21.6**	0.2261	67.8303	58.5203	0.5683	92.6820	0.6314
10	**24**	0.3733	111.9906	102.6806	0.9971	102.9800	0.9971

Table 15 Basic Analysis of Experiment 10 for PV_{BT}

Experiment 10; 1,000 psi, 10 cc/min							
Sections	**Lengths (in)**	**Breakthrough time (hours)**	**Apparent Breakthrough volume (cc)**	**Actual Breakthrough Volume (cc)**	**Breakthrough Pore Volume (total)**	**Pore Volume till section end**	**Breakthrough Pore Volume from face till section end**
1	**2.4**	0.0177	10.6356	5.4456	0.0526	9.1760	0.5935
2	**4.8**	0.0250	15.0150	9.8250	0.0949	18.3520	0.5354
3	**7.2**	0.0348	20.9064	15.7164	0.1518	27.5280	0.5709
4	**9.6**	0.0447	26.8086	21.6186	0.2088	36.7040	0.5890
5	**12**	0.0548	32.8836	27.6936	0.2674	45.8800	0.6036
6	**14.4**	0.0796	47.7444	38.4344	0.3712	55.0560	0.6981
7	**16.8**	0.0880	52.8222	43.5122	0.4202	64.2319	0.6774
8	**19.2**	0.1026	61.5774	52.2674	0.5048	73.4079	0.7120
9	**21.6**	0.1192	71.5314	62.2214	0.6009	82.5839	0.7534
10	**24**	0.1299	77.9274	68.6174	0.6626	91.7599	0.7478

Table 16 Basic Analysis of Experiment 4 for PV_{BT}

Experiment 11; 5,000 psi, 10 cc/min							
Sections	**Lengths (in)**	**Breakthrough time (hours)**	**Apparent Breakthrough volume (cc)**	**Actual Breakthrough Volume (cc)**	**Breakthrough Pore Volume (total)**	**Pore Volume till section end**	**Breakthrough Pore Volume from face till section end**
1	**2.4**	0.0141	8.4420	3.2520	0.0312	10.4110	0.3124
2	**4.8**	0.0197	11.8050	6.6150	0.0635	20.8220	0.3177
3	**7.2**	0.0267	16.0254	10.8354	0.1041	31.2330	0.3469
4	**9.6**	0.0352	21.1002	15.9102	0.1528	41.6440	0.3820
5	**12**	0.0408	24.4632	19.2732	0.1851	52.0550	0.3702
6	**14.4**	0.0585	35.0940	25.7840	0.2477	62.4660	0.4127
7	**16.8**	0.0703	42.1938	32.8838	0.3158	72.8770	0.4512
8	**19.2**	0.0860	51.6300	42.3200	0.4065	83.2880	0.5081
9	**21.6**	0.0959	57.5430	48.2330	0.4633	93.6990	0.5148
10	**24**	0.1072	64.2966	54.9866	0.5282	104.110	0.5282

Table 17 Basic Analysis of Experiment 12 for PV_{BT}

Experiment 12; 5,000 psi, 5 cc/min							
Sections	**Lengths (in)**	**Breakthrough time (hours)**	**Apparent Breakthrough volume (cc)**	**Actual Breakthrough Volume (cc)**	**Breakthrough Pore Volume (total)**	**Pore Volume till section end**	**Breakthrough Pore Volume from face till section end**
1	**2.4**	0.0292	8.7651	3.5751	0.0348	10.2790	0.3478
2	**4.8**	0.0351	10.5348	5.3448	0.0520	20.5580	0.2600
3	**7.2**	0.0475	14.2494	9.0594	0.0881	30.8370	0.2938
4	**9.6**	0.0565	16.9410	11.7510	0.1143	41.1160	0.2858
5	**12**	0.0621	18.6261	13.4361	0.1307	51.3950	0.2614
6	**14.4**	0.1074	32.2212	22.9112	0.2229	61.6740	0.3715
7	**16.8**	0.1192	35.7633	26.4533	0.2574	71.9530	0.3676
8	**19.2**	0.1293	38.7957	29.4857	0.2868	82.2320	0.3586
9	**21.6**	0.1456	43.6785	34.3685	0.3344	92.5110	0.3715
10	**24**	0.1543	46.3029	36.9929	0.3599	102.7900	0.3599

APPENDIX C: SEM/EDX Data Analysis

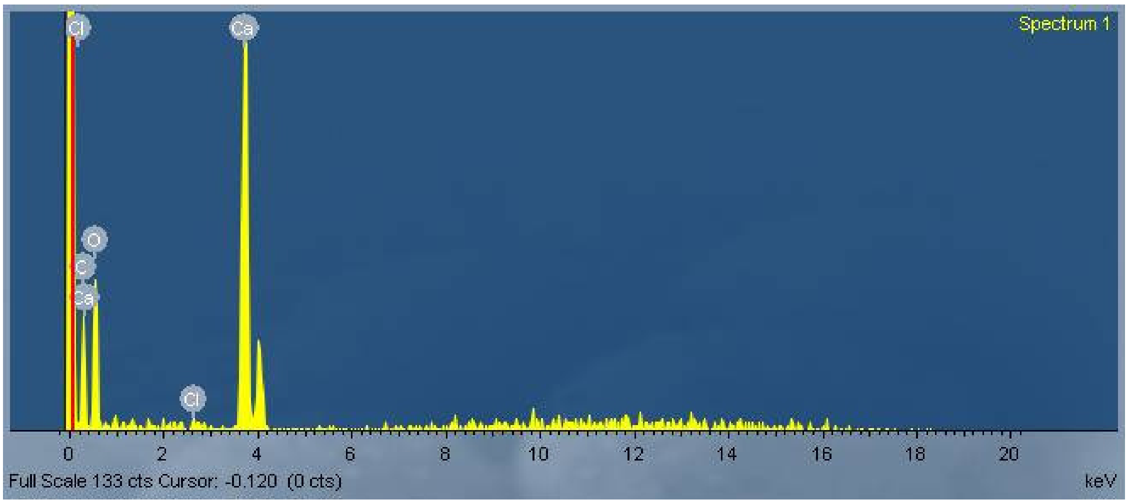

Figure 78 Spectrum for Section 2 IL-16

Table 18 Elemental Analysis at Section 2 IL-16

Spectrum	In stats.	C	O	Cl	Ca
Spectrum 1	Yes	39.59	51.37	0.09	8.94
Spectrum 2	Yes	32.51	47.73	0.25	19.50
Spectrum 3	Yes	32.60	51.34	0.07	15.99
Spectrum 4	Yes	26.25	39.57	0.03	34.14
Spectrum 5	Yes	45.20	51.51	0.02	3.27
Spectrum 6	Yes	20.07	46.89	0.15	32.90
Mean		32.70	48.07	0.10	19.12
Std. deviation		9.00	4.63	0.09	12.49
Max.		45.20	51.51	0.25	34.14
Min.		20.07	39.57	0.02	3.27

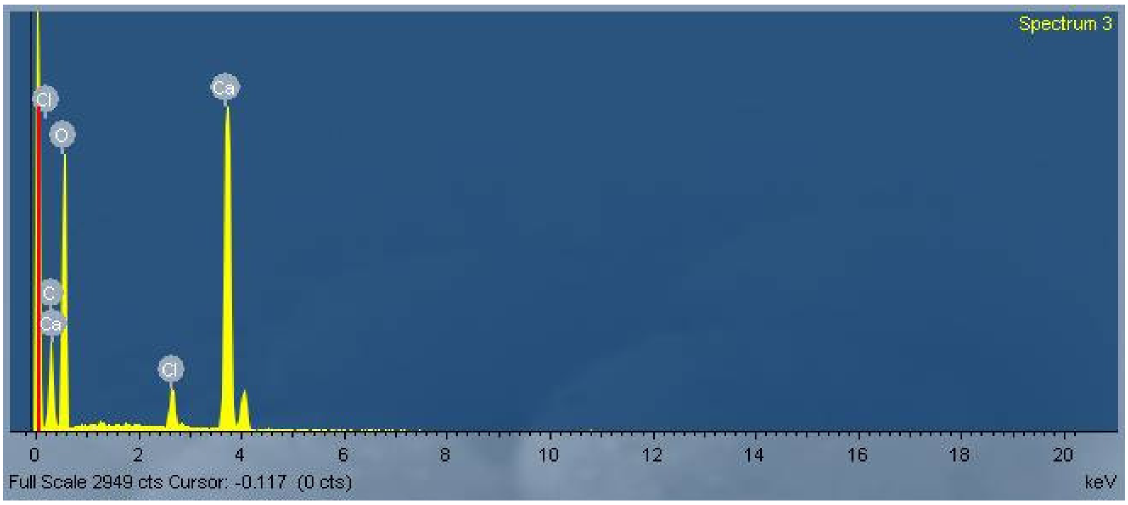

Figure 79 Spectrum for Section 7 IL-17

Table 19 Elemental Analysis Section 7 IL-17

	In stats.	C	O	Cl	Ca
Spectrum 1	Yes	19.21	56.28	0.58	23.93
Spectrum 2	Yes	15.91	49.24	2.22	32.64
Spectrum 3	Yes	27.20	65.38	0.74	6.68
Spectrum	Yes	19.94	59.28	1.34	19.44
Spectrum 5	Yes	20.78	50.92	1.31	26.98
Spectrum 6	Yes	27.29	56.71	0.64	15.36
Spectrum 7	Yes	29.07	56.78	0.79	13.36
Mean		22.77	56.37	1.09	19.77
Std. deviation		5.02	5.33	0.59	8.82
Max.		29.07	65.38	2.22	32.64
Min.		15.91	49.24	0.58	6.68

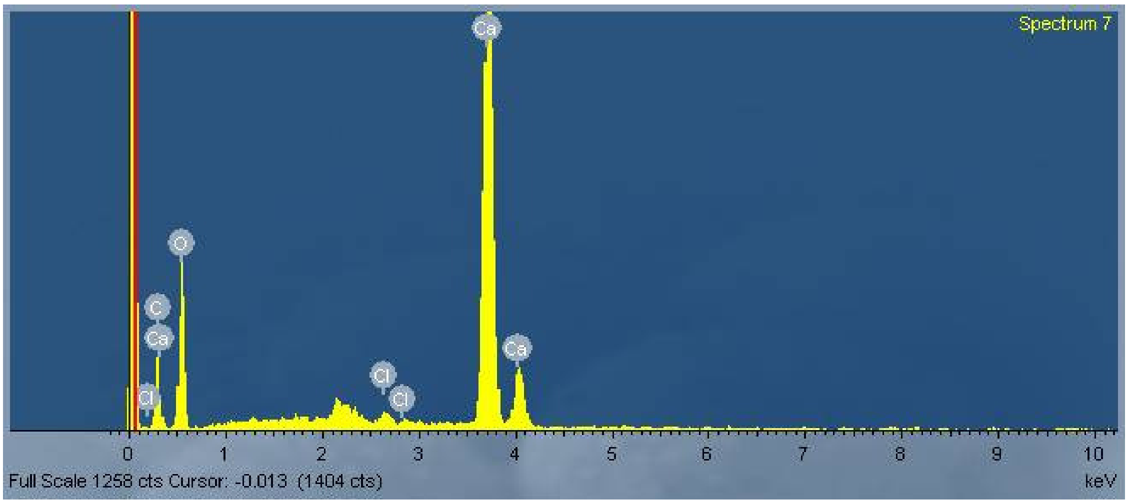

Figure 80 Spectrum for Section 2 IL-20

Table 20 Elemental Analysis for Section 2 IL-20

Spectrum	In stats.	C	O	Cl	Ca	Total
Spectrum 1	Yes	11.75	53.24	0.32	34.70	100.00
Spectrum 2	Yes	15.87	58.74	0.06	25.33	100.00
Spectrum 3	Yes	18.41	60.44	0.20	20.94	100.00
Spectrum 4	Yes	16.62	57.83	0.20	25.34	100.00
Spectrum 5	Yes	16.19	55.07	0.11	28.63	100.00
Spectrum 6	Yes	15.89	56.68	0.21	27.21	100.00
Spectrum 7	Yes	16.47	55.38	0.46	27.69	100.00
Mean		15.89	56.77	0.22	27.12	100.00
Std. deviation		2.02	2.44	0.13	4.17	
Max.		18.41	60.44	0.46	34.70	
Min.		11.75	53.24	0.06	20.94	

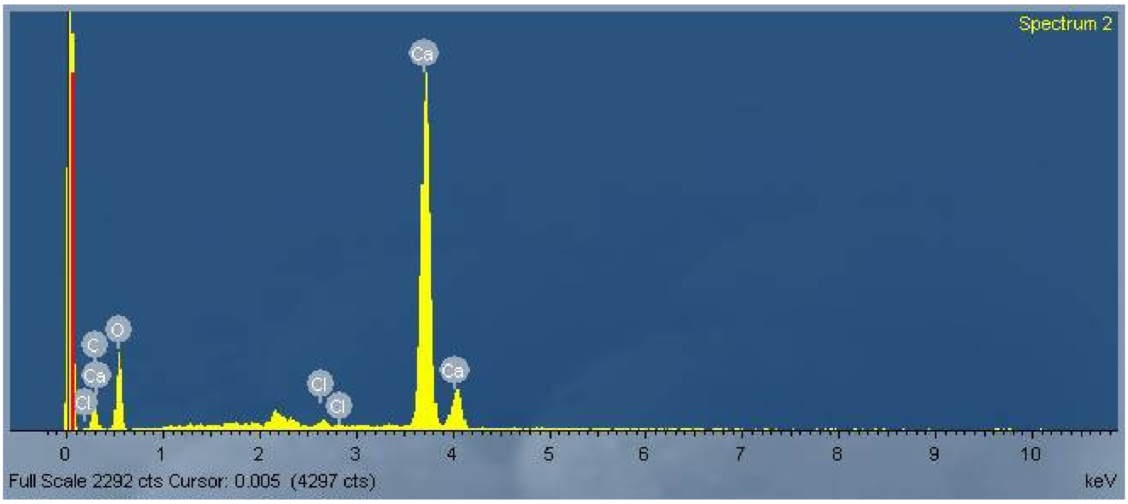

Figure 81 Spectrum for untreated IL-21

Table 21 Elemental Analysis for untreated IL-21

Spectrum	In stats.	C	O	Cl	Ca	Total
Spectrum 1	Yes	12.39	51.71	1.38	33.59	100.00
Spectrum 2	Yes	11.13	53.43	0.46	34.49	100.00
Spectrum 3	Yes	13.58	52.66	0.51	32.83	100.00
Mean		12.37	52.60	0.78	33.64	100.00
Std. deviation		1.22	0.86	0.52	0.83	
Max.		13.58	53.43	1.38	34.49	

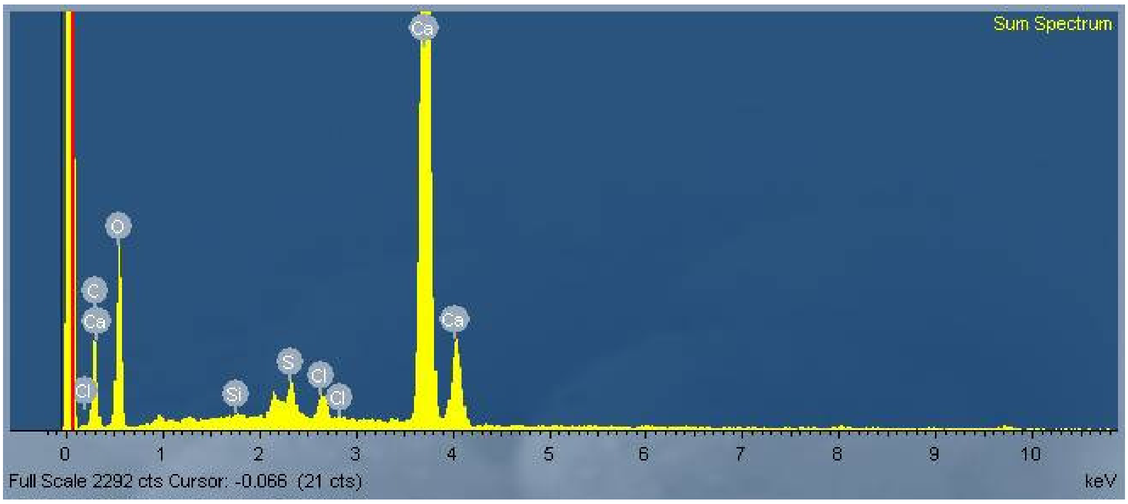

Figure 82 Spectrum for Section 7 of IL-21

Table 22 Elemental Analysis for Section 7 of IL-21

Spectrum	In stats.	C	O	S	Cl	Ca	Total
Spectrum 1	Yes	36.16	52.58	0.37	0.37	10.53	100.00
Spectrum 2	Yes	20.88	47.84	0.61	0.47	30.21	100.00
Spectrum 3	Yes	32.60	46.82	0.32	0.57	19.68	100.00
Spectrum 4	Yes	18.00	50.68	0.77	0.83	29.72	100.00
Spectrum 5	Yes	16.21	51.06	0.82	1.02	30.89	100.00
Spectrum 6	Yes	17.55	50.69	0.89	1.50	29.37	100.00
Spectrum 7	Yes	20.50	49.54	0.91	0.98	28.08	100.00
Mean		23.13	49.89	0.67	0.82	25.50	100.00
Std. deviation		7.93	1.98	0.24	0.39	7.62	
Max.		36.16	52.58	0.91	1.50	30.89	
Min.		16.21	46.82	0.32	0.37	10.53	

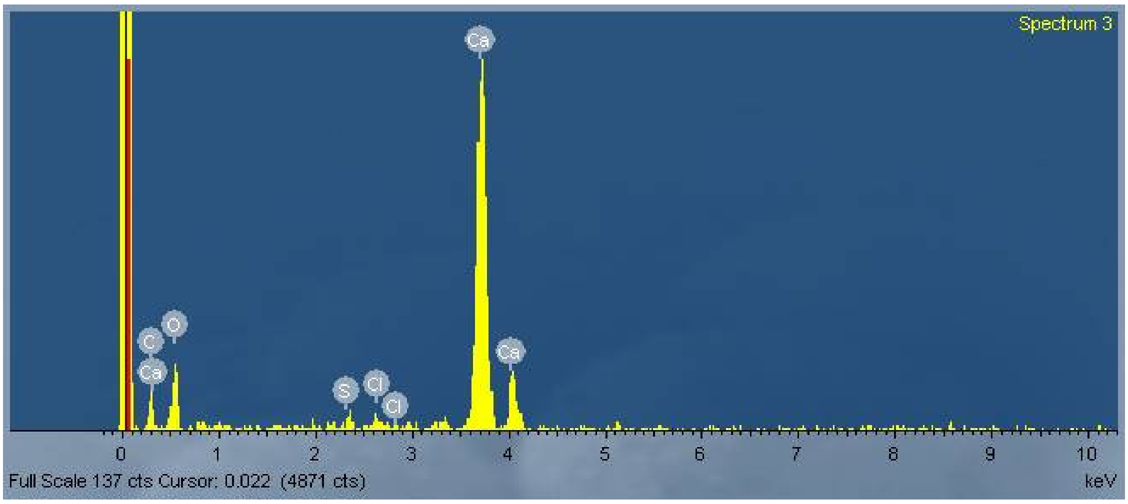

Figure 83 Spectrum for Section 2 of IL-30

Table 23 Elemental Analysis for Section 2 of IL-30

Spectrum	In stats.	C	O	S	Cl	Ca	Total
Spectrum 1	Yes	34.40	54.21	0.13	0.61	10.65	100.00
Spectrum 2	Yes	19.18	36.85	0.83	0.59	42.56	100.00
Spectrum 3	Yes	21.69	44.26	0.87	0.44	32.73	100.00
Spectrum 4	Yes	17.29	51.49	1.36	1.40	28.46	100.00
Spectrum 5	Yes	15.64	50.26	1.49	1.58	31.03	100.00
Spectrum 6	Yes	15.81	50.53	1.21	1.48	30.97	100.00
Spectrum 7	Yes	15.01	48.51	1.24	1.40	33.84	100.00
Mean		19.86	48.01	1.02	1.07	30.04	100.00
Std. deviation		6.83	5.78	0.46	0.50	9.65	
Max.		34.40	54.21	1.49	1.58	42.56	
Min.		15.01	36.85	0.13	0.44	10.65	

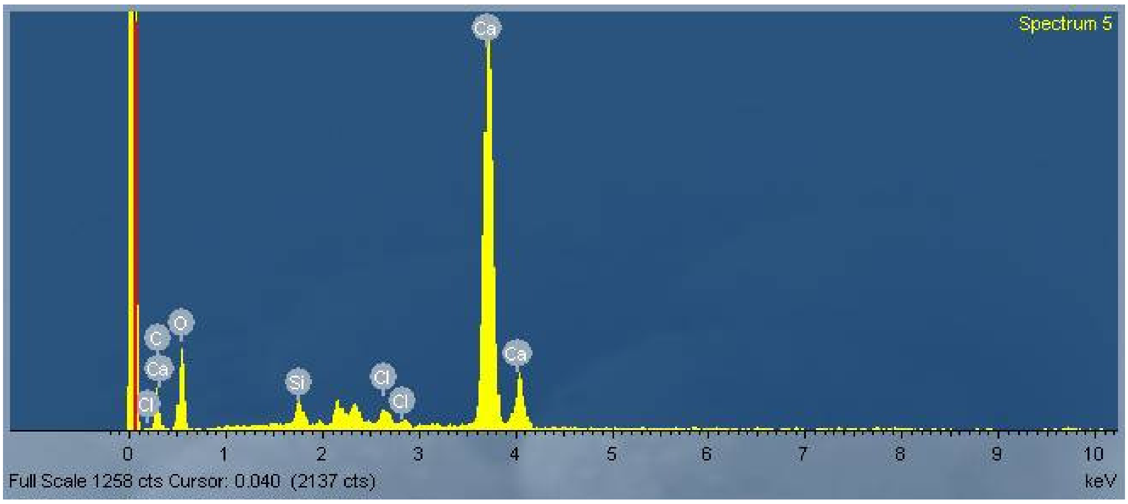

Figure 84 Spectrum for Section 2 of IL-32

Table 24 Elemental Analysis for Section 2 of IL-32

Spectrum	In stats.	C	O	Si	Cl	Ca	Total
Spectrum 1	Yes	33.09	44.61	0.38	0.35	21.56	100.00
Spectrum 2	Yes	17.19	46.80	0.10	0.18	35.73	100.00
Spectrum 3	Yes	11.92	50.58	0.31	0.32	36.88	100.00
Spectrum 4	Yes	15.74	49.53	0.42	1.43	32.89	100.00
Spectrum 5	Yes	15.02	48.95	1.30	1.04	33.68	100.00
Spectrum 6	Yes	13.48	51.21		0.97	34.34	100.00
Spectrum 7	Yes	15.33	55.29	0.45	0.43	28.49	100.00
Max.		33.09	55.29	1.30	1.43	36.88	
Min.		11.92	44.61	0.10	0.18	21.56	

REFERENCES

1. Hung, K. M., Hill, A. D. 1989. A mechanistic model of wormhole growth in carbonate matrix acidizing and acid fracturing. J. Pet. Tech. January. 59-66. SPE-16886

2. Hoefner, M. L., Fogler, H. S. 1989. Fluid velocity and reaction rate effects during carbonate acidizing; Application of a network model. SPE Prod. Eng, February 1989. 56-62. SPE-15573

3. Fredd, C. N., Fogler, H. S. 1999. Optimum Conditions for Wormhole Formation in Carbonate Porous Media: Influence of Transport and Reaction. SPE J. 4 (3) 196-205. SPE-56995

4. Wang, Y., Hill, A. D., Schechter, R. S. 1993. The optimum injection rate for matrix acidizing of carbonate formations. Paper SPE 26578 presented at Annual Technical Conference & Exhibition of the Society of Petroleum Engineers held in Houston, Texas, 3-6 October.

5. Huang, T., Hill, A. D., Schechter, R. S. 1997. Reaction rate and Fluid Loss: The keys to wormhole initiation and propagation in carbonate acidizing. Paper SPE 37312 presented at the SPE International Symposium on Oilfield Chemistry held in Houston, Texas, 18-21 February

6. Glasbergen, G., Kalia, N., Talbot, M. 2009. The optimum injection rate for wormhole propagation: Myth or reality? Paper SPE 121464 presented at SPE European Formation Damage Conference held in Scheveningen, The Netherlands, 27-29 May

7. Shedid, S. A. 2007. Experimental Approach of Matrix acidizing of permeability damaged carbonate reservoirs. Paper SPE 106956 presented at SPE Europec/EAGE Annual Conference & Exhibition held in London, United Kingdom, 11-14 June.

8. Talbot, M. S., Gdanski, R. D. 2008. Beyond Damkohler Number – A New interpretation of wormholing. Paper SPE 113042 presented at 2008 SPE Europec/EAGE Annual Conference & Exhibition held in Rome, Italy, 9-12 June.

9. Hayatdavoudi, A., Chiu, C. B., Kalra, S. K., LeBlanc J. L. & Schluntz, E. K. 1982. Carbonate Acidizing: A Thermodynamic analysis. Paper SPE 10667 presented at the SPE Formation Damage Control Symposium held in Lafayette, L. A., 24-25 March.

10. Shukla, S., Zhu, D. and Hill, A. D. 1999. The Effect of Phase Saturation conditions on wormhole propagation in carbonate acidizing, Paper SPE 82273

presented at the European Formation Damage Conference held at the Hague, the Netherlands, 13-14 May.

11. Huang, T., Zhu, D. and Hill, A. D. 1999. Prediction of Wormhole Population Density in Carbonate Matrix Acidizing. Paper SPE 54723 presented at the European Formation Damage Conference held at the Hague, the Netherlands, 31 May- 01 June.

12. Huang, T., Ostensen, L. and Hill, A. D. 2000. Carbonate Matrix Acidizing with Acetic Acid. Paper SPE 58715 presented at SPE Interational Symposium on Formation Damage Controlheld in Lafayette, Louisiana, 23-24 February

13. Chang, F. F., Nasr-El-Din, H. A., Lindwig, T., Qiu, X. W. 2008. Matrix Acidizing of Carbonate Reservoirs Using Organic Acids and Mixture of HCl and Organic Acids. Paper SPE 116601 presented at SPE Annual Technical Conference & Exhibition in Denver, Colorado, USA, 21-24 September

14. Mahmoud, M. A., Mohamed, I. M., Nasr-El-Din, H. A. 2011. When should we use chelating agents in carbonate stimulation? Paper SPE 149127 presented at the SPE/DGS Saudi Arabia Section Technical Symposium & Exhibition held in Al-Khobar, Saudi Arabia, 15-18 May

15. McDuff, D., Shuchart, C. E., Jackson, S. K. Postl, D., Brown, J. S. 2010. Understanding wormholes in carbonates , unprecedented experimental scale and 3D visualization. Paper SPE 134379 presented at SPE Annual Technical Conference & Exhibition held in Florence, Italy, 19-22 September

16. Qiu, X., Zhao, W., Chang, F., Dyer, S. 2013. Quantitative modeling of acid wormholing in carbonates – what are the gaps to bridge. Paper SPE 164245 presented at the SPE Middle East Oil and Gas Show and Conference held in Manama, Bahrain, 10-13 March

17. Buijse, M., Glasbergen, G. 2005. A semiempirical model to calculate wormhole growth in carbonate acidizing. Paper SPE 96892 presented at SPE Annual Technical Conference held in Dallas, Texas, U.SA, 9-12 October

18. Mahmoud, M. A., Nasr-El-Din, H. A., De Wolf, C. A., Alex, A. K. 2011. Effect of lithology on the flow of chelating agents in porous media during matrix acid treatments. Paper SPE 140149 presented at the SPE Production and Operation Symposium held in Oklahoma City. Oklahoma, USA, 27-29 March

Vitae

Name :Sarmad Zafar Khan

Nationality :Pakistani

Date of Birth :10/17/1987

Email :sarmadzafar@hotmail.com

Address :House No. 3, Mir Street No. 49, Islampura, Lahore

Academic Background :Holds B. Sc. (Hons) in Petroleum & Gas Engineering from University of Engineering & Technology, Lahore, completed in 2009.